1 2  9 0

UNIVERSIDADE D
COIMBRA

Luís Filipe Fragoso Grilo

Obesity – induced hepatic changes during pregnancy

Dissertação no âmbito do Mestrado em Bioquímica,
orientada pela Doutora Susana P. Pereira e pelo Professor Doutor António J. Moreno
e apresentada ao Departamento de Ciências da Vida da Faculdade de Ciências e Tecnologia
da Universidade de Coimbra.

Setembro de 2019

UNIVERSIDADE D
COIMBRA

Obesity – induced hepatic changes during pregnancy

Luís Filipe Fragoso Grilo

Master Dissertation in Biochemistry

CNC CENTER FOR NEUROSCIENCE AND CELL BIOLOGY
UNIVERSITY OF WYOMING
NIH National Institutes of Health
COMPETE 2020
PORTUGAL 2020
UNIÃO EUROPEIA Fundo Europeu de Desenvolvimento Regional
FCT Fundação para a Ciência e a Tecnologia

This work was performed at the Center for Neuroscience and Cell Biology, UC Biotech Building, Biocant Park, University of Coimbra, Portugal, in MitoXT group under the supervision of Dr. Susana P. Pereira (CNC, University of Coimbra) and Prof. Dr. António J. Moreno (Department of Life Sciences, University of Coimbra).

This work was financed by the COMPETE 2020 - Operational Programme for Competitiveness and Internationalisation and Portuguese national funds via FCT – Fundação para a Ciência e a Tecnologia, under projects PTDC/DTP-DES/1082/2014, POCI-01-0145-FEDER-016657 and UID/NEU/04539/2019, the fellowships SFRH/BPD/116061/2016, and the NIH grant R01HD070096-01A1.

Acknowledgments

Este trabalho resulta de um longo ano de trabalho que não era possível sem a intervenção, suporte e apoio de muitas outras pessoas. Foi um ano de grande crescimento para mim, tanto a nível profissional e científico, como a nível pessoal.

Um agradecimento aos meus orientadores, Doutora Susana P. Pereira e Professor Doutor António J. Moreno, por permitirem a realização desta tese. Agradeço igualmente ao Doutor Paulo J. Oliveira por me aceitar no seu laboratório e pelo esforço em sempre garantir todas as condições necessárias ao sucesso deste trabalho.

I would also like to thank to Dr. Peter W. Nathanielsz and Dr. Stephen P. Ford for all the work, time and money invested in this animal model. I am really thankful for their collaboration with MitoXT group and for kindly provide the animal samples used in this work.

Gostaria de expressar o meu agradecimento a todas as entidades de financiamento que suportaram as infraestruturas e os recursos humanos que permitiram a realização desta tese (COMPETE 2020 - Operational Programme for Competitiveness and Internationalisation and Portuguese national funds via FCT – Fundação para a Ciência e a Tecnologia, under projects PTDC/DTP-DES/1082/2014, POCI-01-0145-FEDER-016657 and UID/NEU/04539/2019, the fellowship SFRH/BPD/116061/2016 and the NIH grant R01HD070096-01A1).

Agradeço à Universidade de Coimbra, em particular ao Departamento de Ciências da Vida, ao CNC- Centro de Neurociências e Biologia Celular da Universidade de Coimbra e ao UC Biotech por me acolherem e proporcionarem as instalações e as condições físicas para a realização deste trabalho.

Agradeço, muito particularmente, à Doutora Susana P. Pereira por todo o esforço, dedicação, ajuda, compreensão e paciência que demonstrou durante estes últimos anos para comigo, por não se limitar a ser uma orientadora. Agradeço todos os ensinamentos a nível científico e da vida. Agradeço a confiança depositada, todo o apoio e a constante motivação para que esta tese fosse possível. Grande parte deste trabalho reflete a sua dedicação e generosidade.

Um agradecimento muito especial ao Mestre João Martins pela sua enorme paciência, pelas horas que passou comigo no laboratório, pelo seu rigor científico e por todo o trabalho que teve a rever esta tese. Sem dúvida um exemplo de como a ciência deve ser feita!

Agradeço igualmente a todos os membros do MitoXT -presente e passado - pela boa disposição diária, por todas as conversas/discussões após almoço e por toda a ajuda prestada durante este último ano. Agradeço em particular ao Ricardo Amorim por estar sempre pronto a ajudar e por todo o seu contributo neste trabalho.

Um obrigado a todos os meus companheiros de mestrado, que de diferentes maneiras conseguiram tornar esta caminhada mais fácil. Em especial reconheço a boa disposição diária do André, Óscar e Sara durante o caminho até Cantanhede e agradeço por tantas vezes ficarem à espera que acabasse as minhas experiências.

Aos meus amigos agradeço toda a sua amizade e presença, assim como toda a compreensão por todos os cafés e finos que ficaram por tomar durante as últimas semanas.

Por fim, à minha família pela sua presença constante, compreensão pelas minhas faltas, dedicação e suporte durante toda a minha vida. Que cada vez mais consiga ser o vosso reflexo. Um agradecimento muito especial à minha mãe e ao meu pai por sempre estarem presentes, por todo o suporte que me dão e por todos os sacrifícios feitos. Obrigado ao meu irmão por me estar constantemente a lembrar que estou a fazer uma tese e por todos os debates, muitas vezes inúteis, que me obriga a ter. Aos meus avós pelo exemplo de vida e amizade, um agradecimento especial ao meu avô Fragoso que nunca negou emprestar-me o carro e patrocinou todas as viagens Cantanhede-Coimbra.

Um agradecimento a todos os que de alguma forma permitiram que este trabalho fosse realizado, sem vocês não teria sido possível.

Muito Obrigado!

Abstract

Obesity is rising worldwide and is accompanied by increased incidence of diabetes mellitus and NAFLD. Maternal obesity during pregnancy represents more than a half of total world pregnancies. Pregnancy is a critical period in a woman's life representing a challenge to mother's metabolism. Pregnancy-associated increase in energy and nutrient requirements stress maternal hepatic metabolism which could exacerbate obesity-related hepatic disease. In fact, Maternal Obesity during pregnancy (MO) has been associated with the development of numerous metabolic diseases during and after the gestation. Mitochondrial dysfunction and metabolic alterations are often present in such conditions.

The goal of this study was to characterize the effects of maternal obesity during pregnancy on the maternal hepatic mitochondrial function.

We used a well-established and characterized MO ovine model resulting from 150% recommended global nutrient intake from 60 days before conception, throughout gestation. At 90% gestation, ewes were euthanized under general anesthesia and maternal hepatic tissue collected. Hepatic redox state, metabolic remodulation, mitochondrial function, antioxidant defenses and autophagic mechanisms were determined by Western blot as well as enzymatic activities and molecular quantifications using spectroscopy assays. Data were compared between MO (ML-MO, n=8) and control groups (ML-C, n=10) in total hepatic tissue and in right and left hepatic lobes separately, using the most pertinent statistical test, and $p < 0.05$ considered as statistically significant.

MO induced alterations in maternal hepatic metabolism by increasing NAD^+/NADH ratio, mainly by decreasing NADH levels, decreasing PKA activity and PPAR-γ protein expression. Although no alteration in mitochondrial content was observed, through mtDNA copy number, citrate synthase activity and TOM20 and VDAC protein expression, the hepatic protein content for several subunits of mitochondrial respiratory chain complexes subunits was decreased. Surprisingly, hepatic complex I and IV activities increased due to MO while complex II follow the same behavior than its protein expression, decreasing. Despite no alteration in mitochondrial content indicators, mitochondrial fusion is decreased, and mitochondrial fission is increased without alterations in mitochondrial biogenesis. Additionally, MO resulted in a hepatic increase in lipid peroxidation (MDA levels), decrease in GSH/GSSG ratio and increase in SOD activity, while catalase, glutathione reductase and glutathione peroxidase activities are compromised. Autophagic flux, measured as the LC3-II/LC3-I ratio, was increased although cathepsin B activity, and Beclin-1 and Bcl-2 protein levels were decreased in the livers of MO without alterations in p62 levels. Moreover, Bcl-2 phosphorylation in Thr 56 is increased in MO livers.

In conclusion, MO before and during pregnancy leads to hepatic mitochondrial metabolic alterations, inducing increase in oxidative stress, mitochondria degradation and inducing an imbalanced liver redox state which may exacerbate mitochondrial dysfunction predisposing to hepatic diseases later in life. Monitoring hepatic function during the challenging window of pregnancy can provides new insights for the understanding the origin of hepatic disease.

Keywords: maternal obesity; pregnancy; metabolism; mitochondrial dysfunction; liver; NAFLD; sheep

Resumo

A obesidade é uma doença cuja incidência no mundo continua a aumentar, sendo acompanhada pela incidência de diabetes mellitus e NAFLD (Doença do Fígado Gordo Não Alcoólico). Obesidade em mulheres durante a gravidez representa mais de metade do número total de gestações no mundo. A gravidez é um período delicado nas vidas das mulheres que representa um desafio para o seu metabolismo. Associada à gravidez está um aumento das necessidades energéticas e nutricionais que podem destabilizar o metabolismo hepático das mulheres e exacerbar doenças hepáticas associadas à obesidade. A obesidade durante a gravidez tem, de facto, sido associada ao desenvolvimento de várias doenças de origem metabólica durante e após a gestação. Disfunção mitocondrial e alterações metabólicas estão normalmente presentes nestes tipos de situações.

O objetivo deste estudo é caraterizar os efeitos da obesidade durante a gestação na função mitocondrial hepática.

Foi utilizado um modelo ovino de obesidade durante a gravidez bem validado o qual consiste no consumo de 150% da dieta recomendada a partir de 60 dias antes da fertilização e que continuou durante o período de gestação. A 90% deste tempo, as ovelhas foram eutanasiadas sob anestesia geral e o tecido hepático materno foi recolhido. O estado oxidativo, remodelação metabólica, função mitocondrial, defesas antioxidantes e mecanismos de autofagia do fígado foram determinados por imunodeteção e atividades enzimáticas e quantificações moleculares, os últimos por métodos espetrofotométricos. Os resultados foram avaliados através da comparação do grupo controlo (ML-C, n=10) e o grupo de obesidade durante a gravidez (ML-MO, n=8). Esta comparação foi efetuada no tecido total e nos lóbulos esquerdo e direito do fígado separadamente. Foi utilizado o teste estatístico mais pertinente e valores com $p < 0.05$ foram considerados significativos.

A obesidade durante a gravidez induziu alterações no metabolismo hepático através do aumento da razão NAD^+/NADH (devido à diminuição dos níveis de NADH), diminuindo a atividade da PKA e a expressão proteica do PPAR-γ. Ainda que não tenha sido encontrada qualquer variação nos indicadores de conteúdo mitocondrial (através do número de copias de ADN mitocondrial, atividade da citrato sintetase, e expressão proteica do TOM20 e VDAC), a abundância relativa de várias subunidades dos complexos da cadeia respiratória mitocondrial encontra-se diminuída. Surpreendentemente a atividade dos complexos I e IV estava aumentada com a obesidade durante a gravidez, enquanto que a do complexo II estava diminuída, seguindo a tendência da expressão proteica. Apesar de não existirem alterações na quantidade de mitocôndrias, a fusão mitocondrial está diminuída e a fissão aumentada, sem alterações na biogénese mitocondrial. A obesidade durante a gravidez resulta num aumento da peroxidação lipídica hepática (maiores níveis de MDA), uma diminuição da razão GSH/GSSG e um aumento da atividade da SOD, enquanto as atividades da catalase está diminuída e a da glutationa redutase e da glutationa peroxidase estão comprometidas. O fluxo autofágico, medido através da razão LC3-II / LC3-I, está aumentado apesar da diminuição das atividades das catepsinas e da expressão proteica da Beclin-1 e Bcl-2, sem alterações nos

níveis de p62. Ainda, a fosforilação da Bcl-2 na Thr 56 está aumentada devido à obesidade durante a gravidez.

Em conclusão, a obesidade antes e durante a gravidez leva a alterações mitocondriais hepáticas, aumentando o stress oxidativo, a degradação de mitocôndrias e induzindo um desequilíbrio no estado oxidativo do fígado, o qual pode exacerbar disfunções mitocondriais e predispor para doenças metabólicas. A monitorização da função hepática durante a desafiante janela da gravidez pode fornecer novas pistas sobre a origem das doenças hepáticas.

Palavras-chave: obesidade materna; gravidez; metabolismo; disfunção mitocôndria; fígado; NAFLD; ovelha

Part of this thesis work has been presented in national and international scientific meetings in the form of oral or poster communications.

Oral Communication

1. Susana P. Pereira, Luís Grilo, Chiara H. Cavallaro, João D. Martins, Inês Cardoso, Inês Baldeiras, Teresa Cunha-Oliveira, Stephen Ford, Peter W. Nathanielsz, Paulo J. Oliveira. ***Obesity-induced mitochondrial hepatic changes during pregnancy***. 11th MiPschool, Tromso-Bergen, Norway, 8th – 11th July, 2018.

Poster Communication

1. Luís Grilo, Susana P. Pereira, João D. Martins, Chiara H. Cavallaro, Inês Cardoso, Inês Baldeiras, Teresa Cunha-Oliveira, Stephen Ford, Peter W. Nathanielsz, Paulo J. Oliveira. ***Hepatic oxidative response to maternal obesity during pregnancy in an ewe model.*** 53rd Annual Scientific Meeting of the European Society for Clinical Investigation "The Clocks of Metabolism and Disease", Coimbra, Portugal, 22nd – 24th May, 2019.

2. Luis Grilo, Susana P. Pereira, João Martins, Chiara H. Cavallaro, Inês Cardoso, Inês Baldeiras, Teresa Cunha-Oliveira, Stephen Ford, Peter Nathanielsz, Paulo J. Oliveira. ***Adaptações na fosforilação oxidativa hepática provocadas pela obesidade durante a gravidez num modelo ovino***. 15º Congresso Português de Diabetes, Algarve, Portugal, 8th – 10th March, 2019.

3. Susana P. Pereira, Chiara H. Cavallaro, Luis Grilo, João D. Martins, Inês Cardoso, Teresa Cunha-Oliveira, Inês Baldeiras, Stephen P. Ford, Peter W. Nathanielsz, Paulo J. Oliveira. ***Being obese during pregnancy: the mitochondrial impact on maternal hepatic tissue***. MitoPorto – Advances in Mitochondrial Research, Oporto, Portugal. 13th July, 2018.

4. Susana P. Pereira, Chiara H. Cavallaro, Luis Grilo, João D. Martins, Inês Cardoso, Inês Baldeiras, Teresa Cunha-Oliveira, Stephen Ford, Peter W. Nathanielsz, Paulo J. Oliveira. ***Mitochondrial Changes in the Maternal Liver in a Model of Obesity (MO) During Pregnancy***. 52nd Annual Meeting of the European Society for Clinical Investigation, Barcelona, Spain, 30th May – 1st June, 2018.

5. Luis Grilo, Susana P. Pereira, Chiara H. Cavallaro, Inês Cardoso, Inês Baldeiras, Teresa Cunha-Oliveira, João Martins, Stephen Ford, Peter Nathanielsz, Paulo J. Oliveira. ***Alterações Mitocondriais no Fígado Materno num Modelo de Obesidade Gestacional***. 14º Congresso Português de Diabetes, Algarve, Portugal, 9th – 11th March, 2018.

6. Susana P. Pereira, Chiara H. Cavallaro, Luis Grilo, Inês Cardoso, Inês Baldeiras, Teresa Cunha-Oliveira, Stephen Ford, Peter W. Nathanielsz, Paulo J. Oliveira. Maternal Nutrient ***Excess and Obesity (MO) in pregnant ewes alters hepatic mitochondrial biology and redox balance***. SRI 2018 – Society for Reproductive Investigation, San Diego, CA, USA. 6th – 10th March, 2018.

7. Teresa L. Serafim, Cláudia M. Deus, Sónia Pinho, Tatiana R. Martins, Vilma A. Sardão, Luis Grilo, Chiara H. Cavallaro, Shanshan Yang, Ablat Tuerxun, Fred Odhiambo, Adel B. Ghnenis, Ashley M. Smith, Junfei Li, Teresa Cunha-Oliveira, Susana P. Pereira, Peter W. Nathanielsz, Stephen P. Ford, Paulo J. Oliveira. ***Impact of Maternal Obesity During Pregnancy on Fetal Hepatic Redox Profile and Quality Control Proteins***. MitoPorto – Advances in Mitochondrial Research, Oporto, Portugal. 26th May, 2017.

Table of Contents

List of Images

List of Tables

List of Acronyms and Abbreviations

4-HNE	4-Hydroxynonemal
ACC	Acetyl-CoA Carboxylase
ACL	Adenosine Triphosphate Citrate Lyase
ACO2	Aconitase 2
ACOX	Acyl-CoA Oxidase
ACP	Acyl Carrier Protein
ACSL1	Long-chain Acetyl-CoA Synthetase 1
AFLP	Acute Fatty Liver of Pregnancy
AFP	Alpha Fetoprotein
AGPAT	Acylglycerol-Phosphate Acyl Transferase
AhR	Aryl Hydrocarbon Receptor
ALP	Alkaline Phosphatase
ALT	Alanine Transaminase
AMPK	AMP-activated protein Kinase
ANT	Adenosine Nucleotide Translocator
AST	Aspartate Aminotransferase
ATG	Autophagy-Related protein
ATP	Adenosine Triphosphate
Bad	BCL2 associated Agonist of Cell death
Bcl-2	B-Cell Lymphoma 2
BMI	Body Mass Index
BSA	Bovine Serum Albumin
BW	Body Weight
C	Control group
CACT	Carnitine/Acylcarnitine Transporter
CaMK	Calcium/calmodulin-dependent Kinase
Cat	Catalase
CD14	Cluster of Differentiation 14
CD68	Cluster of Differentiation 68
ChREBP	Carbohydrate Response Element Binding Protein
CoA	Coenzyme A
COPII	Coat Protein II
CPT	Carnitine Palmitoyl Transferase
CRP	C-Reactive Protein
CVD	Cardiovascular Diseases
Cyc D	Cyclophilin D
Cyt C	Cytochrome C
DAG	Diacylglycerol
DCPIP	2,6-Dichlorophenolindophenol
DGAT	Diacylglycerol Acyl Transferase
DH	Dehydratase
DNA	Deoxyribonucleic Acid
DNL	*de novo* Lipogenesis
DNM1L	Dynamin-1-like protein
DOC	2,5-Dimethoxy-4-Chloroamphetamine
DTAB	Dodecyltrimethylammonium Bromide
DTNB	5,5-dithio-bis-(2-nitrobenzoic acid)

DTT	Dithiothreitol
ECH	2-Enoyl-CoA Hydratase
EDTA	Ethylenediamine Tetraacetic Acid
EGTA	Ethylene Glycol-bis(β-aminoethyl ether)-N,N,N′,N′-Tetraacetic Acid
ELISA	Enzyme-Linked Immunosorbent Assay
ELOVL6	Elongation Of Very Long-chain fatty acids protein 6
EMR1	EGF-like module-containing Mucin-like hormone Receptor-like 1
EnR	Enoyl-Reductase
ERR	Estrogen-Related Receptors
ETC	Electron Transport Chain
ε	molar attenuation coefficient
FA	Fatty Acids
FABPpm	plasma membrane Fatty Acid-Binding Protein
FAD/$FADH_2$	Flavin Adenine Dinucleotide (oxidized and reduced form respectively)
FAS	Fatty Acid Synthase complex
FAT/CD36	Fatty Acid Translocase/ Cluster of Differentiation 36
FATP	Fatty Acid Transport Proteins
FFA	Free Fatty Acids
Fis-1	Fission 1 protein
G6P	Glucose-6-Phosphate
GGT	Gamma Glutamyl Transferase
GLUT-1	Glucose Transporter 1
GDM	Gestational Diabetes Mellitus
GPAT	Glycerol-Phosphate Acyl Transferase
Gpx	Glutathione Peroxidase
GR	Glutathione Reductase
GSH/GSSG	Glutathione (reduced and oxidized form respectively)
GTPase	Guanosine-5'-Triphosphate Hydrolyses
HAD	3-Hydroxyacyl-CoA Dehydrogenase
HCC	Hepatocellular Carcinoma
HELLP	Haemolysis, Elevated Liver enzymes and Low Platelets
HNF-4α	Hepatocyte Nuclear Factor 4 alpha
ICP	Intrahepatic Cholestasis of Pregnancy
IL-6	Interleukin-6
IMM	Inner Mitochondrial Membrane
INSIG	Insulin-Induced Gene
IOM	Institute Of Medicine
IRS-1	Insulin Receptor Substrate 1
KR	β-ketoreductase
KS	β-ketosynthase
l	length
LAMP-2A	Lysosome-Associated Membrane Protein 2
LC3	microtubule-associated protein 1A/1B-Light Chain 3
LCAD	Long chain Acyl-CoA Dehydrogenase
LCFA	Long-Chain Fatty Acids
LCHAD	Long-Chain 3-Hydroxyacyl-Coenzyme A Dehydrogenase
LDH	Lactate Dehydrogenase
LDL	Low-Density Lipoprotein

LPA	Lysophosphatidic Acid
LXR	Liver X Receptor
MAPK	Mitogen Activated Protein Kinases
MAT	Malonyl/Acetyl transferase
MCDA	Medium chain Acyl-CoA Dehydrogenase
MDA	Malondialdehyde
Mfn	Mitofusin
MIG12	Midline-1-Interacting G12-like protein
ML	Maternal Liver
MLL	Maternal Left liver Lobe
MLN64	Metastatic Lymph Node protein 64
MLR	Maternal Right liver Lobe
MO	Maternal Obesity group
mPTP	mitochondrial Permeability Transition Pore
MRI	Magnetic Resonance Imaging
mRNA	Messenger Ribonucleic Acid
mtDNA	mitochondrial Deoxyribonucleic Acid
mTORC1	mammalian Target Of Rapamycin Complex 1
MTP	Microsomal Triglyceride transfer Protein
NAD^+/NADH	Nicotinamide Adenine Dinucleotide (oxidized and reduced form respectively)
$NADP^+$/NADPH	Nicotinamide Adenine Dinucleotide Phosphate (oxidized and reduced form respectively)
NAFLD	Non-Alcoholic Fatty Liver Disease
NAM	N-Acetylmuramic acid
NASH	Non-Alcoholic Steatohepatitis
NF-κB	Nuclear Factor κB
NRC	National Research Council
NRF	Nuclear Respiratory Factor
OAT	3-oxoacyl-CoA thiolase
OMM	Outer Mitochondrial Membrane
OPA-1	Optic Atrophy 1
OXPHOS	Oxidative Phosphorylation
PA	Phosphatidic Acid
PAI-1	Plasminogen Activator Inhibitor-1
PB	Phosphate Buffer
PBS	Phosphate Buffer Saline
PGC-1α	Peroxisome proliferator-activated receptor alpha (PPAR-α) and its co-activator PPAR gamma co-activator 1 alpha
PIK3/PKB	Phosphoinositide-3 kinase/Protein Kinase B
PINK1	Phosphatase and tensin homolog-Induced putative Kinase 1
PKA	Portein Kinase A
PKC	Protein Kinase C
PMSF	Phenylmethylsulfonyl Fluoride
PP2A	Protein Phosphatase 2A
PPAR	Peroxisome Proliferator-Activated Receptor
PVDF	Polyvinylidene fluoride
PXR	Pregnane X Receptor
ROS	Reactive Oxygen Species
RT-PCR	Real Time Polymerase Chain Reaction

RXR	retinoid X Receptor
SCAP	SREBP Cleavage-Activated Protein
SCD1	Stearoyl-CoA Desaturase 1
SDS	Sodium Dodecyl Sulfate
SIK	Salt Inducible Kinase
Sirt-1	Silent mating type information regulation 2 homolog 1 (*S. cerevisiae*)
SOD	Superoxide Dismutase
SPECT	Single-Photon Emission Computed Tomography
SREBP	Sterol Regulatory Element Binding Protein 1c
T2D	Type 2 Diabetes
TCA	Trichloroacetic Acid
TE	Thioesterase
Tfam	mitochondrial Transcription factor A
TFB	Transcription Factor B proteins
TG	Triglycerides
TLR-4	Toll-like Receptor 4
TNB	2-nitro-5-thiobenzoate
TNF-α	Tumor Necrosis Factor-alpha
TOM20	Translocase of Outer Membrane 20
TSPO	Translocator Protein
U	enzymatic Units
UCP	Uncoupling Protein
VDAC	Voltage-Dependent Anion Channel
VLDL	Very-Low-Density Lipoprotein
WHO	World Health Organization

Chapter 1 - Introduction

1.1 Maternal obesity: a burden for the rest of the life?

1.1.1 Obesity, a multifactorial disease

Obesity is a chronic condition that results from an unbalance between energy uptake and energy expenditure[1]. Several factors contribute to the development of this condition, namely social, behavioral, physiological and metabolic/molecular attributes[2]. The multifactorial nature of this disease turns it in an embarrassing condition affecting a huge percentage of world population[3]. Nowadays, obesity is probably the biggest problem in public health all over the world[4]. Obesity is highly related to the development of several other disorders, such as Type 2 Diabetes (T2D), Cardiovascular Diseases (CVD) and various types of cancers, that might lead to increased overall mortality[2,4].

Obesity is defined according to the Body Mass Index (BMI), a ratio of a person's weight (in kilograms) and the square of height (in meters). A BMI over than 25 kg/m^2 is considered overweight and 30 kg/m^2 or greater as obesity (class I 30≤BMI<35; class II 35≤BMI<40; class III BMI≥40)[5,6]. However, BMI stratification fails in some cases because it ignores other factors such as the location of adiposity, individual characteristics and muscle mass. Other methods such as dual energy X-ray absorptiometry, magnetic resonance imaging (MRI) and computerized tomography present more accurate results but they are more expensive[4].

During evolution, several genes that determine fat storage became essential as a survival advantage in starvation periods[1]. The need of a system that was able to store the excess of energy led to the development of the adipose tissue[2]. However, the alterations in lifestyle and diet in the last decades compromised this evolutionary adaptation leading to the increase of obesity incidence[2]. In humans, the adipose tissue is divided into brown adipose tissue and white adipose tissue. The last is responsible for fat storage and is composed by fibroblasts, preadipocytes and macrophages[2]. In obesity, white fat accumulation induces adipocytes hypertrophy and hyperplasia leading to a decrease in insulin receptors' density and an increase in beta-3 adrenergic receptors[7,8]. This adaptation facilitates monocytes diapedesis to visceral adipose stroma initiating a proinflammatory status, increasing reactive oxygen species (ROS) production, inducing insulin resistance and pancreatic beta cells apoptosis[2]. Together, these events and the generation of several lipid intermediates induce a state of lipotoxicity, causing anatomical and functional damage in several cell types[2,9].

There are several physiological factors that predispose to obesity, including subtle variations of the endocrine system, the digestive system and (epi)genetics regulation[4]. Recent studies demonstrated that the microbiota can also regulate metabolism and adiposity[10–12]. The ratios between *Bacteroidetes* and *Firmicutes* populations appears to be a crucial factor in obesity, which is related to an increase in the *Firmicutes* population[11]. In fact, it is believed that these bacteria metabolize the consumed food more

efficiently than *Bacteroidetes,* which results in weight gain[11]. One study as shown that replacing normal mice microbiota with the microbiota from obese mice resulted in increased obesity[12]. Hereditary factors are also very important in obesity development. So far, 140 genes have been identified that are associated with the regulation of the individual weight[13]. Indeed, several genetic syndromes are associated with hyperphagia, e.g. the Prader-Willi syndrome[4].

Numerous evidence suggest that women's nutrition and health status during pregnancy can modulate the offspring risk factor to develop chronic diseases later in life[14]. This can contribute to the perpetuation of a vicious cycle that can explain the continuous increase in obesity incidence. Pregnancy itself, is a demanding process that requires critical maternal adaptations to support the gestation of a new life in the womb and can be regarded as a metabolic challenge for the mother. When the mother is obese, she already holds an altered metabolism, thus becoming pregnant and support fetus development can be a metabolic challenge too demanding for this already weakened organism and push it out the plasticity limit triggering unrecoverable alterations that lead to disease in the mother. Furthermore, historical reports have already associated alterations in nutrition and metabolic conditions to the increase of pregnancy-related complications and offspring disease development[15].

1.1.2 Looking to the past, the historical relevance

Pregnancy is described as a sensitive period in women life all over the history[16,17]. Many factors have been pointed as crucial for a successful pregnancy, such as the ideal gestational weight gain, which still not consensual and has been changing in different guidelines over time.

During World War I, with the decline in food supply, a decrease in incidence of pre-eclampsia was observed that led to medical guidelines advising the restriction of weight gain in pregnant women[18]. However, a nutritional deprivation during the Dutch famine in 1944 led to several complications throughout pregnancy, including an increased incidence of stillbirths, low birth weight and infant mortality[18]. These factors went against the previous guidelines leading to a liberalization of the gestational weight gain. Nowadays, the dogma has changed and the popular idea of "eating for two" is well accepted [18].

In 1990 emerged the first guidelines for the minimal weight gain during pregnancy proposed by the Institute of Medicine (IOM)[19]. The ensuing large increase in obesity incidence led to a review of these guidelines in 2009[20]. In this occasion, the IOM suggested not only a minimum but also a maximum weight gain. In addition, the guidelines were adjusted according to the women's BMI, a classification adopted by the World Health Organization (WHO) already described in section 1.1.1.

1.1.3 Obesity Epidemiology: to understand the present

Obesity has been increasing worldwide over the last 30 years mainly in developed and developing countries[4,21]. This trend is also followed by the increasing prevalence of childhood overweight, supporting the hypothesis of a vicious cycle involving maternal obesity and the consequent overweight of the offspring (Figure I.1).

In Portugal a similar trend is observed regarding the increase of obesity prevalence affecting, so far, 61.8% of male and 56.6% of female total populations [21–23]. In Portuguese women, overweight and obesity conditions increase with age affecting a significant percentage of the population in the reproductive age (Figure I.2)[21]. Although there are several complications described for the obese mother and their offspring that may result from being obese during pregnancy, the percentage of pregnant overweight and obese women still increasing all over the world. In the last 30 years conception by overweight women increased 24%, a variation from 30% of global pregnancies in 1983 to 54% in 2011 (Figure I.3)[18]. This results mainly from the increasing obesity incidence. In addition, 48% of all pregnant women exceed the gestational weight gain recommended by IOM[24]. Obese and overweight women are twice likely to surpass IOM guidelines[18].

1.1.4 Maternal Obesity During Pregnancy: a risk too heavy?

Overweight during pregnancy is a risk for both maternal and fetal health and this risk increases as the maternal BMI increases[17]. The health complications that may result for the mother can occur at long-term, far beyond the perinatal period[25]. Maternal obesity is related to increased odds ratios for future development of maternal obesity, metabolic syndrome, T2D and CVD[25]. Several physiological, cellular and molecular mechanisms, involving genetics, nutrition, oxidative stress, insulin resistance, inflammatory changes and vascular alterations, might be behind long-term disease development. Maternal obesity is also associated with a higher risk of developing pregnancy-related disorders. Those complications include gestational diabetes mellitus (GDM), hypertensive disorders, venous thromboembolism, cesarean delivery, wound infection and postpartum anemia[17].

Obese women are 4.8 to 8.7 times more likely to develop gestational hypertension[26]. Curiously, gestational hypertension has higher incidence rates in obese white women than in obese African Americans, although the inverse occurs in healthy women[27]. Epidemiological studies also associate an increased risk of developing pre-eclampsia with obesity. The risk is 3-fold higher in women with BMI of 30 kg/m^2 and 5-fold higher with BMI of 35 kg/m^2 compared to lean women[27]. In addition, pre-eclampsia itself is related to future maternal CVD development[16,17]. Pelvic pain is a usual disorder during late pregnancy caused by the increase of fetus weight. Pelvic pain prevalence increases directly with increasing BMI. The odds ratios are increased to 1.4 in overweight women, 1.7 in obese women with BMI between 30 and 35 kg/m^2 and 2.3 for obese women with BMI over 35 kg/m^2 [28].

Gestational diabetes mellitus is characterized by the development of a state of insulin resistance that only happens during pregnancy. It is not only associated with women who were overweight or obese before pregnancy, but also with excessive weight gain during the gestation[17]. Commonly, GDM is diagnosed between 24 and 28 weeks of pregnancy by screening blood glucose fluctuations after the ingestion of a high dose of glucose. Women with a pre-pregnancy BMI of 30 kg/m^2 have 2.90 to 4 higher risk of developing GDM compared to lean women, while this risk is 5.55 to 9-fold higher for pre-pregnancy severe obese women[29–31]. Diet and physical activity showed positive effects in reducing GDM[16].

Obesity is also associated with increased risks of several complications during delivery. It was reported that the first stage in labor is significantly longer in obese women and that it is less probable that these women fully complete this stage[17]. Cesarean delivery risk is also increased 1.41-fold in overweight and 1.75-fold in obese women, usually associated with numerous delivery complications such as protracted labor and cephalopelvic disproportion that result from fetal macrosomia[32]. Cholesterol deposits in the myometrium of obese women can also affect contractions since an increase in soft tissue inside the pelvis may explain the higher rate of cesarean delivery and the lower response to oxytocin administration[16].

In addition, fetus of overweight women present an elevated risk of incidence of structural birth defects, including neural tube defects, prematurity, macrosomia, hypoglycemia and birth injury from shoulder dystocia, and stillbirth[17]. Preterm birth prior to 28 weeks happens 2.99 times more in obese women with BMI over than 40 kg/m^2 when compared to normal weight women[33]. Neonatal mortality is more common in overweight and obese mother and, when combined with preterm premature rupture of membranes, the risk of incidence is even higher, reaching 3.5-fold in overweight women and 5.7-fold in obese women[34]. Stillbirths occurrence is also increased, being twice more likely to happen in obese women. These odds are even higher in black women[17].

Table 1.1 *– Prevalence Increased risk for several pregnancy-related disorders in function of BMI.*

Condition	**Increased risk (compared to normal-weight women)**		
	Overweight (25 – 29.9 kg/m^2)	Obesity (30 – 34.9 kg/m^2)	Severe Obesity (> 35 kg/m^2)
Gestational hypertension		4.5-8.7 [26]	
Pre-eclampsia		3 [27]	5 [27]
Gestational Diabetes	3.76 [29]	2.9 – 4 [29–31]	5.55 – 9 [29,30]
Pelvic Pain	1.4 [28]	1.7 [28]	2.3 [28]
Cesarean Delivery	1.41 [32]	1.75 [32]	
Preterm Birth			2.99 [33]
Premature rupture membranes with neonatal mortality	3.5 [34]	5.7 [34]	

Several evidences suggest that the womb environment can predispose the offspring for the development of future disorders such as obesity, metabolic syndrome, asthma, autism spectrum disorder, attention-deficit, hyperactivity disorder and cardiac diseases that may arise even during childhood of the offspring[17]. The combination of obesity and GDM represents an even higher risk of disease development for the offspring[17]. The above-mentioned epidemiological studies, summarized in Table 1.1, highly relate maternal obesity with maternal and fetal disease. Therefore, better understanding of the pathways involved in the pathogenesis of maternal obesity is essential, only then it will be possible to develop appropriate and tailored therapeutic approaches to minimize, or even completely abrogate, the harmful consequences of obesity during pregnancy to the maternal and fetal health.

1.2 Pregnancy: a metabolic challenge

Pregnancy is a period characterized by several body adaptations mainly related to the needs for supporting the healthy development of the fetus, being thus a time of high energy demand[35]. For example, maternal heart rate rises, cardiac output increases 40% and the peripheral vascular resistance decreases[36]. In order to maintain the ideal supply of metabolic fuels, the women body suffers metabolic and endocrine adaptations[25].

One of the pregnancy progress hallmarks is weight gain. Although it is a highly variable factor in each women, it is an important adaptation which provides the nutritional support to a healthy fetal development[18]. The gestational weight gain is the sum of fetal and maternal tissues development, including the placenta and amniotic fluid, as well as increase in blood volume, mammary glands and maternal adipose tissue[18].

Energy intake and energy expenditure are essential components in energy balance. During pregnancy, the energy requirements increase over time to support fetal development[18], in average 375, 1200 and 1950 kJ/day for the first, second and third trimester, respectively[35]. Usually, there is an increase of 12 kg in women weight during pregnancy, in which 3.7 kg are fat accretion[35]. While energy requirements increase with the progress of pregnancy, fat accumulation does not. Average rates of fat accumulation are 8 g/day in the first trimester, 26 g/day in the second trimester and a variable number between 7g/day and 23 g/day has been reported for the third trimester[35]. Maternal fat mass accumulation depends on individual factors, such as race, ethnicity and nutrition[25], which can explain the discrepancy of fat accumulation in late pregnancy[35]. Fat can be deposited into visceral (central) and subcutaneous (peripheral) adipose tissue[18]. Fat accumulation in visceral adipose tissue and around other tissues such as liver, pancreas and heart is well correlated to the risk of developing disorders such as CVD, insulin resistance and metabolic syndrome[18,37]. In healthy women, fat is mainly accumulated subcutaneously in the hips and thighs before it starts to be deposited in visceral adipose tissue during late pregnancy. However, in obese women with significant subcutaneous fat, fat tends to accumulate in visceral adipose tissue during all phases of pregnancy[18].

Lipid metabolism during pregnancy can be split into two separated periods: during the first half, triglycerides (TG) are synthesized and stored as energy reserves in maternal adipose tissue; during the second half of the pregnancy, lipids are mobilized to the peripheral tissues preparing for lactation[25]. As a consequence, circulating TG and cholesterol levels increase during pregnancy in the form of very-low-density lipoprotein (VLDL) and low-density lipoprotein (LDL), while circulating free fatty acids (FFA) decrease with pregnancy progression when compared to preconception levels[25]. These factors lead to an hyperlipidemic environment in the mother-fetus interface[25].

A study in women about the fat distribution during pregnancy showed that individuals who gain more visceral fat during the beginning of gestation are more likely to develop impaired glucose tolerance[38]. Another study in a rodent model demonstrated that visceral fat removal before pregnancy reduce the risk of insulin resistance development[37]. The stimulus for body composition changes, physiologically required during pregnancy, might represent an ultimate challenge for the compromised metabolism of an obese woman. Therefore, a better understanding of the mechanisms that lead to fat accumulation in obese women during pregnancy might be pertinent to explain the metabolic and inflammatory alterations that contribute to disease development during and after an obesogenic pregnancy.

1.2.1 Pregnancy in obese women: is that different?

Obese pregnant women usually gain a smaller percentage of gestational weight comparing to healthy individuals. It is reported that during the late phases of pregnancy there is an increase in plasma circulating TG levels, TG related lipoprotein levels, plasma cholesterol and FFA levels independently of the BMI of the mother[25]. Studies showed that the energy costs of any pregnancy are directly dependent on the pre-pregnancy BMI, and that the main cause for differences is the amount of fat accumulated[39]. In accordance, IOM guidelines suggest that the ideal gestational weight gain must take in consideration the maternal BMI (11.5 to 16 kg for a normal pregnancy, 7 to 11.5 kg for overweight women and 5 to 9 kg for obese women)[20].

Globally, 89% of women with normal-weight BMI become overweight or obese five years after a pregnancy[40]. This fact implies that in a second pregnancy a substantial part of women does not have the ideal initial weight[18]. Several studies suggest that metabolic and endocrine alterations during pregnancy persist and play a role in maternal health even after delivery.

1.2.2 Maternal Obesity: the whole picture

Pregnancy and Obesity are two different conditions that involve hormonal adaptations that are fundamental for the homeostasis of these physiologic processes (**Figure 1.1**)[25]. Apart from the traditional endocrine glands, several tissues can contribute to these hormonal alterations, namely liver, pancreas, skeletal muscle and adipose tissue,

among others[25]. Indeed, adipose tissue not only stores TG, but it also produces crucial substances that have endocrine, paracrine and autocrine functions including, for example, adipokines or adipocytokines such as plasminogen activator inhibitor-1 (PAI-1), tumor necrosis factor-alpha (TNF-α), resistin, leptin and adiponectin[2].

During pregnancy the placenta plays an essential role on endocrine regulation through the production of several hormones released at specific time-points, e.g. human chorionic gonadotropin, human placental lactogen and placental growth hormones[25]. Steroid hormones are also essential to regulate pregnancy. The sexual hormones estrogen and progesterone levels are increased when compared to non-pregnant women[25]. Steroid hormones are produced in the ovaries only during the first 8 to 9 weeks of pregnancy. Following this time period, the placenta controls the synthesis of these hormones from cholesterol[25]. Because *de novo* synthesis of cholesterol is very limited in placenta, steroid hormone production depends on the cholesterol available in maternal circulation[41]. Cholesterol uptake in placenta is mediated by two transporters: metastatic lymph node protein 64 (MLN64); and translocator protein (TSPO)[42,43].

The increased levels of steroid hormones in circulation, particularly estradiol and progesterone, facilitates TG metabolism, energy storage and mobilization[44]. Estradiol also stimulates TG circulating levels by up-regulating VLDL secretion in liver[44]. After the first trimester of pregnancy the maternal cortisol concentrations double, leading to an increase of FFA concentrations and promoting pancreatic insulin secretion, which exerts diabetogenic effects[45]. During gestation in obese individuals a huge decrease in the circulating levels of steroid hormones is observed. This decrease is particularly significant during the late phases of pregnancy, when progesterone and estradiol placental production decreases 20% [25]. This hormonal feature in obese women is probably a consequence of a decreased TSPO expression in placental mitochondrial membranes[41].

Insulin also plays a crucial role in the metabolic adaptations during pregnancy. Its production rates well as its mechanisms of action are altered[25]. During pregnancy, women present a high sensitivity to food deprivation and to short-term fasting, which leads to a relative fasting hypoglycemia, hyperlipidemia and hypoaminoacidemia, therefore inducing a mild diabetogenic state[46]. These alterations are mainly caused by a natural and general insulin resistance at the level of several tissues. However, the mechanisms underlying the development of insulin resistance are not yet well described. It has been hypothesized that alterations at the level of the maternal-fetal interface might induce such adaptations[25].

One of the proposed mechanisms is the development of a low grade inflammation state induced in placenta and adipose tissue by the production of cytokines, e.g. IL-6, that are released to maternal circulation[47]. IL-6 can act as counter regulator of genes such as IRS-1 which can interfere with insulin resistance. It is known that cytokines cannot cross the placental barrier and, therefore, it is unlikely that they do interfere with fetal development[25]. In addition, there is an increase in Toll-like receptor 4 (TLR-4) protein and mRNA levels in the adipose tissue during pregnancy[25]. TLR-4 is activated by

saturated fatty acids and it has been proposed as the link between inflammation and insulin resistance[48].

In normal conditions, insulin is a crucial hormone in the regulation of glucose metabolism and glucose plasma levels. It promotes glucose uptake in skeletal muscle, adipose tissue and liver, and suppresses hepatic glycogenolysis and gluconeogenesis[49]. During insulin resistance the pancreas is stimulated to increase insulin secretion to counteract defects in glucose uptake and to decrease hepatic glucose production[50]. Obesity is a condition that highly affects these regulation mechanisms. During the late stages of pregnancy in obese women the severity of insulin resistance is 2 to 3-fold higher than in healthy women[51]. This leads to an increased reliance on lipid substrates as energy sources and to greater adipose tissue mass[25]. Carbohydrate oxidation decreases progressively during gestation while fat oxidation increases until 5 times[52], probably as a response mechanism in order to decrease fat accretion. In addition, insulin promotes *de novo* lipogenesis (DNL) in liver, being associated with Non Alcoholic Fatty Liver Disease (NAFLD) development and the promotion of TG accumulation and hepatic steatosis[53]. On the other hand, FFA oxidation leads to mitochondrial dysfunction by the uncoupling of mitochondrial respiration and increased ROS production[54]. Indeed, increased placental ROS production has been reported in pregnancies of obese women[54].

The dysregulation of the mechanisms controlled by insulin can trigger the development of T2D and fasting hyperglycemia[55]. NAFLD and T2D are commonly related since insulin prompts fibrogenesis by stellate cells[56] and can induce Non Alcoholic Steatohepatitis (NASH). The stimulation of *de novo* lipogenesis and palmitate synthesis increases the risk of lipotoxicity and, consequently, hepatic injuries[57].

Glucagon is produced by pancreatic alpha cells and has an effect contradictory to that of insulin. It stimulates glucose production, inhibits glycolysis, increases peripheral lipolysis and fatty acid oxidation and can also be involved in amino acid metabolism[58]. Increased glucagon secretion is associated to the accumulation of fat in liver[58] which, in turn, may have a crucial role in the development of hyperglucagonemia through mechanisms that are still not yet fully understood[59].

Adiponectin is a cytokine that is only expressed by differentiated adipocytes and can decrease inflammation by inhibiting NF-κB and TNF-α expression in macrophages, for example. Its expression is usually inversely proportional to the levels of inflammatory molecules such as C-reactive protein (CRP)[60]. In opposition, high levels of inflammatory molecules such as TNF-α or IL-6 can also inhibit adiponectin expression and secretion[2]. Adiponectin expression and release is a process well-regulated and its serum levels are determined by the metabolic status: they are increased during a high-carbohydrate diet[61]; and decreased when adipocytes become insulin-resistant[62]. In addition, the decrease in expression of adiponectin mRNA occurs due to gene methylation in the adipose tissue[63]. Reduction in plasma adiponectin levels are also associated to liver fat content and hepatic insulin resistance[64]. High levels of adiponectin improve insulin sensitivity, decrease the flow of FA and induce their mitochondrial oxidation. Although adiponectin levels are always higher in pregnant than in non-pregnant women, they decrease during gestation in

parallel with the increasing insulin resistance[65]. Adiponectin levels are decreased in obese women and they are inversely proportional to maternal BMI[2,64].

Leptin is another cytokine produced by the adipose tissue that has a crucial role in the regulation of body weight and fat mass[66]. It is related to the content of TG by controlling lipid metabolism through the inhibition of lipogenesis and the induction of lipolysis, consequently, decreasing lipid content in skeletal muscle, pancreatic cells and liver, and improving insulin sensitivity[67]. The main controller of leptin plasma levels is glucose metabolism, although catecholamines and glucocorticoids can also influence leptin production[2]. High leptin levels are associated with less insulin secretion and glucose uptake as well as with an increase of gluconeogenesis[68].

Plasma leptin levels are increased two-fold during pregnancy, a unique time window in which it is produced not only by adipose tissue but also by the placenta[69]. An increase in leptin plasma levels also occurs in obesity probably as an attempt mechanism to induce weight loss[67]. Leptin levels are also increased in obese pregnant women despite no changes in mRNA expression were observed[63]. This suggests a lower metabolic plasticity during maternal obesity comparing to healthy pregnancies. In fatty liver diseases higher levels of plasma lectin are also observed and are well-related to the severity of the disease[70]. Leptin can recruit macrophages, stimulating their phagocytic activity and inducing cytokines production, leading to inflammation[71]. Also, leptin is able to stimulate endothelial and smooth muscles cells proliferation and migration inducing oxidative stress and vascular inflammation[2].

Adipsin is another protein characteristic of obesity that is produced in adipocytes and associated with insulin resistance, dyslipidemia and CVD[67]. Adipsin regulates the rate of FA uptake by adipocytes, and therefore their accumulation of TG, through a pathway dependent on the action of lipoprotein lipase[72]. Several other adipokines, including visfatin, omentin and apelin, are also upregulated in obesity[2]. Angiotensinogen is also expressed in adipose tissue, mainly in the visceral adipose tissue, and its levels are correlated to the severity of the metabolic syndrome[67]. Plasminogen activator inhibitor-1 (PAI-1) is an inhibitor of plasminogen activators in blood and is linked to insulin resistance and increased levels of pro-inflammatory citokines[1]. Both angiotensinogen and PAI-1 regulate adipose tissue blood supply and the FA flow from it[2].

Inflammation is associated with obesity and insulin resistance. During maternal obesity, the expression of macrophage-specific markers such as CD68, EMR1 and CD14 in the adipose tissue and the placenta is increased 3-fold due to the infiltration of activated macrophages[73]. The increased FFA levels characteristic of hyperinsulinemia conditions can trigger the activation of TLR4 signaling pathways and lead to chronic inflammation[74]. Indeed, the plasma levels of the inflammatory cytokines CRP and IL-6 are increased by 30% in pregnant obese women. Interestingly, TNF-α levels present no alterations[75,76].

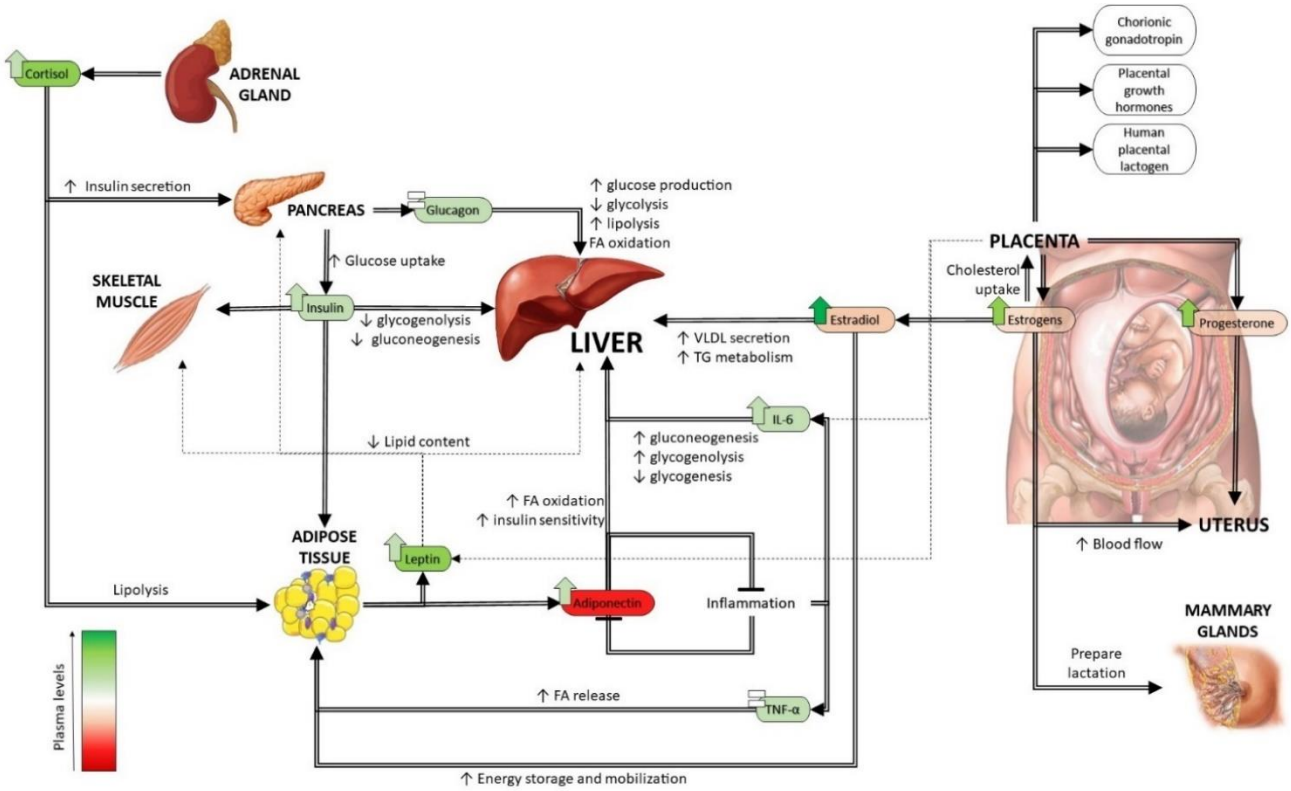

Figure 1.1 –Tissues' interactions in endocrine and metabolic regulation during pregnancy and maternal obesity. *The color of the boxes represents the plasma levels alterations during an obese pregnancy comparing with a healthy pregnancy. The color of the arrows represents the plasma levels alterations of endocrine molecules due to pregnancy and comparing with the levels in non-pregnant women. All comparisons were done using values typical of the third trimester of pregnancy.*

TNF-α is associated with the development of insulin resistance, linking obesity with diabetes and participating in the pathogenesis of obesity-associated metabolic syndrome[2]. TNF-α effects in insulin sensitivity are explained by its stimulation of the release of FFA from adipocytes, the inhibition of adiponectin synthesis and the interference with tyrosine-residue phosphorylation systems[77]. TNF-α also activates nuclear factor κB (NF-κB), stimulating the progress of inflammation in the adipose tissue[77]. Resistin circulating levels are also traditionally related to the degree of adiposity[78], and this adipokine constitutes another link between diabetes and obesity[7]. IL-6 is another inflammatory cytokine produced by macrophages and adipocytes that influences glucose tolerance and blocks adiponectin secretion[67]. IL-6 increases gluconeogenesis and glycogenolysis while it inhibits glycogenesis leading, therefore, to an elevation of TG levels[67]. IL-6 circulating levels are also well correlated to BMI and insulin resistance[77].

Hepatic tissue seems to play an important role in all these processes of endocrine regulation. It is a tissue that, due to its metabolic plasticity, can switch its activity according to the body's hormonal context. Thus, liver might be an ideal organ to evaluate the metabolic adaptive events caused by obesity during pregnancy and provide a metabolic overview that can be useful in the prediction of future pathologies.

1.3 Liver: the key organ in metabolism

The liver is one of the largest organs, in humans is composed by two lobes and represents 2 to 3% of the total body weight. Each lobe can also be divided into four segments which possess different levels of vascularization[79]. The liver plays a crucial role in pregnancy, obesity and in the metabolism, homeostasis and redistribution of amino acids, carbohydrates and lipids, being able to regulate the body's energy balance and weight[80]. Liver is an organ highly exposed to toxic substances and is responsible for their metabolization, being thus a frequent victim of its toxicity[81].

Moreover, the liver is a highly vascularized organ that, at rest, receives more than 25% of the total cardiac output. The hepatic artery is responsible for 25 to 30% of the liver blood supply and divides in left and right hepatic arteries each one connecting to its respective lobe. The right hepatic artery originates the cystic artery that is responsible for the vascularization of the gallbladder[79].

Liver damage is usually a result of hepatocytes' damage, hepatic tumor and/or lipid accumulation[81]. In the present work it is hypothesized that pregnancy can exacerbate the hepatic lipid accumulation characteristic of obesity and trigger further hepatocytes' damage.

1.3.1 Anatomic alterations: two lobes with different roles?

The portal vein provides between 70 to 75% of total liver blood supply. The portal vein is valveless, so it represents a low- and variable-pressure system which pressures usually range between 3 and 5 mm Hg. Similarly, to the hepatic artery, the portal vein also divides in left and right portal vein and each of them has different characteristics. The left portal vein presents a longer extrahepatic course and commonly divides in branches that are initially connected to segment II and then divided to the other segments. On the contrary, the right portal vein quickly divides to the different segments of the liver's right lobe[79].

Intrahepatic veins are responsible for venous drainage in liver. The left and middle hepatic veins either drain into inferior vena cava directly or by forming a short trunk before doing so[79]. The right hepatic vein is usually larger and presents a short intrahepatic course before directly draining into inferior vena cava[79].

In addition to the differences in the liver lobes' vascular system, other observations suggest that the right and left lobes might play some different roles. Post-operative complications after hepatic transplant are more common in right lobe liver donors[82]. Furthermore, magnetic resonance imaging in patients with cirrhosis demonstrated a inhomogeneous distribution of liver function[83] and healthy patients presented differences in the distribution of several radiopharmaceuticals between liver lobes using single photon emission computed tomography[84]. Other factors, such as greater presence of catecholamines and higher sympathetic nerve density in the liver right lobe also suggest different undertakings in each lobe[84]. Despite all these observations, there is not a consensual explanation about liver lobe-dependent differences in metabolic

activity. Maternal obesity effects might be different in each liver lobe both at the level of anatomic alterations and of the regulation of cellular and tissue homeostatic mechanisms, it still not known yet.

1.3.2 Effect of pregnancy in liver: role in disease

The liver plays a crucial role during pregnancy and some physiological and hormonal alterations that are characteristic of pregnancy mimic changes that are also observed in patients with liver disease[36]. Pregnancy-associated liver diseases occur in more than 3% of pregnant women, being the major cause for liver dysfunction in pregnancy[36]. Two different scenarios are possible: the women develop disease during pregnancy or they exacerbate a pre-existing liver disease during pregnancy[36]. A high mortality rate is associated with pregnancy-related diseases, so a quick and good diagnostic is essential to ensure maternal and fetal health[85].

Although there is a rise in blood volume during pregnancy and the liver is a highly vascularized organ, the blood flow in this tissue remains constant during gestation[36]. A compression in the inferior vena cava, due to the enlargement of uterus, and a decrease in the venous return have been described in pregnancy[36].

At the cellular level, an increase of endoplasmic reticulum was reported during pregnancy with altered production and secretion of proteins into blood circulation, so plasma biochemical analysis should be performed minutely[36]. Alkaline phosphatase (ALP) levels are increased during the third trimester of gestation due to its synthesis in placenta as a result of fetal bone development[36]. The alpha fetoprotein (AFP) is also increased since it starts to be secreted by the fetal liver[36]. Fibrinogen and clotting factors (I, II, V, VII, X and XII) are increased during pregnancy, leading to the recognition of pregnancy as a pro-coagulant state[36]. Other molecules' levels in blood, e.g. transaminases, bilirubin or prothrombin, normally do not undergo flutuactions during pregnancy[36].

Hepatic complications can occur in early pregnancy (e.g. hyperemesis gravidarum) or in late pregnancy (e.g. acute fatty liver of pregnancy (AFLP); pre-eclampsia with hepatic involvement including hemolysis, elevated liver enzymes and low platelets (HELLP) syndrome; liver rupture and intrahepatic cholestasis of pregnancy (ICP))[36]. ICP is the most common liver related complication during pregnancy and has a high incidence rate in subsequent pregnancies[36]. HELLP syndrome is characterized by an increase of 2 to 30 times in alanine transaminase (ALT) and represents 22% of the cases with alterations in liver functional tests in pregnant women [86]. HELLP syndrome is considered a severe form of pre-eclampsia, occurring in 10 to 20% of pre-eclampsia cases[87].

The liver is responsible for the synthesis of TG during the first half of pregnancy, in order to store energy, and then controls the lipid oxidation and the energy production from fatty acids[25]. During the second half of pregnancy, the rate of fatty acids oxidation in the liver is increase to fulfill the energy requirements[25]. AFLP is characterized by

mitochondrial hepatopathy and it is directly related to a defect in mitochondrial beta oxidation of fatty acids[88]. AFLP is usually a result of a genetic deficiency in long-chain 3-hydroxyacyl-Coenzyme A dehydrogenase (LCHAD), that is a crucial part of the mitochondrial trifunctional protein complex of the inner mitochondrial membrane[89], and leads to an increase in long-chain fatty acids' levels[89]. Since preeclampsia occurs in 40% of AFLP cases and is highly related to oxidative stress in liver, it might represent a trigger for liver steatosis and mitochondrial dysfunction[90]. After pregnancy, maternal health recovery may be facilitated due to the absence of the placental production of toxic metabolites and oxidative stress species[89].

Although liver disease during pregnancy affects a small portion of pregnancies, it represents a pathological group with significant morbidity and mortality[36]. Better knowledge of the mechanisms behind the development of these disorders is crucial for improving the number of successful pregnancies in these women. Since obesity is a metabolic burden for the organism, the alterations induced by pregnancy, mainly in lipid metabolism, can more easily constitute a trigger for the increased probability of developing liver-related diseases in obese pregnancy.

1.3.3 Liver metabolic function: link between obesity and pregnancy

The liver is an essential organ in carbohydrate and lipid metabolism regulation. It is highly associated with satiety signaling through glucose itself or through the synthesis of some peptides whose levels are determined by glucose concentrations[80]. During the postprandial period, increased concentrations of glucose in the hepatic portal venous system can trigger signaling mechanisms and regulatory pathways such as the promotion of food intake, the decrease in energy expenditure or the increase in fat storage[91].

Fatty acid oxidation in the liver can also be involved in weight regulation, a process sensible to fatty acids' length affected in maternal obesity. In fact, human and animal studies suggest that increased levels of medium-chain triglycerides are able to induce satiety and promote energy expenditure, slowing weight gain[80]. Medium-chain triglycerides can be directly absorbed in the hepatic portal vein and quickly oxidized by hepatic β-oxidation[92]. This factor links directly weight regulation with fatty acids length and oxidation which are influenced by diet, intestinal metabolism and lipid transport[80].

In addition, an increase in the ROS levels in liver, mainly superoxide anion, and their reaction with nitric oxide leading to peroxynitrite formation, causes a decrease in the nitric oxide levels that leads to vasoconstriction in the hepatic vasculature[2,93]. Thus, high ROS levels in liver are usually associated with hepatic injury. Moreover, the rate of secretion of several liver enzymes is also commonly used as a marker of liver damage[94]. Alterations in the circulating levels of proteins such as aminotransferases (Aspartate aminotransferase – AST, Alanine Aminotransferase – ALT), alkaline phosphatase (ALP), gamma glutamyl transferase (GGT) or Lactate Dehydrogenase (LDH) are used as liver health markers[94].

Lipid metabolism alterations are common in several conditions, namely in obesity and pregnancy. In both, fatty acids' accumulation is a common pathway that can lead to hepatic injury and steatosis. NAFLD is usually the liver phenotype of an obese organism.

1.4 NAFLD: steatosis as a natural role in maternal obesity

Obesity alters many metabolic functions in the liver and is associated with inflammation and NAFLD-associated steatosis development[95]. These conditions may progress to several other liver complications such as hepatitis C which, in turn, can develop to cirrhosis and hepatocellular carcinoma (HCC)[80]. NAFLD is present in up to 90 % of obese individuals[96].

NAFLD is the major cause of chronic liver disease in the world and its incidence still increasing mainly due to the epidemic rise in obesity incidence[97]. NAFLD is characterized by more than 5% of hepatic fat infiltration and can evolve to severe states associated with necro-inflammation and fibrosis in liver[97]. NAFLD is a consequence of an excess of metabolic substrates availability that initially leads to alterations in the dynamics of body regulation between liver and adipocytes and then with other organs[50]. In NAFLD, FFA are absorbed in hepatocytes and accumulated in lipid droplets under the form of TG which activate the c-Jun terminal kinase pathway and induce insulin resistance[50].

Currently, the gold standard method for NAFLD diagnosis is a quite invasive process consisting of liver biopsy followed by the quantification of lipid accumulation using histology. So far, blood analysis diagnosis are inconclusive since molecules and/or enzymes already associated with NAFLD might present changes due to other processes in the organism[98]. The search for a better and trustworthy diagnosis using specific biomarkers is a priority of many researches.

Several factors are associated with the development of the NAFLD phenotype, namely nutrition, genetic predisposition and environmental conditions[99]. Pregnancy is a period in which the body is under stress and several metabolic changes occur[25]. Thus, in obese woman, pregnancy can be a trigger for hepatic dysfunction, especially when they already present a fragile balance, as occurs in NAFLD. Consequently, pregnancy may exacerbate pre-conception states of hepatic dysfunction.

1.4.1 Epidemiology

NAFLD is highly associated with numerous other metabolic diseases such as metabolic syndrome and visceral obesity. NAFLD presents a high incidence (20 to 30%) in the general population from developed countries. In some subpopulations the prevalence is even higher, such as in people with T2D (42.6 to 69.5% in Europe) or with morbid obesity (75 to 92%)[100,101]. Since NAFLD is asymptomatic, a silent disease, it is not possible to perform precise studies that can trustily predict the world real prevalence.

However, it is well known that NAFLD incidence is increasing at a dangerous rate mainly caused by the rise in obesity cases, which have doubled since 1960's[102].

Diabetes, hypertension, dyslipidemia and obesity are considered risk factors for the progression of NAFLD to NASH[103,104]. In addition, genetic predisposition has been linked to NASH development. Subjects harboring the PNPLA3 I148M or TM6SF2 genotypes develop liver fibrosis with increased severity[105,106], whereas the EFCAB4B phenotype is associated with lobular inflammation[107]. Polymorphisms in the TM6SF2 gene are associated with a 40 to 88% increased risk of developing NAFLD[106]. A family history of diabetes is also considered to be a risk marker for the predisposition of patients to develop NASH[107]. These facts suggest that genetic analysis can be important to improve the follow-up of NAFLD and/or to prevent its progression to more harmful conditions.

Apparently, predisposition to NAFLD is independent of the individual gender[108]. However, some studies show that post-menopausal women have an increased risk of developing fibroses[109]. Aging is indeed correlated to NAFLD[110], although this dependence might be a consequence of the absence of diagnosis due to the asymptomatic nature of NAFLD, making the discovery of the disease more likely in older people. Differences in NAFLD prevalence were also dependent of race and ethnicity[111]. However, they might be potentiated by other factors such as diet. Hispanics present a higher risk to develop T2D and, therefore, they appear to have a stronger predisposition to suffer from NAFLD comparing to Caucasians. However, this tendency is not maintained for the evolution of the disease towards liver injury[111,112]. Both the Hispanic population and the non-Hispanic white population have a higher incidence of NAFLD and NASH, and fibrosis with increased severity comparing to the African-American population[113,114].

It is well described that NAFLD can evolve to NASH and then to cirrhosis or HCC. Indeed, NAFLD is one of the principal causes of HCC in the United Sates and is almost surpassing the leading cause, viral hepatitis[115]. In a 10 years follow-up study of NASH patients, 20% of them developed cirrhosis and 8% died from liver-related complications[116]. In another study, 43 out of the 87 patients with NASH developed HCC without an intermediate state of cirrhosis[117]. NAFLD can also trigger other diseases, being the cardiac events the main NAFLD-related cause of death[118].

HCC is the sixth most common cancer in the world and the third cancer-related-death cause[119]. HCC constitutes a natural progression of NAFLD that may occur independently of the development of fibrosis. Insulin resistance and hepatic steatosis are considered the triggers for adipokines' hormonal changes, oxidative stress, lipotoxicity, adipose tissue-related inflammation and stimulation of insulin-like growth factor signaling, factors that lead to the disease progression[120].

1.4.2 NAFLD progression

NAFLD is characterized by a state of liver steatosis with or without low inflammation levels. If inflammation and ballooning are present the liver is already in a NASH state. While NAFLD is described as a state with hepatic insulin resistance, increased fasting glucose levels and an atherogenic profile[121], NASH is characterized by an increase of the inflammatory levels of pro-atherogenic cytokines, hyper-coagulable factors and adhesion molecules[122]. It is reported that during a three years period 20 to 30% of the NAFLD cases evolve to NASH, while this percentage increases to 42-44% if a six years period is considered[123,124].

NASH cases in which the liver presents no fibrosis the disease can evolve to a NAFLD-related cirrhosis, a progression that occurs quickly in 5 to 18% of the cases. However, if fibrosis is present, cirrhosis development happens in 38% of the cases. They can also evolve directly to HCC by mechanisms that still unknown[125–127]. After this transition the risk of developing portal hypertension is increased 17%, 23% and 52% after one, three or ten years, respectively[128]. Patients with decompensated liver cirrhosis have a median survival time of two years and currently the only solution available is a liver transplant[129].

1.4.3 Pathophysiology

NAFLD is associated to a spectrum of alterations in liver functionality that can result in an inter-organ deregulation and potentiate diseases in other tissues. Increase in liver fat content can lead to cardiovascular, kidney and/or metabolic diseases and even cancer[130]. Reports point that insulin resistance has a crucial role in NAFLD development. NAFLD can impair body dynamics, mainly in circulating lipids and hormones[99].

It is well characterized that hepatocytes injury is a consequence of an overload of primary metabolic substrates, mainly lipids, glucose and fructose[131]. The main source of fat accumulation in hepatocytes are the circulating free fatty acids, which are a result of adipose tissue lipolysis and lipoprotein spill over[50].

Cholesterol plays a significant role in many human metabolic disorders and is considered the most lipotoxic molecule[132]. An increased accumulation of cholesterol has been reported in NAFLD and NASH patients[133]. It is well documented that cholesterol is able to induce inflammatory responses by stimulating macrophages to release cytokines, such as tumor necrosis factor-α and interleukin-6, that activate the NLRP3 inflammasome pathway[134].

As previously described, hormonal alterations also have an impact in liver homeostasis. Hormones can modulate hepatocyte's metabolism and their regulatory actions can be crucial to understand NAFLD. In addition, hormonal regulation is dependent on several mechanisms, e.g. the hormones released by the gut microbiome, namely glucagon-like peptide 1 and ghrelin[50,99]. All the alterations described previously

have a significant effect in liver homeostasis and the hepatic metabolism is one of the most affected systems.

1.4.4 Liver metabolism

1.4.4.1 Metabolic flexibility in liver

Hepatic tissue is able to metabolize or produce several crucial nutrients with a great compliance and can quickly adapt according to the involved circunstances[135]. Modern life style together with foods' and drinks' abuse overtakes this original liver capability of adaptation and adjustability[135].

Metabolism in liver can adapt many times each day to maintain the blood nutrient levels essential to the body homeostasis[135]. As an example, liver can shift lipid metabolism according to a fed or a starvation period, promoting fatty acid synthesis or the quick fatty acid breakdown, respectively[135].

1.4.4.2 Lipid Metabolism

Fatty acids are efficient, economic and storable fuel molecules[136]. Fatty acids present two main roles in the body: they can be used as a fuel storage system after synthesis from aminoacids and carbohydrates during the postprandial phase; or they can be absorbed from the diet or released from the adipose tissue and transported to the hepatic tissue where they are catabolized, which occurs mainly during starvation periods[135].

After ingestion, fatty acids are absorbed mainly as reconstructed complex lipids in chylomicrons that are transported predominantly in lymph vessels to the adipose tissue where they are stored as triglycerides[135]. Storage and mobilization of triglycerides are regulated by several hormones such as glucagon, adrenalin and glucocorticoids[137].

During the starved state, triglycerides can be broke down in adipocytes originating free fatty acids that are used as an energy source in the liver[135]. In hepatocytes long-chain fatty acids (LCFA) levels (C12-C20) must be tightly regulated due to their importance in several signaling, transcription and metabolic pathways[138]. Therefore, liver developed several mechanisms to control fatty acid metabolism (**Figure 1.2**)[136].

Numerous studies revealed that the protein-mediated transport of fatty acids is the first step in the control of their uptake rate[138,139]. Fatty acids are then activated to acyl-CoA and must be transported to mitochondria in order to produce energy by the β-oxidation[135,136]. This transport occurs via the carnitine shuttle whose rate is another control point in lipid metabolism[140]. Fatty acids can also have an endogenous origin through the *de novo* synthesis pathway, which is regulated essentially by protein expression[136]. Fatty acyl-CoA can also be modified in ER to produce other important cellular lipids, such as phospholipids and triglycerides, or to be secreted[135,141].

1.4.4.3 Lipid uptake regulation

Long-chain fatty acids are, indeed, one of the major sources of energy in the human body and they are essential for the synthesis of molecules such as the phospholipids[138]. LCFA are associated with signaling pathways involving Ca^{2+} release and Protein Kinase C (PKC) transduction cascades[142], the regulation of metabolic enzymes, such as acetyl-CoA carboxylase[143] and glucokinase[144,145], and the binding to several transcript factors that regulate protein expression, e.g. Peroxisome proliferator-activated receptors (PPARs), Sterol regulatory element-binding protein (SREBP), Carbohydrate-response Element-binding Protein (ChREBP), Liver-X nuclear receptor (LXR), Hepatocyte nuclear factor 4 alpha (HNF-4α) and Nuclear factor kappa-light-chain-enhancer of activated B cells (NF-κβ)[145–148].

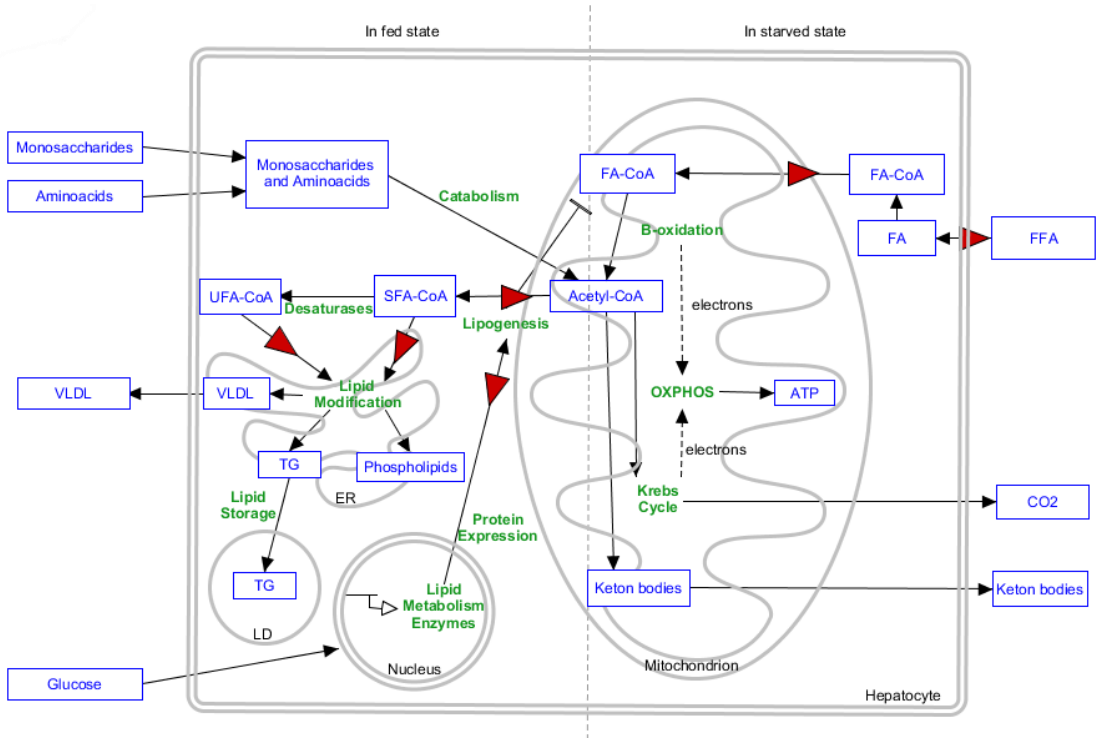

Figure 1.2- Hepatic lipid metabolism in fed and starved state.
Relationship between fatty acids uptake, degradation and synthesis are summarized. In the fed state fatty acids are mainly synthetized from excessive nutrient levels in the blood, and they are stored, exocyted or integrated into other molecules. In the starved state, fatty acids are mainly released in blood circulation by adipocytes, and they are uptake and used as energetic fuel by hepatocytes. Red triangles represent crucial steps that control each mechanism; in green are the different pathways; in blue are represented the metabolites or families of metabolites. Abbreviations: ATP – Adenosine Triphosphate; CO2 – Carbon Dioxide; ER – Endoplasmic Reticulum; FA – Fatty Acids; FA-CoA – Fatty Acyl-CoA; FFA – Free Fatty Acids; LD – Lipid Droplet; SFA-CoA – Saturated Fatty Acyl-CoA; TG - Triglycerides; UFA-CoA – Unsaturated Fatty Acyl-CoA; VLDL – Very Low-Density Lipoprotein.

While short-chain fatty acids can diffuse through the cellular membranes, the majority (over than 90%) of LCFA cellular uptake is dependent on protein-mediated transport[149]. Different proteins with distinct functioning mechanisms are responsible for LCFA transport across hepatocytes' cellular membrane. Some examples are the plasma membrane fatty acid-binding protein (FABPpm), the scavenger receptor FAT/CD36

(fatty acid translocase/ cluster of differentiation 36) and the fatty acid transport proteins 2 and 5 (FATP2/5)[81].

FABPpm is a peripheral membrane protein located in outer leaflet of the cellular membrane[150]. This protein is derived from the gene of the mitochondrial aspartate aminotransferase. However, when it is localized at the cellular membrane it is responsible for the uptake of fatty acids[151,152]. A possible mechanism of fatty acid transport by FABPpm in collaboration with FAT/CD36 was proposed[153], although the response to different stimuli is dissimilar for both proteins[141,154–156]. An important role of FABPpm in the fatty acids uptake to the cell nucleus has also been described[157].

FAT/CD36 is a protein well known for its role in the uptake of oxidized low-density lipoprotein in macrophages and for FA uptake in adipose tissue, skeletal muscle and heart[81,158]. Recently, FAT/CD36 was also associated with fatty liver disease[159]. In cells it is localized in the cell surface caveolae, intracellular vesicles and mitochondria. In mitochondria it is associated to carnitine palmitoyltransferase 1 (CPT1), a key protein in β-oxidation[139,160].

FAT/CD36 expression has been associated with several transcriptional factors, such as cytosolic aryl hydrocarbon receptor (AhR), and several nuclear hormone receptors, e.g. pregnane X receptor (PXR), liver X receptor (LXR) and Peroxisome proliferator-activated receptor gamma (PPARγ)[159]. Plasma levels of soluble FAT/CD36 were also related to a phenotype of insulin resistance, carotid atherosclerosis and fatty liver in a study with more than one thousand healthy European subjects[161]. Moreover, increased FAT/CD36 expression has been linked with AMP-activated protein kinase (AMPK) activation[162] and with fatty liver disease due to an increase in fatty acid uptake and TG storage[81,141,159,163–165]. In normal conditions, its expression in healthy hepatocytes is low but it is hugely increased with lipid rich diets, hepatic steatosis and NAFLD[164].

The mechanism behind FA transport by FAT/CD36 is still not completely understood, although it is speculated that FABPpm acts like an outsider receptor for LCFA and then interacts with FAT/CD36 mediating the transmembrane uptake by facilitating LCFA flip-flop across the bilayer[153].

FATP are a family of proteins involved in fatty acids uptake that can be differentiated from each other due to the location of genes that encode them and the tissue where they are expressed[138]. In liver four different FATP isoforms (2 to 5) are expressed, being the FATP-2 and FATP-5 the more abundant[166]. Indeed, FATP-5 is specific to liver tissue and both FATP-2/5 have been linked to fatty liver diseases[138].

The mechanism of LCFA transport by FATPs is still not completely understood. FATPs might facilitate the transfer of LCFA by forming homo- or heterodimers[166,167]. On the other hand, FATPs can also act by inducing LCFA activation, thus stimulating their uptake. FATPs facilitate the thioester-CoA bond formation that traps the LCFA inside cells[138]. Association of FATP-1 with ACSL1 (long-chain acetyl-CoA synthetase 1) supports the second hypotesis[168]. A model that also involves FAT/CD36 fatty acid

recognition and FABPpm intracellular FA buffering after FATPs uptake has also been proposed[166].

FATP-2-AAV knockdown in mice with hepatosteatosis significantly improved liver morphology and decreased intracellular fat depots as well as TG levels[169]. A similar study with a FATP-5-AAV treatment also improved hepatic steatosis[170], while FATP-5 knockout mice uptake of LCFA is reduced 40 to 50% in a high-fat diet context[171].

The role and the possible therapeutic strategies associated with FA transporters are still not completely clear. However, their relationship with fatty liver disease seems indisputable. Assessing tissues' capability of FA uptake can be valuable for the detection of increased levels of intracellular FA, although FA oxidation can also have a significant impact on FA homeostasis.

1.4.4.4 Beta-oxidation

Under certain conditions, such as prolonged fasting, illness or periods of increased physical activity, liver uses fatty acids oxidation to obtain energy[172]. Furthermore, FA oxidation can also occur associated with the synthesis of ketone bodies to produce metabolites such as β-hydroxybutyrate and acetoacetate that can be used as energy source in other tissues, namely in brain when blood glucose levels are low[135,137]. Fatty acid oxidation can occur in three different organelles: β-oxidation in lysosomes and mitochondria; and ω-oxidation in the endoplasmic reticulum[173].

Mitochondrial β-oxidation is the dominant FA oxidative pathway[172]. Although short- (< C8) and medium-chain (C8 to C12) fatty acids are able to freely cross mitochondrial membrane, mitochondrial uptake of LCFA requires a specific mechanism regulated by CPT1[174]. In fatty acid cellular synthesis, elevated levels of acetyl CoA in the mitochondria are converted to citrate that is transported to cytosol, the subcellular location where FA synthesis starts[135]. In this process, malonyl-CoA (a metabolic intermediate) is produced and it can inhibit CPT1 activity[172].This regulation is a crucial step in β-oxidation rate control, preventing the formation of a futile cycle of fatty acids' synthesis and consumption[136].

CPT1 is responsible for the FA-CoA conversion into fatty acyl-carnitines, promoting their transport to the mitochondrial matrix by the carnitine/acylcarnitine transporter (CACT)[175]. Then, the mitochondrial carnitine palmitoyltransferase 2 (CPT2) converts fatty acyl-carnitines into FA-CoA allowing the start of β-oxidation cycle[175]. In this process, CACT is a crucial protein that restores cytosolic carnitine levels[176].

In the mitochondrial matrix, FA-CoA undergo a first step of dehydrogenation, to form acyl-CoA esters, catalyzed by chain length-specific acyl-CoA dehydrogenases such as VLCAD, LCAD or MCAD[175]. Deficiencies in these enzymes induce hepatic steatosis and alterations in lipid metabolism[177,178]. A hydration step performed by 2-enoyl-CoA hydratase (ECH) followed by another dehydration by 3-hydroxyacyl-CoA dehydrogenase (HAD) and a thiolysis performed by 3-oxoacyl-CoA thiolase (OAT) end the cycle[172,175].

In each cycle an Acetyl-CoA molecule is released and the fatty acid chain is reduced in 2 carbons until it is fully converted into Acetyl-CoA[172].

Chronic starvation has been linked to the increased expression of β-oxidation genes through transcriptional mechanisms[173]. Peroxisome proliferator-activated receptor alpha (PPAR-α) and its co-activator PPAR gamma co-activator 1 alpha (PGC-1α) are associated with the increased expression of several target genes such as CPT1, Long-Chain Acyl-CoA Dehydrogenase (LCAD), Medium-Chain Acyl-CoA Dehydrogenase (MCAD), and acyl-CoA oxidase (ACOX)[173]. Starvation also leads to acetyl-CoA carboxylase (ACC) inhibition by AMPK, preventing malonyl-CoA formation, thus increasing the FA oxidation rate and activating PGC-1α through sirtuins activity[179,180].

The role of β-oxidation in fatty liver disease still not completely elucidated. However, its importance in the regulation of the fatty acid pool is irrefutable mainly due to its direct connection with the *de novo* lipogenesis pathway.

1.4.4.5 *De novo* lipogenesis

De novo lipogenesis is an essential pathway in the liver which allows fatty acid synthesis for energy storage or secretion[181]. *De novo* lipogenesis is highly related and controlled by the carbohydrate metabolism in order to convert sugars into lipids during a post-prandial state. The synthetized lipids can be used as energy fuel during starvation periods[182]. Indeed, a high-carbohydrate diet leads to an increase in *de novo* lipogenesis rate[183] and this abnormal rate contributes to NAFLD pathogenesis[57].

The process starts by the conversion of cytoplasmatic citrate into acetyl-CoA, by Adenosine triphosphate citrate lyase (ACL), which is then used to produce malonyl-CoA by ACC. Malonyl-CoA is then transferred to the Fatty acid synthase complex (FAS), an enzyme complex with seven protein domains that catalyzes the remaining reaction steps leading to the synthesis of palmitate[184]. The elongation process catalyzed by FAS initially requires that an acetyl-CoA molecule binds to acyl carrier protein (ACP). The acetyl-ACP formed establishes a thiol bond with the Cys161 of the β-ketosynthase (KS) active site, promoting the connection between an acetyl-ACP and FAS. To proceed, the elongation reaction of the acetyl-Cys161, or of any previously existing acyl-Cys161 complex, requires malonyl-ACP molecules as a carbon source[182]. The generation of the malonyl-ACP molecules is catalyzed by malonyl/acetyl transferase (MAT), which promotes the binding of malonyl-CoA to ACP with the release of CoA[185]. KS catalyzes the connection between acetyl-Cys161 (in the first cycle) or acyl-Cys161 to Malonyl-ACP forming β-ketoacyl-ACP, which is then reduced to β-hydroxyacyl-ACP by the action of β-ketoreductase (KR)[186]. The formed β-hydroxyacyl-ACP suffers a dehydration catalyzed by dehydratase (DH) followed by a reduction catalyzed by NADPH-dependent enoyl-reductase (EnR), leading to the formation of an acyl-ACP[187].

This cycle repeats until the acyl chain reaches 16 carbons. Thioesterase (TE), an enzyme that is also part of FAS, has a high specificity for 16 carbon long acyl chains and

cleaves their bond with ACP, leading to the release of a palmitate (16:0)-CoA molecule[182,188]. To a lesser extent, FAS can also produce stearate (18:0). However, elongation reactions of palmitate catalyzed by the enzyme elongation of very long-chain fatty acids protein 6 (ELOVL6) are a far major source of stearate[188,189]. Both palmitate and stearate can suffer desaturation by stearoyl-CoA desaturase 1 (SCD1) leading to the production of the unsaturated fatty acids palmitoleate (16:1 n-7) and oleate (18:1 n-9), respectively[190]. Those unsaturated fatty acids can then suffer further elongation and/or unsaturation reactions[191].

De novo lipogenesis is controlled at multiple levels by a large number of different regulatory mechanisms. For example, polyunsaturated FAs decrease *de novo* lipogenesis by preventing gene expression[192]. The enzyme complex FAS constitutes the rate-limiting step in fatty acid synthesis[193] and its depletion leads to fatty liver disease due to the hampering of β-oxidation caused by malonyl-CoA accumulation[194]. ACC is also a well-regulated enzyme through different mechanisms: polymerization, via allosteric control; phosphorylation; and expression[188,195]. ACC inhibition reduces TG levels in liver by preventing fatty acid synthesis and activating FA oxidation[193]. Firstly, this protein is expressed in low-activity dimers that can suffer polymerization stimulated by cytosolic proteins, e.g. midline-1-interacting G12-like protein (MIG12), or glutamate levels, thus presenting higher enzymatic activity[196–198]. Indeed, not only glutamate but also citrate levels regulate allosterically the increase of ACC activity through its polimerization[182].

Secondly, ACC activity can be inhibited by phosphorylation, a quick response to stimuli such as adrenaline or glucagon[199]. Atypical phosphorylation states of cAMP-AMPK in Ser79, Ser1200 and Ser1215, and of PKA in Ser77 and Ser1200 present an increased potential to phosphorylate ACC[182]. Glutamate activation of protein phosphatase 2A (PP2A) leads to the removal of phosphate groups from ACC increasing its activity[200]. The last level of ACC activity regulation is by the control of its expression mediated by transcriptional factors such as SREBP1c, ChREBP and LXRs[182].

In detail, *de novo* lipogenesis rate is highly dependent on transcriptional regulation by this two different pathways: the SREBP1c and the ChREBP[201]. Activation of these proteins is stimulated by increased insulin signaling and increased glucose concentrations, respectively[202,203]. Inactive SREBP1c exists in the endoplasmic reticulum associated with the proteins SREBP cleavage-activated protein (SCAP) and insulin-induced gene (INSIG)[204]. Sterol biding or phosphorylation of SCAP induce a conformational change and the consequent INSIG dissociation from the complex[205]. This process exposes an amino acid sequence that is recognize by the coat protein II (COPII) and the newly formed SREBP1c-SCAP complex is transported to the Golgi apparatus where both proteins are split due to proteases' activity releasing SREBP1c in its mature form[205]. SREBP1c mature form can be activated by two different mechanisms[182]. The first activation pathway is phosphorylation by mammalian target of rapamycin complex 1 (mTORC1) through phosphoinositide-3 kinase/protein kinase B (PI3K/PKB) pathway[206]. SREBP1c transcriptional activity can also be induced by the regulation of protein expression through the heterodimerization of LXRα with retinoid X receptor

(RXR), a process dependent on mTORC1 activity[207]. SREBP1c activity can be inhibited by PKA, AMPK and salt inducible kinases (SIKs)[175].

ChREBP activation is a mechanism that is still not completely understood although its relationship with the postprandial increase of glucose uptake in hepatocytes seems evident[182]. Several metabolites produced during glycolysis, such as glucose-6-phosphate (G6P) and fructose-2,6-bisphosphate, were proposed as ChREBP regulators[208,209]. ChREBP acetylation is also associated with an increase of its activity, while phosphorylation by AMPK or PKA of Ser196 prevent ChREBP translocation to nucleus[203,210].

Both SREBP1c and ChREBP are associated with the expression of pyruvate kinase and several lipogenesis-related enzymes, such as FAS, SCD1, ELOVL6 and ACC. This can be a mechanism to increase acetyl-CoA availability and, therefore, to increase lipogenesis activity[182]. After fatty acids synthesis, these enzymes can suffer several alterations and be associated in complex molecules to decrease FA-related toxicity.

1.4.4.6 Fatty acids' storage and modifications

During the fed state, newly synthesized free and non-esterified fatty acids are not directly released to blood circulation. Instead, they are converted into complex lipids such as triglycerides, phosphoglycerolipids or cholesteryl esters in the endoplasmic reticulum membrane[211].

FA-CoA can be used to synthesize phospholipids through several cellular pathways[212]. The specificity of fatty acids' utilization and the consequent membrane lipid saturation is determined by the distinct affinity of several lysophospholipid acyltransferases to the different acyl-CoA chains[135]. The mechanisms that modulate membrane constitution will be discussed further ahead.

Triglycerides synthesis starts with the acylation of glycerol-3-phosphate by a FA-CoA molecule, a reaction that yields a lysophosphatidic acid (LPA) and is catalyzed by the glycerol-phosphate acyl transferase (GPAT)[213]. LPA suffers another acylation catalyzed by the acylglycerol-phosphate acyl transferase (AGPAT) forming phosphatidic acid (PA) that can be dephosphorylated by Lipin-1 to form diacylglycerol (DAG)[202].

PA and DAG are essential lipid intermediates in phospholipid synthesis[213]. DAG can be acylated to TG by the diacylglycerol acyl transferase (DGAT). TG are inert molecules whose synthesis decreases the FA-related toxicity[182]. Triglycerides can then be associated to ApoB100 by the microsomal triglyceride transfer protein (MTP) in the ER lumen and assembled to VLDL that can be exocytosed from the cell[214].

TGs can also be stored in hepatocytes inside of cytoplasmic lipid droplets that constitute the major form of hepatic fat[131]. Lipid droplets represent an important mechanism in cell dynamics since they are able to move between endoplasmic reticulum and mitochondria leaflets. This enables the correct delivery of triglycerides according to

the metabolic demand[215,216]. This process of intracellular accumulation also allows storage of neutral lipids, thus preventing accumulation of lipid intermediates and the consequent lipotoxicity[216].

1.4.4.7 Lipid metabolism in NAFLD

The Regulation of cellular lipid metabolism pathways is crucial to the definition of the fatty acid pool and its intracellular balance, and has an impact on the whole-body lipid homeostasis[81]. As discussed before, in NAFLD there is an accumulation of fat in hepatocytes that results from metabolic abnormalities such as increased FA uptake, increased *de novo* FA synthesis, impaired VLDL secretion and TG accumulation (**Figure 1.3**)[81,217].

When the lipid secretion capability of liver is exceeded by FA synthesis, TG start to accumulate, when excessive intrahepatic triglyceride reach >5% of liver volume constitutes the hallmark of steatosis[135]. These processes begin with hepatic stress that, in its turn, induces an inflammatory reaction and the consequent insulin resistance that decrease FA release from adipocytes and increase TG mobilization[218]. However, the constant TG storage in adipocytes leads to the enlargement of the visceral adipose tissue resulting in a high release of FFA directly to the liver through blood circulation. This increased FA uptake overcomes the hepatic β-oxidation capability causing FA and TG accumulation[135].

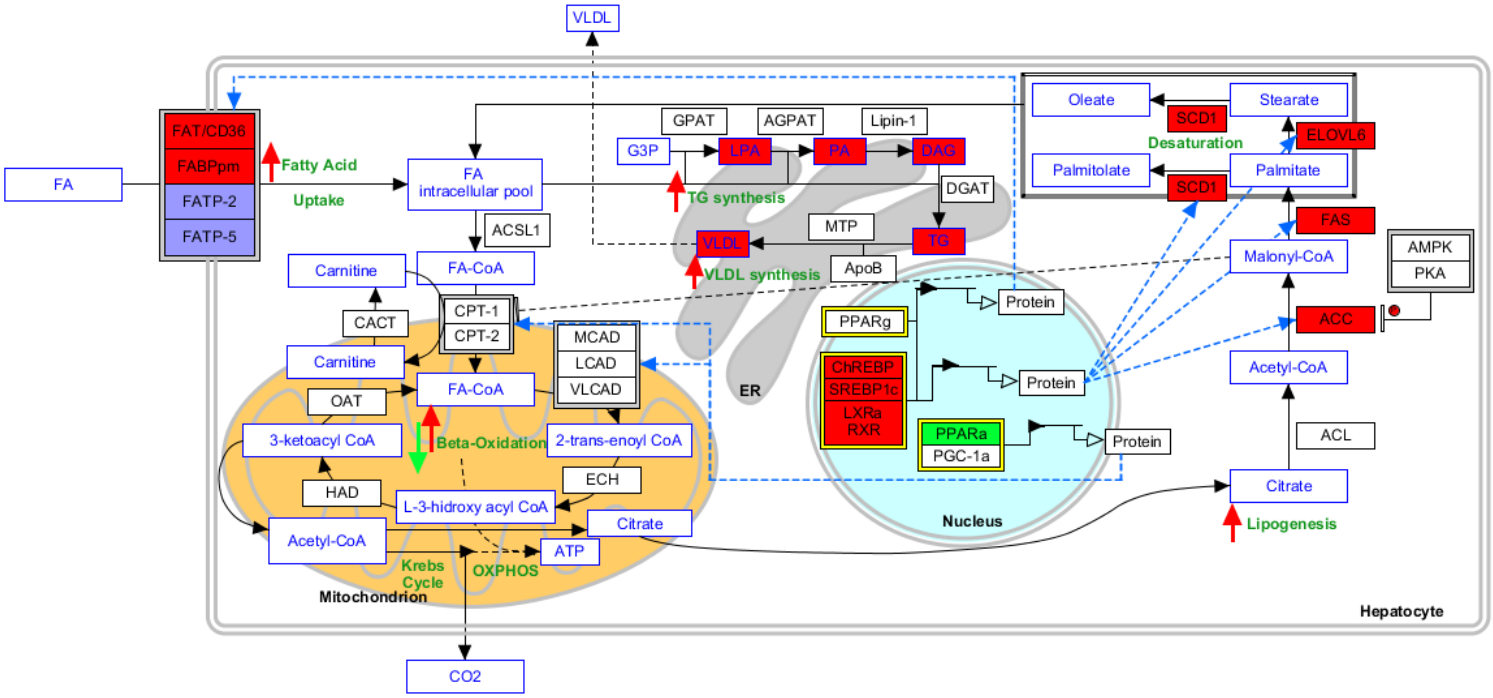

Figure 1.3- Lipid metabolism in liver, its regulation and alterations in NAFLD.
The role of lipid metabolism pathways and their regulation and dynamics in NAFLD. Boxes in red represent an increase in metabolite/protein levels; in blue represent reported unchanged levels; and in green decrease of levels. Black arrows represent enzymatic reactions; and blue dashed arrows protein expression alterations due to transcriptional factors action. FA uptake, de novo lipogenesis, TG and VLDL synthesis, and lipid-related transcriptional activity seem to be increased while β-oxidation rate has contradictory reports.

Indeed, the role of β-oxidation in NAFLD is still not well understood due to several contradictory reports[219] that associate the disease with increased [220–222], unchanged[223] or decreased[224] fatty acid oxidation. This discrepancies between studies may be explained by the utilization of different markers and techniques or by a variation of hepatic response during NAFLD evolution. Indeed, a study demonstrated that the mRNA levels and protein expression of several lipid-related enzymes change with disease severity[225].

In opposition, several studies point to increased rate of *de novo* lipogenesis during NAFLD as a strong cause of lipid hepatic accumulation[226,227]. In a study about obese patients with NAFLD it was reported that 26% of the hepatic TG were obtained from *de novo* lipogenesis and that these patients were unable to adjust their *de novo* lipogenesis during the fasting-fed state transition[57].

Moreover, hepatic lipid accumulation is related to several pathways usually associated with cellular impairment, namely endoplasmic reticulum stress, mitochondria stress, oxidative stress, autophagy and a state of lipotoxicity. Indeed, lipotoxicity is highly related to the inflammatory response in Kupffer and hepatic stellate cells that control NAFLD progression to NASH[131,175]. A strong relationship has been proposed between abnormalities in lipid metabolism and mitochondria dysfunction[96].

1.5 Mitochondria

1.5.1 Structure and function

Mitochondria are cellular organelles with a double membrane that play crucial roles in metabolism. They provide the energy required to cell homeostasis through ATP production via oxidative phosphorylation (OXPHOS) and they regulate free radicals' production, calcium homeostasis, and cell survival and death (**Figure 1.4**)[228]. Alterations in mitochondrial pathophysiology are linked to several metabolic diseases by enhanced generation of ROS, decreased antioxidative capability and reduced OXPHOS with the concomitant decrease in ATP production[229].

Each mitochondrion contains between 800 and 1000 copies of a self-replicating genome, the mitochondrial DNA (mtDNA), which is maternally inherited[230]. This circular genome encodes 13 proteins that are essential for the respiratory complexes' function[231]. mtDNA molecules are packaged in highly ordered structures, the nucleoids, which are located in the mitochondrial matrix often near the cristae[230]. Alterations in the mtDNA copy number were associated with numerous diseases, such as obesity[232], a depletion in mtDNA was also associated with fatty liver diseases[233,234] and in NASH patients was reported a lower expression of mtDNA encoded polypeptides[235].

The outer and inner mitochondrial membranes are separated by a small intermembrane space. While the outer mitochondrial membrane (OMM) is relatively permeable, the inner mitochondrial membrane (IMM) surrounding the mitochondrial matrix has a restricted permeability that allows the generation of a proton-motive force

across it and, consequently, the efficient operation of the OXPHOS system (Figure 1.4)[229].

Cells might respond to metabolic challenges such as nutrient availability by changing mitochondrial morphology and distribution within the cell[232]. It has been previously demonstrated that obesity causes alterations in the mitochondrial structure. In patients with obesity and T2D the skeletal muscle mitochondria were significantly shorter[237]. High glucose availability was also correlated to mitochondrial reticulum fragmentation[238]. Abnormal mitochondria morphology has been associated with NASH development[233,239]. Ideally, longer mitochondria network are more protected from degradation, and have a tighter and more efficient cristae structure that allows a higher oxidative phosphorylation efficiency[240].

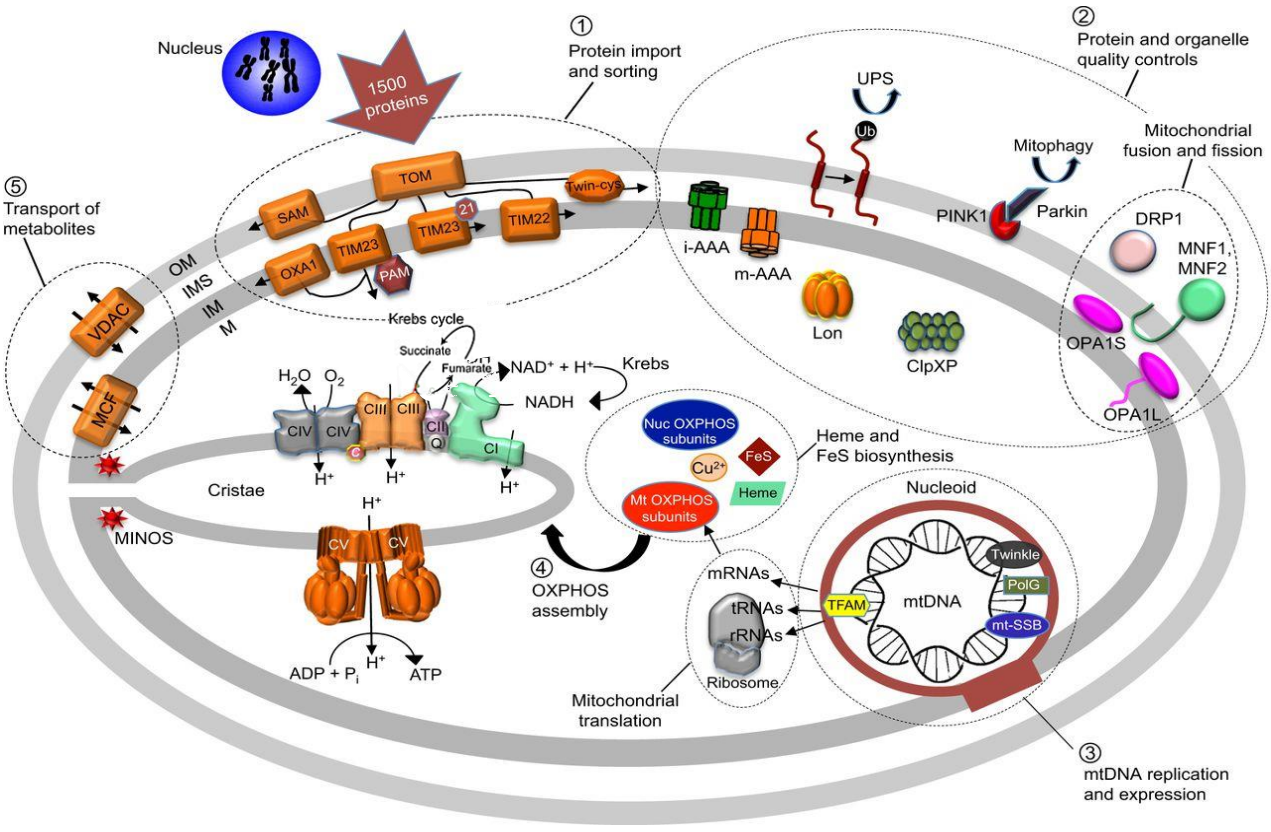

Figure 1.4 – Simplified representation of mitochondria structure and some of its functions. Source: Lasserre et.al, 2015[236].

It is possible to see differences between the protein composition of the outer mitochondrial membrane (OMM) and the inner mitochondrial membrane (IMM), and also the proton movement in OXPHOS. The image depicts several proteins involved in the trans-membrane transport of metabolites and proteins, as well as proteins responsible for mitochondrial dynamics and quality control. mtDNA associated proteins and their role in gene transcription of OXPHOS subunits are summarized.

Mitochondria enclose a class of mitochondrial uncoupling proteins (UCP) that are able to separate oxidative phosphorylation from ATP synthesis. UCPs are transporters in mitochondrial membrane that can deplete the proton gradient. Mutations in UCP3 gene

have being associated with obesity, diabetes and NAFLD[241–243]. It was also described that UCP3 protects mitochondria from lipotoxicity[244] and is an important mediator of thermogenesis. UCP2 is widely express and its main function is the control of mitochondria-derived ROS, and some reports also suggest that it might controls ATP synthesis, regulates FA metabolism and mobilize FFA outside the mitochondrial matrix towards the intermembrane space[245–247].

A significant part of the mitochondrial functions are in some way related to the opening or activation of the mitochondrial permeability transition pore (mPTP), a high-conductance channel that allows a sudden increase in the IMM permeability to ions and small solutes[248]. It has been reported that the mPTP plays a role in the regulation of the mitochondrial membrane potential, calcium homeostasis, ROS generation, ATP production and cell death[248]. The protein constitution of the mPTP in not consensual. However, cyclophilin D (CyPD), adenosine nucleotide translocator (ANT), voltage-dependent anion channel (VDAC), BH3 proteins, p53 and ATP synthase were proposed as part of the mPTP or of its regulators[249–251].

Mitochondria content changes according to different physiological homeostatic conditions. In part, this can be caused by mitochondrial quality alterations, such as mitochondrial dysfunction, in response to several stimuli[252,253]. Due to the large number of pathways involved in mitochondrial dynamics there are not reliable and direct methods to assess the mitochondrial content. Usually, the molecular levels or enzymatic activities of mitochondria restricted macromolecules are used as markers. Some examples are the determination of citrate synthase activity, mtDNA copy number, cytochrome c oxidase activity, cardiolipin content or TOM20 protein levels[254,255].

1.5.2 Mitochondrial Dynamics: biogenesis, fission, fusion and mitophagy

Mitochondria are highly dynamic organelles which can be formed (mitochondrial biogenesis), degraded (mitophagy), fused with other mitochondrion or undergo fission to form several mitochondria from a unique mitochondrion[231,256]. All these processes are well regulated and are a consequence of the mitochondrial state or dysfunction, amongst other numerous stimuli[231].

Mitochondrial biogenesis is the process by which mitochondria number and/or size is increased by the synthesis of new mitochondrial mass requiring both nuclear and mitochondrial genes[229]. PGC-1α is a transcription factor that regulates this process by stimulating the activity of others transcription factors and proteins such as nuclear respiratory factor-1 (NRF-1), NRF-2, mitochondrial transcription factor A (Tfam), Estrogen-related receptors (ERRs), UCP2 and PPARs[257,258]. NRF-1, NRF-2 and Tfam are responsible for the transcription of mitochondrial essential proteins and mtDNA replication (**Figure 1.5**)[259].

PGC-1α is regulated according to the cell metabolic state through phosphorylation by AMPK and deacetylation by NAD-dependent protein deacetylase sirtuin 1 (SIRT1)[258]. Furthermore, cytosolic calcium concentration can modulate PGC-1α activity via p38

mitogen-activated kinase and calcium/calmodulin-dependent kinase (CaMK)[260,261]. A decrease in PGC-1α gene expression has been associated with a high-fat diet, thus decreasing mitochondrial biogenesis[262]. Also, a reduced Tfam expression is associated with a decrease in mtDNA copy number[234].

NRF1 transcriptional activity has been related to the expression of several nuclear genes, such as subunits of the mitochondrial oxidative phosphorylation complexes, proteins involved in the mitochondrial import machinery, mitochondrial ribosomal proteins and tRNA synthases[264]. Together with NRF2, it regulates Tfam and transcription factor B proteins (TFBs) transcription which, on their turn, are the main regulators of mtDNA transcription and replication[264]. ERR-α regulates the transcription of many nuclear genes involved in oxidative phosphorylation, FA oxidation, Krebs cycle and mitochondrial fusion and fission[265].

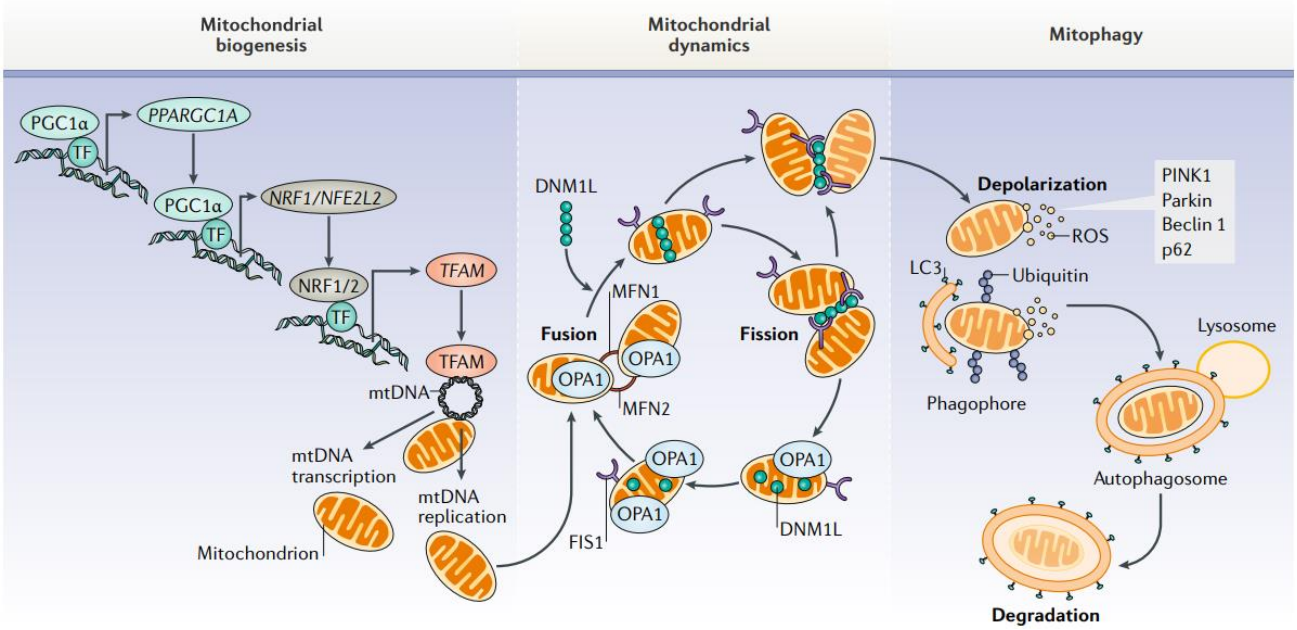

Figure 1.5- Schematic representation of the mechanisms involved in mitochondrial dynamics. *Source: Picca et.al 2018[263].*
The image shows transcriptional mechanisms behind mitochondrial biogenesis, the proteins related to fusion and fission events and the process of mitophagy in a depolarized mitochondrion.

Mitochondrial dynamics represent a delicate balance of mitochondrial fission and fusion events that maintain the ideal physiologic conditions for regulating cell death and growth pathways and remove damaged mitochondria (**Figure 1.5**)[266,267]. Several proteins have been identified as key regulators of those processes. Mitochondrial fusion is regulated by three GTPases mitofusin 1 (Mfn1), Mfn2 and optic atrophy 1 (Opa1)[268,269]. Mfn1 and Mfn2 are located in the OMM while Opa1 is in the IMM. They are responsible for the fusion events taking place on their respective membranes[229]. Two other GTPases, mitochondrial fission 1 protein (Fis1) and Dynamin-1-like protein (DNM1L), are responsible for mitochondrial fission. They are located in the OMM and the cytosol, respectively[270]. Disturbed mitochondrial dynamics are associated with mitochondrial

dysfunction in response to nutrient excess. There are reports showing an up-regulation of the mitochondrial fission machinery in obesity and T2D[238].

Autophagy is a process that includes all the pathways involved in the degradation of cytosol components and organelles through their delivery to lysosomes. There are three distinct types of autophagy: microautophagy; chaperone-mediated autophagy; and macroautophagy[271]. In microautophagy, portions of the cytoplasm are engulfed by invaginations of the lysosomal membrane. In chaperone-mediated autophagy, substrate proteins are unfolded by chaperone activity, translocated across the lysosomal membrane through a LAMP-2A mediated process and degraded[272]. Macroautophagy is a process involving the formation of a double membrane (phagophore) which surrounds a portion of cytoplasm or an organelle, such as a mitochondrion. The elongation of the phagophore leads to the formation of a double-membraned vesicle, the autophagosome, which fuses with a lysosome promoting the degradation of its content[271].

Mitophagy is an autophagic process specific for the removal of damaged mitochondria (**Figure 1.5**)[273]. Mitophagy is essential for the maintenance of the mitochondrial content and integrity. It has been described that it initially proceeds through a step of mitochondrial fission to allow a better separation of healthy and dysfunctional mitochondria[231]. Mitophagy can be triggered by mitochondrial membrane potential loss[96]. Phosphatase and tensin homolog-induced putative kinase 1 (PINK1) starts this process by communicating mitochondrial membrane potential loss to Parkin through its kinase activity[274,275]. Activated Parkin promotes the ubiquitination of several mitochondrial membrane proteins, such as VDAC1, Mfn-1 and Mfn-2, triggering mitochondrial degradation by autophagosomes and lysosomes (Figure 1.6)[274,276]. Furthermore, Mfn-1 and Mfn-2 ubiquitination prevents fusion of damaged mitochondria[276].

Autophagy can be divided in five sequential steps, whether a bulk of cytoplasm or a mitochondrion are being degraded[277]: phagophore initiation; phagophore elongation; autophagosome formation; autophagosome fusion with lysosome; and lysosomal degradation[278].

The elongation step is mediated by two different ubiquitin-like conjugation systems. In the first, autophagy-related protein 12 (ATG12) can be conjugated with ATG5 through ATG7 ligase activity, forming the ATG5-ATG12-ATG16L1 complex. Alternatively, if ATG12 is conjugated with ATG3 instead of ATG5, a specific mitophagic degradation of depolarized mitochondria is promoted. The mechanisms involved in this mitophagy process remain poorly understood[280]. The second ubiquitin-like conjugation system involves microtubule-associated protein 1A/1B-light chain 3 (LC3). LC3 has a mature cleaved form, LC3-I, that can suffer ubiquitin-like reactions with phosphatidylethanolamine forming LC3-II, which is required for the phagophore elongation and the autophagosomes completion[278].

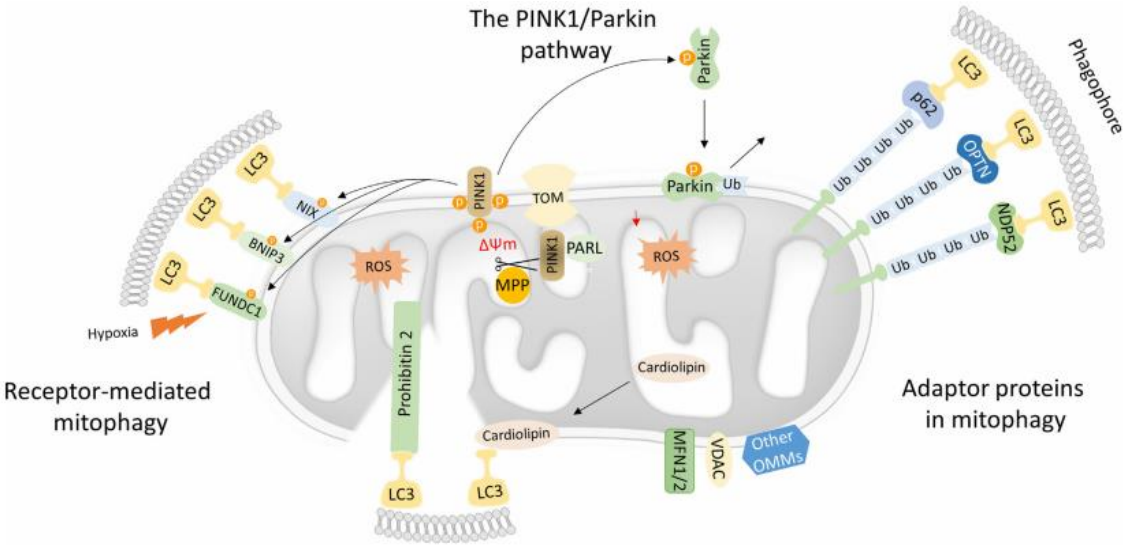

Figure 1.6- Schematic representation of the mitophagy mechanisms. *Source: Gkikas et.al, 2018*[279]*.*

The ubiquitin-binding adaptor protein p62/SQSTRM1 accumulates in depolarized mitochondrial membranes and might be responsible for LC3 recruitment to damaged mitochondria[281]. PINK1 and Parkin can also interact with the Beclin-1/PI3K complex, thus activating the nucleation of pre-autophagosomal membranes around damaged mitochondria[271]. Parkin can also stimulate mitochondrial biogenesis through PGC-1α release, probably as a mechanism to replace the degraded mitochondria[282]. Mitophagy can also be mediated by receptors from the OMM, such as BNIP3, NIX and FUNDC1, and by IMM receptors, such as PHB2 and cardiolipin, which become exposed to cytosol in response to mitochondrial damage and recruit LC3 (**Figure 1.6**)[279]. Mitophagy may occur in response to nutrient excess and cellular dysfunction. Therefore a possible dysfunction of hepatocytes mitophagy might be associated with obesity development[256,283]. A defective autophagosome-lysosome fusion has been observed in high fat diet-induced obese mice due to alterations in membrane lipid composition[284]. Indeed, obese patients with NASH showed an increase in the LC3-II/LC3-I ratio and higher levels of p62 that impair the hepatic autophagic flux[285].

Accumulated evidence suggest a possible role of autophagy in cellular metabolism implication in metabolic disorders[286]. Although autophagy is frequently connoted with the digestion of cellular proteins, it can also degrade lipid stores, such as lipid droplets. This process is called lipophagy and allows the removal of lipid excess and the maintenance of adequate lipid levels in liver cells[286]. ATG7 haploinsufficient mice present reduced lipophagy and increased obesity and diabetes development[287]. Cathepsins are a class of proteases that have a crucial role in lysosomes due to their endo- or exopeptidase activities[288]. Cathepsins B, D and L have been proposed as fibrosis markers in liver[288,289] and NAFLD patients also present a significant decrease in cathepsins B and D expression[290]. In an obese mice model were reported defects in lysosomal acidification and a reduction in cathepsins[291].

Alterations in mitochondrial dynamics are associated with cells requirements of energy, i.e. oxidative phosphorylation, and can lead to mitochondrial dysfunction. Thus, an imbalance of either of these processes can have an impact on the remaining ones and, ultimately, compromise the whole organism function. Indeed, impairment of mitochondrial dynamics directly affect mitochondrial metabolism capability which together with the excessive nutrient supply might lead to pronounced mitochondrial metabolism impairment.

1.5.3 Mitochondria and Metabolism

Mitochondria produce energy under the form of ATP via oxidative metabolism in two crucial steps: reduction of NAD^+, FAD or succinate during glycolysis, Krebs cycle or FA β-oxidation; and oxidative phosphorylation[229]. Over than 90% of body's cellular energy is produced through the coupling of the electron transport chain (ETC) with Krebs cycle[292].

Krebs cycle is a cyclic metabolic pathway that consists in the oxidation of acetyl-CoA resulting from carbohydrate, lipid and aminoacids metabolism[293]. In the first step acetyl-CoA and oxaloacetate are converted by citrate synthase into citrate, a six-carbon molecule also involved in *de novo* lipogenesis[294]. If citrate follows the Krebs cycle it is converted into *cis*-aconitate and further into isocitrate, being both reactions catalyzed by aconitase[294].

Aconitase is an enzyme with an iron-sulfur cluster that is crucial in the Krebs cycle, is sensible to the cellular redox state and regulates intracellular iron metabolism[295]. The mitochondrial aconitase isoform (ACO2) undergoes a reversible inactivation by reacting with superoxide anion ($^{\bullet}O^{2-}$) and forming H_2O_2, thus regulating mitochondrial metabolism. This reaction leads to a release of a Fe^{2+} which can then participate in the Fenton reaction with H_2O_2 and form $^{\bullet}OH$, a molecule with high oxidative potential to cellular biomolecules[296].

Moreover, the inactive form of aconitase can be degraded by Lon protease, a mitochondrial protease. This process permanently regulates the Krebs cycle rate, decreasing OXPHOS activity[295]. Aconitase in its inactive form is also associated with nucleoids and has an important role in the stabilization and protection of mtDNA[297]. However, high levels of ROS production lead to an increase in aconitase inactivation inducing aconitase aggregates which cannot be degraded by Lon and lead to mitochondrial dysfunction[295].

Aconitase activity might also be partially inhibited by 4-Hydroxynonemal (4-HNE), a product from lipid peroxidation commonly associated with oxidative stress mechanisms[298]. 4-HNE inhibition of aconitase stimulates ACC activity due to citrate accumulation. In obese subjects this process induces fat accumulation and acts like a paradoxical mechanism that maintains the pathological condition[299].

In the Krebs cycle, isocitrate is subjected to two steps of decarboxylation catalyzed by the isocitrate dehydrogenase and α-ketoglutarate dehydrogenization complex. The reaction product formed is succinyl-CoA which is then converted to succinate. Succinate is the substrate of succinate dehydrogenase, an enzyme also involved in OXPHOS. During succinate oxidation to fumarate, the succinate dehydrogenase cofactor FAD is reduced and stimulates ETC activity[293]. Fumarate is then hydrated to malate in a reversible reaction catalyzed by fumarase, a relatively conserved enzyme in the Krebs cycle[300]. Malate dehydrogenase consumes malate and regenerates the oxaloacetate necessary to start another cycle[294].

OXPHOS system is formed by five multi-subunit enzyme complexes which are located in the IMM[301]. The electrons donated to NAD^+ and FAD during the Krebs cycle are used by complex I (NADH ubiquinone reductase) and complex II (succinate dehydrogenase), respectively. The electrons are then transferred to complex III (ubiquinol-cytochrome c reductase) via a ubiquinone-ubiquinol dependent mechanism. Finally, the electrons are passed to complex IV (cytochrome c oxidase) by cytochrome c. This process is coupled to proton transport across the IMM from the matrix to the intermembrane space in all complexes except succinate dehydrogenate (Figure 1.7)[302]. In complex IV the electrons are accepted by oxygen in a reaction that ends with the production of water molecules[303]. The proton-motive force produced by the ETC is used by complex V (F_oF_1 ATP synthase) to produce ATP[229]. All ETC complexes are composed by several subunits encoded by nuclear and mitochondrial DNA except for complex II, which is composed exclusively by nuclear subunits[304].

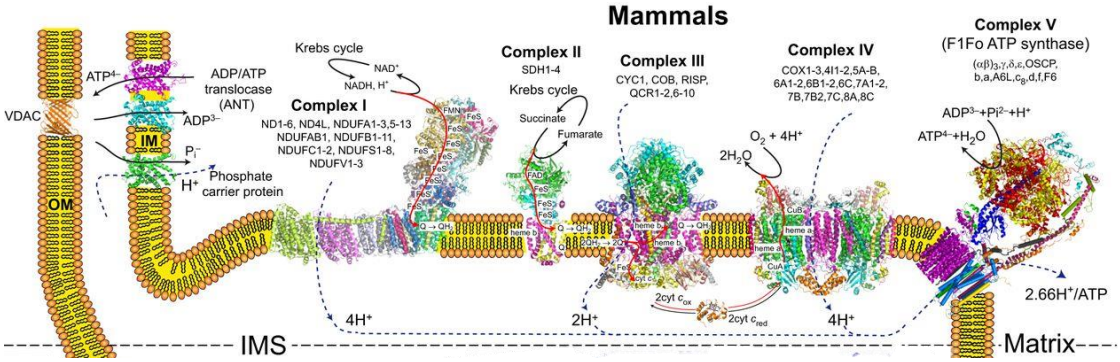

Figure 1.7- Representation of the enzymatic complexes of the OXPHOS system. Adapted from Lasserre et.al, 2015[236].

Reactions taking place in each enzymatic complex as well their protein subunits composition are schematized. The role of proton translocator in complexes' activity is also depicted.

Several studies have reported that different complexes can be assembled into supercomplexes which organization vary among tissues and depends on the metabolic and physiological conditions[305]. These superstructures can be stabilized by cardiolipin and might represent a way to improve the efficiency of electron flux in the ETC, stabilize complex I and decrease accidental ROS formation[303].

High-fat diet induces a decrease in the expression of oxidative phosphorylation-related genes[262]. Indeed, both the content[234] and the respiratory chain complexes activity[306] is reduced in NAFLD patients. PGC-1α is able to improve mitochondrial respiration in cells harboring a complex III or IV deficiency[307].

It is well described that electron flow through the ETC can lead to the production of ROS. This happens either accidently or on purpose and is due to the interaction between high-potential reduced OXPHOS complexes intermediates and oxygen molecules. ROS are molecules with a crucial role in the cell homeostasis regulation. However, they are also commonly associated with cellular oxidative damage.

1.5.4 Oxidative Stress

Oxidative stress is a condition that results from the unbalance between reactive species production and the cells' antioxidant defense capability to deal with them[228]. This imbalance is crucial to the development of pathophysiological cellular states, since high ROS levels can lead to oxidative damage and cell death. However, at low levels ROS are vital to the regulation of several cellular signaling pathways[228].

Systemic oxidative stress is highly related to obesity due to an abnormal production of adipokines, a feature of the metabolic syndrome. Metabolic syndrome is characterized by the presence of high sugar and lipids levels in blood circulation combined with insulin resistance and a large waist circunference[240].

In obesity, there are five main sources of ROS: peroxisomal FA metabolism, that leads to hydrogen peroxide formation; cytochrome P450 microsomal reactions, forming superoxide anion; phagocytic cells, that produce ROS as part of an inflammatory response leading to damage of several tissues; NADPH oxidase activity, which is increased in adipocytes due to an increase in angiotensin II secretion; and ETC, the main source of ROS, where superoxide anion is generated due to a reaction between oxygen and electrons escaped from the ETC (Figure 1.8)[2,240]. ROS formation and the ensuing cell damage promote the formation of even more ROS in a self-perpetuating vicious cycle.

Pregnancy-induced metabolic and endocrine adaptations convey on the regulation of several physiological processes responsible for the production of reactive oxygen species. The former include placental formation, cholesterol synthesis in placenta mitochondria and the up-regulation of energetic metabolism[309]. As occurs in the generality of conditions, ROS play a dual role during gestation. During oxidative stress they can lead to cell injury and induce several diseases, such as pre-eclampsia. When their levels are near physiological concentrations, they are essential to many crucial events, such as embryo implantation and cell replication, maturation and differentiation. Animal studies showed that twins pregnancy are more likely to generate oxidative stress conditions than singleton pregnancies[309].

Mitochondria continuous function is, indeed, the main source of ROS production due to imperfections in the electron flow through the ETC, This happens mainly in

complex I and III where 0.4 to 4% of the oxygen consumed by mitochondria is reduced to superoxide anion ($^{\bullet}O_2^-$)[229]. Since cellular ROS production is an inevitable process, cells possess numerous defense systems, both enzymatic and non-enzymatic, to deal with it (Figure 1.8)[310].

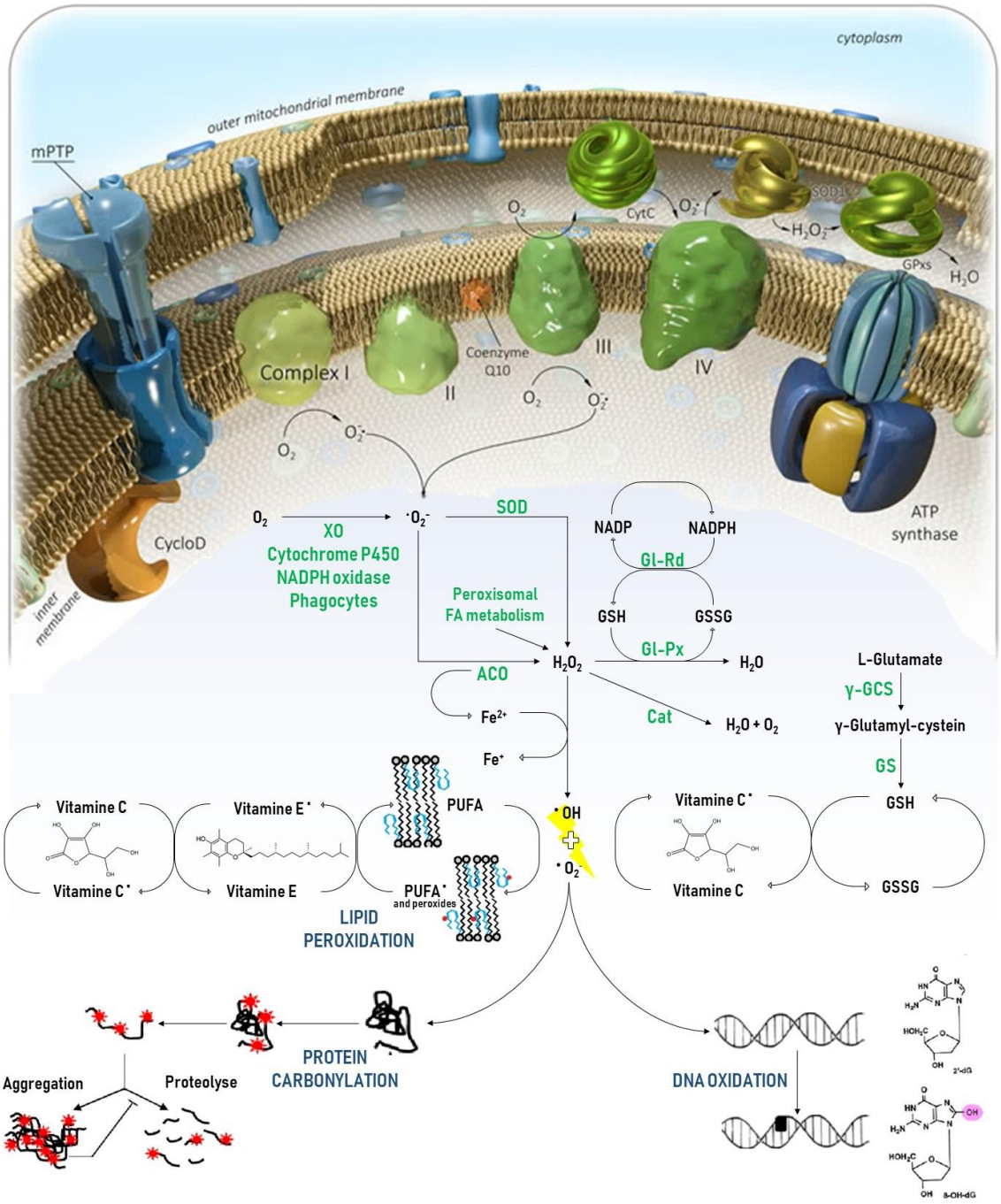

Figure 1.8- ***Mechanisms of ROS production, antioxidant defenses and oxidative damage. Adapted from Kudryavtseva et.al, 2016***[308]***.***
The mechanisms of ROS formation and the enzymatic antioxidant defenses responsible for their degradation are depicted. If the ROS degrading systems are overwhelmed by ROS production, oxidative damage in lipids (lipid peroxidation), proteins (protein carbonylation) and DNA (DNA oxidation) occurs. Lipid peroxidation can be recovered by non-enzymatic antioxidant defenses such as Vitamin E and C.

$^{\bullet}O_2^-$ cannot cross the mitochondrial membrane. However, if it is formed in the intermembrane space, it might be scavenged by oxidized cytochrome c or diffuse to the cytosol through VDAC[311]. Superoxide dismutase (SOD) is the antioxidant enzyme responsible for $^{\bullet}O_2^-$ disposal through its conversion to H_2O_2[312]. As previously discussed, aconitase can catalyze the same reaction. Two different SOD isoforms are expressed in liver: SOD1 (CuZn-SOD) present in the cells' cytoplasm; and SOD2 (Mn-SOD) localized in mitochondria. Both catalyze the same reaction[313].

However, in the presence of iron ions it can undergo the Fenton reaction forming $^{\bullet}OH$. In addition, H_2O_2 can freely cross membranes, being an important regulator of numerous cells signaling pathways[314]. Glutathione peroxidase and catalase are the principal enzymes responsible for H_2O_2 levels regulation. Catalase is mainly expressed in peroxisomes and is responsible for peroxisomal H_2O_2 degradation[315]. Catalase activity can be regulated indirectly by the ROS levels in cells. Its activity is promoted upon serine 231 and 386 phosphorylation. Catalase is ubiquitinated and degraded when cells can no longer deal with oxidative stress[316].

Glutathione (GSH) is an important mitochondrial molecule which can be oxidized to GSSG by glutathione peroxidase (Gl-Px). Gl-Px reaction is coupled to the reduction of H_2O_2 or lipid hydroperoxides[317]. Gl-Px1 is the main expressed isoform and is located in the cytoplasm. Gl-Px4 (phospholipid hydroperoxide glutathione peroxidase) is predominantly linked to the mitochondrial membrane[228]. Glutathione reductase (Gl-Rd) is the enzyme responsible for reestablishing GSH levels. It catalyzes GSSG reduction in a reaction coupled with NADPH oxidation[317]. The other non-enzymatic antioxidant defenses include Vitamin E, Vitamin C, and several carotenoids and flavonoids[229].

When the cells' capability to deal with ROS is exceeded by their production, ROS can interact with several biomolecules, such as lipids (i.e. lipid peroxidation), proteins (i.e. protein carbonylation) and DNA (i.e. DNA oxidation), inducing cell damage (Figure 1.8)[310]. Several reports mention DNA purine and pyrimidine nitrogenous bases' damage due to interactions with $^{\bullet}OH$[229]. Overproduction of ROS is associated with mitochondrial lipids, proteins and mtDNA damage, leading to abrogation of ATP production and other mitochondrial dysfunctions[318,319]. mtDNA damage is increased in NASH, causing a decreased expression of mtDNA-encoded proteins that further leads to an impaired oxidative respiration ending up in a vicious cycle[320,321].

In the obesity scenario, antioxidant capacity is also compromised, contributing to the perpetuation of the oxidative imbalance. In obese subjects the serum levels of vitamin E, vitamin C and glutathione are decreased[322]. In addition, antioxidant enzymes such as SOD and catalase also present a decreased activity in the human plasma from obese subjects[323]. Moreover, it is described that in obesity the increase in TG levels inhibits ANT activity which further promotes ROS production[324]. Numerous evidences point steatosis as an important cause of oxidative stress in the hepatic tissue. However, the role of GSH in NAFLD is not well understood since contradictory results have been reported[325,326].

All these molecular, cellular and physiological mechanisms can contribute to the development of the numerous disorders that frequently accompany obesity. Those include diabetes mellitus, systemic arterial hypertension, ischemic heart diseases, stroke, and other CVD, sleep apnea, asthma, gout, hyperlipidemia, peripheral vascular disease, physiological problems, rheumatological and orthopedic problems, as well as cancer or liver and kidney failure[2,4].

1.6 Model

Numerous animal models were developed to study the effect of compromised pregnancies as rodents, non-human primates and domestic ruminants. No animal is able to truly recapitulates human pregnancy however. Sheep model is considered a good model for experiment gestational negative outcomes since is not so expensive as non-human primates and can better replicate human pregnancy than rodents[327].

When compared with rodents, sheep model presents a most similar fetal size to human, higher pregnancy time, is a monotocous specie, is tolerant to invasive procedures and a placenta interface similar to humans[327,328]. Therefore, is a good model to study not only effect of pregnancy over the fetus as to understand the opposite effect[328].

Due to these characteristics, sheep model has been used in scientific research during the last decades what results in a large knowledge about sheep gestation. The specific model for maternal obesity used in this work was previously validated by the increase in total sheep weight gain, percentage of body fat[329]

1.7 Aim of the work

The successful establishment, maintenance and outcome of pregnancy is the goal of the reproductive system. The effects of a successful pregnancy are not restricted to the gestational and delivery time period, they can have long-term health consequences both to the mother and the offspring. In fact, pregnancy is a time period which requires a huge metabolic effort from the mother to totally compensate the increase in energy requirements.

Metabolic disorders are highly associated with unsuccessful outcomes in pregnancies. Obesity can represent a burden too high during this period mainly because of the metabolic dysregulations typical of excessive overweight. Even after a successful gestation, maternal obesity can lead to several consequences in the mothers' health by inducing disease or pre-disease status. A better understanding of the consequences of maternal obesity during pregnancy is crucial to the development of suitable medical approaches and therapeutics to use in such cases.

Liver has a vital role in body metabolism. Thus, we propose that together, obesity and pregnancy, might cause maternal hepatic dysfunction which can constitute a primordial stage in metabolism imbalance leading to the development of other diseases. To address this hypothesis, we set two different goals: 1) characterize liver metabolism alterations caused by maternal obesity during pregnancy, with a special focus in mitochondrial changes; and 2) assess the possible dichotomy between liver lobes and therefore, better understand the hepatic metabolism in a lobe-dependent manner.

Chapter 2 - Materials and Methods

2.1 Reagents

All the reagent used were of the highest grade of purity available and all the aqueous solutions were prepared in ultrapure water (type I, Milli-Q Biocel A10 with pre-treatment via Elix 5, Millipore). For nonaqueous solutions, ethanol (99.5%, Sigma-Aldrich, Barcelona, Spain) or dimethyl sulfoxide (DMSO, Sigma-Aldrich) were used as solvents.

Table 2.1 lists all the reagents used in the present work, their suppliers and commercial references.

Table 2.1- *List of the reagents used in the present work, their respective suppliers and commercial references.*

Reagent	CAS number	Supplier	Reference
7-Amino-4-methylcoumarin	26093-31-2	Sigma-Aldrich	A9891
Acetic acid	64-19-7	Panreac	131008.1611
Acetyl-CoA	102029-73-2	Sigma-Aldrich	A2056
Antimycin A	1397-94-0	Sigma-Aldrich	A8674
BioRad – DC protein assay	-	Bio-Rad	5000116
Bioxytech MD kit	-	OxisResearch	21044
Brij-35 (Polyoxyethyleneglycol dodecyl ether)	9002-92-0	Sigma-Aldrich	858366
Bromophenol blue	34725-61-6	Sigma-Aldrich	B5525
BSA (Bovine Serum Albumin)	9048-46-8	Sigma-Aldrich	A7030
Catalase from bovine liver	9001-05-2	Sigma-Aldrich	C1345
Clarity Western ECL substrate	-	Bio-Rad	1705060
Cytochrome C from bovine heart	9007-43-6	Sigma-Aldrich	30398
DCPIP (2,6-Dichloroindophenol sodium salt)	620-45-1	VWR	230212X
Decylubiquinone	55486-00-5	Sigma-Aldrich	D7911
Dimethyl malonate	108-59-8	Sigma-Aldrich	136441
DMSO (Dimethyl sulfoxide)	67-68-5	Sigma-Aldrich	34869
DNase/RNase-free water	-	Qiagen	1017979
DTAB (Dodecyltrimethylammonium bromide)	1119-94-4	Thermo Fisher	128271000
DTNB (5,5′-Dithiobis(2-nitrobenzoic acid)	69-78-3	Sigma-Aldrich	D8130
DTT (DL-1,4-Dithiothreitol)	3483-12-3	Sigma-Aldrich	D9779
EDTA (Ethylenediaminetetraacetic acid disodium salt)	6381-92-6	VWR	20296.291
EGTA (Ethylene-bis(oxyethylenenitrilo)tetraacetic acid)	67-42-5	Sigma-Aldrich	E4378

Glycerol	56-81-5	Sigma-Aldrich	G6279
Glycine	56-40-6	NZY tech	MB01401
GSSG (L-Glutathione oxidized)	27025-41-8	Sigma-Aldrich	G4376
HCl (Hydrochloric acid)	7647-01-0	Panreac	131020,1212
Hemoglobin from bovine blood	9008-02-0	Sigma-Aldrich	H2625
Hydrogen Peroxide	7722-84-1	Merck	107210
Isopropanol	67-63-0	Sigma-Aldrich	190764
K_2HPO_4 (Monobasic potassium phosphate)	7778-77-0	Sigma-Aldrich	NIST200B
KCl (Potassium chloride)	7447-40-7	Sigma-Aldrich	P9541
KCN (Potassium cyanide)	151-50-8	Fisher Scientific	P/4600/50
KH_2PO_4 (Potassium phosphate monobasic)	7778-77-0	Sigma-Aldrich	P0662
KOH (Potassium hydroxide)	1310-58-3	Sigma-Aldrich	P5958
Methanol	67-56-1	Sigma-Aldrich	M/4000/17
$MgCl_2$ (Magnesium chloride)	7786-30-3	Thermo Fisher	223211000
MOPS (4-Morpholinepropanesulfonic acid sodium salt)	71119-22-7	Alfa Aesar	A17214
Na_2HPO_4 (Sodium phosphate dibasic)	7558-79-4	Sigma-Aldrich	S5136
NaCl (Sodium chloride)	7647-14-5	Fisher Scientific	S/3160/60
NAD/NADH-Glo™ Assay	-	Promega Corporation	G9071
NADH (β-Nicotinamide adenine dinucleotide reduced)	606-68-8	Sigma-Aldrich	8129
NADPH (β-Nicotinamide adenine dinucleotide 2′-phosphate reduced tetrasodium salt)	2646-71-1	Panreac	A1395,0100
NAF (Sodium fluoride)	7681-49-4	VWR	27859.293
NaOH (Sodium hydroxide)	1310-73-2	Sigma-Aldrich	S8045
Nicotinamide	98-92-0	Sigma-Aldrich	N0636
NP40	127087-87-0	Sigma-Aldrich	NP40S
Oxaloacetate	328-42-7	Acros Organics	416600050
PhosSTOP (phosphatase inhibitor)	-	Sigma-Aldrich	4906845001
PKA kinase activity kit	-	Enzo Life Sciences	ADI-EKS-390A
PMSF (Phenylmethylsulfonyl fluoride)	329-98-6	Sigma-Aldrich	P7626
Ponceau S	6226-79-5	Sigma-Aldrich	P3504
Potassium carbonate	584-08-7	VWR	26724.291
Precision Plus ProteinTM Standard Dual Color	-	Bio-Rad	161-0374
Protease inhibitor cocktail	-	Sigma-Aldrich	P8340
QIAmp DNA mini-kit	-	Qiagen	51304
Rotenone	83-79-4	Sigma-Aldrich	R8875

SDS (Sodium dodecyl sulfate)	151-21-3	NZY tech	MB01501
SOD activity kit	-	Enzo Life Sciences	ADI-900-157
Sodium acetate	127-09-3	Sigma-Aldrich	S8750
Sodium azide	26628-22-8	Sigma-Aldrich	S2002
Sodium bicarbonate	144-55-8	Sigma-Aldrich	S6297
Sodium butyrate	156-54-7	Sigma-Aldrich	B5887
Sodium dithionite	7775-14-6	Fisher Scientific	S/3800/53
Sodium orthovanadate	13721-39-6	Sigma-Aldrich	S6508
Sodium succinate	6106-21-4	Fisher Scientific	S/6480/53
SsoFast Eva Green Supermix	-	Bio-Rad	172-5201
TCA (Trichloroacetic acid)	76-03-9	Sigma-Aldrich	T0699
TEMED (1,2-Bis(dimethylamino)ethane)	110-18-9	NZY tech	MB03501
Tert-butylperoxide	110-05-4	Sigma-Aldrich	168521
Tris HCl	1185-53-1	Sigma-Aldrich	T3253
Triton X-100	9002-93-1	Acros Organics	327371000
Trizma base	77-86-1	Sigma-Aldrich	T1503
Tween-20	9005-64-5	Sigma-Aldrich	P9416
Z-Arg-Arg-7-amido-4-methylcoumarin hydrochloride	136132-67-7	Sigma-Aldrich	C5429
β-glycerophosphate	58409-70-4	Sigma-Aldrich	G6626
B-mercaptoethanol	60-24-2	Sigma-Aldrich	M3148

2.2 Animal treatment

Eighteen nulliparous Western white-faced ewes (Rambouillet/Columbia breeding) were randomly divided into two dietary groups and fed with different amounts of a highly palatable diet. The first group (control - C) was composed by 10 individuals which consumed the National Research Council (NRC) recommendations of nutrition[330]. This diet allows the maintenance of a constant body weight and supports the increase of 10-15% in body weight during early gestation. The other group was composed by 8 individuals which were fed with a global nutrient excess of 50% over of NRC recommendations (150%) in order to promote obesity (maternal obesity – MO) (**Figure 2.1**).

Ewes' adaption from their previous diet of mixed legume-grass hay to the experimental diet (**Table 2.2**, **Table 2.3**) was performed during one week. During this time period all experimental animals were fed with the necessary quantity of experimental diet to fulfill 100% of the NRC nutritional recommendations. After the adaptation period, animals were divided and fed according to the experimental groups previously described. This experimental intervention was maintained during 60 days before the conception and continued throughout all the gestation period. Ewes were fed once daily at approximately

4 PM (GMT-7). They were grouped into six adjacent pens in an open fronted pole barn. Each group (C and MO) was divided into two pens per dietary treatment to allow replication. Food amounts were individually calculated based on body weight (BW) according to NRC guidelines and were adjusted weekly to account for BW increases. An intact ram (white-faced, Rambouillet/Columbia breeding) bearing a marking harness was continuously maintained in each of the six pens for approximately six weeks, and the first day each ewe was marked was considered day 0 of gestation (**Figure 2.2**).

***Table 2.2**-Composition of the diet fed to ewes throughout the study.*

Ingredients	%
Ground bromegrass hay [1]	14.02
Ground corn	63.89
Soybean meal	13.30
Liquid molasses	5.60
Limestone	2.24
Ammonium chloride	0.50
Mineralized salt [2]	0.24
Magnesium chloride	0.10
ADE premix [3]	0.10
Rumensin 80	0.02

[1] Mean particle length = 2.54 cm.

[2] Contained 13% NaCl, 10% Ca, 10% P, 2% K, 1.5% Mg, 0.28% Fe, 0.27% Zn, 0.12% Mn, 0.01% I, 35 p.p.m. Se, and 20 p.p.m. Co.

[3] Contained 110 000 IU kg^{-1} vitamin A, 27 500 IU kg^{-1} vitamin D, 660 IU kg^{-1} vitamin E.

***Table 2.3**- Nutrient analysis of the experimental diet.*

Analyzed Composition	
Dry matter (%)	88.54
Neutral detergent fibre (% DM)	24.09
Acid detergent fibre (% DM)	9.99
Crude protein (% DM)	17.39
In vitro dry matter digestibility (% DM)	93.92

2.3 Tissue collection

At 90% gestation time, ewes were sedated with Ketamine (22.2 mg/kg body weight) and maintained under isoflurane inhalation anesthesia (4% induction, 1-2% maintenance). Under this general anesthesia, ewes were exsanguinated, and the gravid uterus quickly removed. Maternal live BW and total fetal weight were recorded. Both maternal and fetal liver were dissected out and tissue mass recorded. Both fetal and maternal livers were divided into right and left lobes, snap frozen in liquid nitrogen and, stored at -80ºC for future use. All the samples are handled independently throughout all experiments.

All the animal dietary protocol and sample collection were handled by our collaborators at the Department of Animal Science, University of Wyoming, Laramie,

Wyoming, USA. Frozen hepatic tissue from maternal right and left lobes were properly sent to MitoXT laboratory facilities (CNC, Center for Neuroscience and Cell Biology, UC Biotech Building, Cantanhede, Portugal).

Figure 2.1*-Image representative of the individuals used in the present study. Control Rambouillet/Columbia ewe fed with 100% National Research Council nutritional recommendations (NRC, left) and maternal obese Rambouillet/Columbia ewe fed 150% NRC (right).*

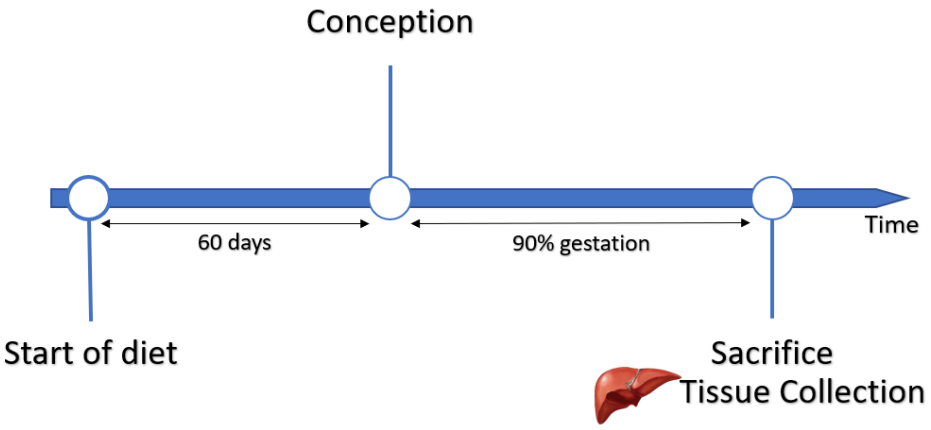

Figure 2.2*- Timeline of the experimental design applied in the present study.*

2.4 DNA extraction

Total DNA for mtDNA copy number quantification was extracted from frozen liver tissue using the QIAamp DNA mini-kit (Qiagen, Düsseldorf, Germany), according to the manufacturer's instructions. Briefly, 20 mg of frozen liver tissue was weighed and incubated with digestion buffer and proteinase K at 56°C overnight. The obtained lysate was centrifuged, and the resulting supernatant was treated with RNase A. After incubation, the lysate was mixed with binding buffer and ethanol and centrifuged through a silica-based spin column. Then, bound DNA was eluted by centrifuging elution buffer

through the column. The extracted DNA samples were quantified spectrophotometrically at A260 nm using a NanoDrop 2000 spectrophotometer (Thermo Scientific, Waltham, MA, USA), diluted to 20 ng/µL in extraction buffer, and stored at −20°C until use.

2.5 mtDNA copy number

RT-PCR was performed using the SsoFast Eva Green Supermix, in a CFX96 real time-PCR system (Bio-Rad, Hercules, CA, USA), with the primers defined in **Table 2.4** at 500 nM. Amplification of 25 ng DNA was performed with an initial cycle of 2 min at 98ºC, followed by 40 cycles of 5 seconds at 98ºC plus 5 seconds at 63ºC (**Figure 2.3**). At the end of each cycle, Eva Green fluorescence was recorded to enable determination of Cq. For quality control, after amplification, melting temperature of the PCR products was determined by performing melting curves. For each set of primers, amplification efficiency was assessed, and no template controls were run. mtDNA copy number was determined in each sample by the ratio between the amount of the mitochondrial gene cytochrome b (CytB) and the amount of the nuclear gene tyrosine 3-monooxygenase/tryptophan 5-monooxygenase activation protein, zeta (YWHAZ), using the CFX96 Manager software (v. 3.0; Bio-Rad).

Table 2.4 *Sequences of the primers used for the quantification of mtDNA copy number.*

Gene	Accession number	Forward primer	Reverse primer
CytB	NC_001941.1 (14159-15298)	CAGGATCCAACAACCCCACA	GTCTCCGAGTAAGTCAGGCG
YWHAZ	NM_001267887.1	GAGCAGGCTGAGCGATATGA	TGACCTACGGGCTCCTACAA

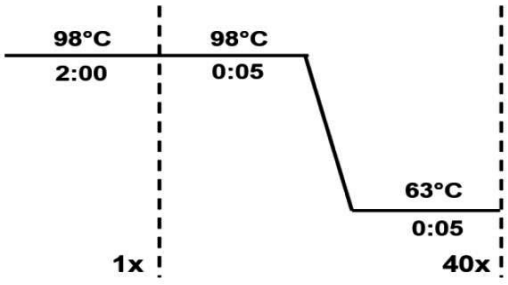

Figure 2.3 *- Experimental design depicting the duration and temperature of the RT-PCR cycles used to assess mtDNA copy number.*

2.6 Protein Quantification

After tissue homogenization, protein concentration in the lysates was determined using BioRad-DC protein assay from BioRad (Hercules, USA), according to the manufacturer's instructions. Briefly, this assay is based on the reaction of protein amino acids (primarily tyrosine and tryptophan, but also cystine, cysteine, and histidine) with an alkaline copper tartrate, followed by the reduction of a Folin substrate that leads to color development. After 15 minutes of reaction, the absorbance at 750 nm was measured using a Cytation 3 multi-mode microplate reader (BioTek Instruments, Inc.). Standard solutions containing 0.25 to 1.5 mg/mL Bovine Serum Albumin (BSA) were prepared using tissue homogenization buffer and used to infer samples' protein concentration. Standards and samples were quantified using duplicates and triplicates, respectively.

2.7 Enzymatic Activities

2.7.1 Catalase

Catalase activity was determined by following hydrogen peroxide decomposition by measuring the 240 nm absorbance decrease. Tissue samples were resuspended in 50 mM Phosphate Buffer 50 mM, pH 7.8 (PB) and homogenized two times during 20 seconds with an UltraTurrax homogenizer from IKA (Staufen, Germany). Total tissue homogenates volumes equivalent to 4 µg of total protein were diluted with 200 µL PB in a multi-well plate. The catalase activity assay was started by the addition of 100 µL hydrogen peroxide solution at 10 mM. The 240 nm absorbance was read every 15 seconds during 3 minutes at 25ºC using the Cytation 3 multi-mode microplate reader (BioTek Instruments, Inc.). Purified catalase was used as a positive control. Separate wells containing the catalase inhibitor sodium azide were used as negative controls. For each sample negative controls were prepared. Samples were measured in triplicates and negative controls in duplicates. The first seven absorbance readings of each sample and respective controls were fitted to an exponential regression curve. The maximal catalase activity was determined using the initial linear part of this fitting curve. Results are expressed in enzyme units (U) obtained directly from the decomposition of hydrogen peroxide using the Beer-Lambert law with $l = 0.691$ cm and $\varepsilon = 43.6\ M^{-1}.cm^{-1}$.

2.7.2 Cathepsin B

The sample preparation was performed as described for the catalase assay. Sample aliquots of 50 µL at 0.2 mg/mL protein concentration (10 µg total protein) were incubated at 37ºC with 70 µL incubation buffer (100 mM sodium acetate pH 5.5, 1 mM EDTA, 5 mM DTT and 0.05% (vol/vol) Brij-35). The cathepsin B activity assay was started by the addition of 70 µL of the substrate Z-Arg- Arg-N-methyl-coumarin at 40 µM. Substrate cleavage was followed during 20 minutes by fluorescence reading at 460 nm emission using 360 nm excitation with the Cytation 3 multi-mode microplate reader (BioTek Instruments, Inc.). A curve with known concentrations of N-methyl-coumarin was used

as standard. Cathepsin B activity was determined from the slope of the linear regression of experimental values and the results were normalized using the amount of protein in each sample.

2.7.3 Cathepsin D

The sample preparation was performed as described for the catalase assay. Sample aliquots of 50 µL at 0.2 mg/mL (10 µg total protein) were incubated at 37ºC for 30 minutes with 125 µL of 3% (wt/vol) hemoglobin in 200 mM acetic acid. After the incubation, 125 µL of 15% (vol/vol) TCA were added to the samples and they were kept for 2 hours at 4ºC. Samples were then centrifuged at 13 400 *g* for 5 minutes. Cathepsin D activity was determined by measuring the absorbance at 280 nm of 70 µL from the supernatants using the Cytation 3 (BioTek Instruments, Inc.) multi-plate reader. Results were normalized using the protein amount of each sample.

2.7.4 Citrate Synthase

The samples were homogenized as described for the catalase assay except that 50 mM phosphate buffer (pH 7.0) was used as buffer. Citrate synthase activity was measured according to a previously described protocol[331]. The reaction was started by the addition of 30 µL of each sample (2 mg/mL) to the wells containing 80 µL of 1 mM 5,5'-Dithiobis(2-nitrobenzoic acid) (DTNB), 10 µL of 4 mM acetyl-CoA, 10 µL of 1% Triton X-100 (in 50 mM phosphate buffer pH 7.0) and 20 µL of 10 mM oxaloacetate. The reaction was followed by the absorbance increase at 412 nm due to the consumption of DTNB and formation of 5-Mercapto-2-nitrobenzoic acid (TNB). The baseline activity was measured during 2 minutes and the increase of absorbance was followed during 5 minutes after starting the reaction. The assay was performed in triplicates. Negative controls were obtained replacing oxaloacetate by the corresponding volume of 50 mM phosphate buffer (pH 7.0). Citrate synthase activity was determined using the slope experimental values' linear regression and was expressed in enzyme units (U) obtained by the Beer-Lambert law with $l = 0.346$ cm and $\varepsilon = 13.6$ $mmol^{1}.cm^{-1}$. Citrate synthase activity of the negative controls was subtracted from their respective samples.

2.7.5 Glutathione Peroxidase

Liver samples were minced with a scalpel in an ice-cold board and repeatedly washed with cold PBS until almost all the blood clots and other debris were removed. Then all the samples were homogenized in 800 µL PBS in a pre-cooled Potter Elvehjem glass homogenizer using a tight-fitting Teflon pestle (wall clearance: 0.10 mm) attached to a mechanical overhead stirrer (Heidolph, Schwabach, Germany) set to 600 rpm for 50-60 strokes. The samples were centrifuged at 250 g for 2 min at 4ºC. The supernatants were collected and stored at -80ºC.

Measurements of glutathione peroxidase (GPx) were performed as described previously[332]. GPx activity was evaluated by spectrophotometry, using tert-butylperoxide as substrate[333], through the quantification of NADPH oxidation at 340 nm. Results are expressed in international units of enzyme activity (U).

2.7.6 Glutathione Reductase

Liver samples were extracted as described for GPx activity determination. Measurements of glutathione reductase (GRd) activity were performed as described previously[332], using GSSG as substrate[333], through the spectrophotometric quantification of NADPH oxidation to $NADP^+$ at 340 nm. Results are expressed in international units of enzyme activity (U).

2.7.7 Protein Kinase A

Protein kinase A (PKA) activity was measured using the PKA kinase activity kit from Enzo Life Sciences (Farmingdale, New York). This assay is based in a solid phase enzyme-linked immuno-absorbent assay (ELISA). The multi-well plates provided in the kit are pre-coated with a synthetic peptide that is a specific substrate for PKA. Kinase activity is determined using a polyclonal antibody that specifically recognizes the phosphorylated form of the substrate (**Figure 2.4**).

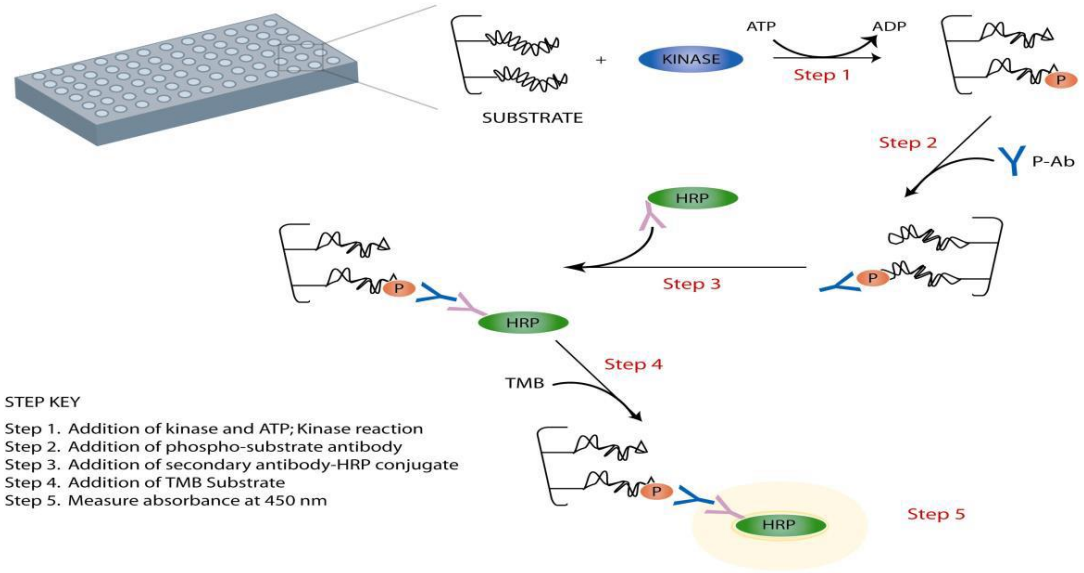

***Figure 2.4**-Schematic outline of protein kinase A kinase activity assay system.*

Tissue homogenization was performed as described for the catalase activity assay, although a different extraction buffer was used (20 mM MOPS, 50 mM β-glycerophosphate, 50 mM sodium fluoride, 1 mM sodium orthovanadate, 5 mM EGTA, 2 mM EDTA, 1% NP40, 1 mM dithiothreitol (DTT), and 1mM phenylmethanesulphonylfluoride (PMSF)). Samples were left on ice for 10 minutes and centrifuge at 15 700 g for 15 minutes. The pellets were discarded, and the supernatants used for PKA activity assessment after protein quantification. Briefly, samples (1 µg of protein) were added to each well, the reaction was started by the addition of ATP and allowed to occur during 90 minutes at 30ºC. The wells were soak with a solution of the phosphorylated substrate-specific antibody and incubated during 60 minutes at room temperature. The wells were washed during 1-2 minutes with the washing buffer provided in the kit in a total of four times. The multi-well plates were subsequently incubated with a peroxidase conjugated secondary antibody (anti-rabbit IgG:HRP conjugate) at room temperature for 30 minutes. Wells were washed again four times as previous described. The assay was completed by the addition of the horseradish peroxidase substrate tetramethylbenzidine (TMB), leading to the generation of a colored product proportional to the PKA phosphotransferase activity. TMB reaction with the secondary antibody was followed at 650 nm for 45 minutes using the Cytation 3. Then, the color development was stopped by adding an acidic stop solution, and the plates re-read at 450 nm. PKA Activity was assessed either using the slope from the kinetic record or the final absorbance, since they provide similar results. PKA activity was normalized to the average of the control group.

2.7.8 OXPHOS Complex I – NADH dehydrogenase

The sample preparation was performed as described for the citrate synthase assay. OXPHOS Complex I (NADH dehydrogenase) activity was determined according to a previously described protocol[334]. To each reaction well was added 130 µL H_2O, 21 µL potassium phosphate buffer (PB) 500 mM pH 7.5, 12.6 µL BSA 50 mg/mL, 6 µL KCN 10 mM, 10 µL NADH 2 mM, and 10 µL of the sample to be tested with a 2 mg/mL protein concentration (20 µg total protein). The reaction was started by the addition of 6 µL decylubiquinone 10 mM and followed by the decrease of absorbance at 340 nm due to oxidation of NADH. The baseline activity was measured for 5 minutes before de addition of decylubiquinone. The decrease of absorbance was followed during 10 minutes after starting the reaction. In order to check the specificity of the reaction, 12.5 µM of the complex I inhibitor rotenone was added in separate wells. In the wells without rotenone the volume was adjusted with 50 mM PB pH 7.0. Each sample was measured in triplicates and negative controls in duplicates. The maximal activity was determined using the slope of the experimental values' linear regression and is expressed in enzyme units (U) obtained by the Beer-Lambert law with $l = 0.484$ cm and $\varepsilon = 6.2$ $mmol^{-1}.cm^{-1}$. NADH dehydrogenase activity of the negative controls was subtracted from their respective samples.

2.7.9 OXPHOS Complex II – Succinate dehydrogenase

The sample preparation was performed as described for the citrate synthase assay. OXPHOS Complex II (succinate dehydrogenase) activity was measured according to a previously described protocol[334]. An aliquot of 80 µL from the sample homogenate at 2 mg/mL protein was incubated with 12.5 µL PB 25 mM pH 7.5, 5 µL BSA 50 mg/mL, 145 µL DCPIP 0.015% and 7.5 µL KCN 10 mM. The reaction was started by the addition of 12.5 µL of the complex II substrate succinate (400 mM). Succinate dehydrogenase activity was followed by the decrease of absorbance at 600 nm due to DCPIP reduction. The baseline activity was measured for 2 minutes and the decrease of absorbance was followed during 3 minutes after starting the reaction. In order to check the specificity of the reaction, 10 µL of the complex II inhibitor malonate (1 M) was added in separate wells. Linear regression of the experimental values was used to obtain slopes. The slope from the baseline was subtracted to the slope from complex II activity. The assay was performed in triplicates. Activities are represented in enzymes units (U) using the Beer-Lambert law with l = 0.628 cm and $\varepsilon = 19.1\ M^{-1}.cm^{-1}$.

2.7.10 OXPHOS Complex I+III – NADH dehydrogenase and cytochrome c reductase

The sample preparation was performed as described for the citrate synthase assay. Complex I/III activity was measured according to a previously described protocol[334]. An aliquote of 25 µL from the sample homogenate at 2 mg/mL protein concentration (25 µL) was incubated with 175 µL H_2O during 10 minutes. After, a mix containing 25 µL PB 50 mM pH 7.5, 5 µL BSA 50 mg/mL, 7.5 µL 10 mM KCN, and 2.5 µL NADH 10 mM was added to each well. The reaction was started by the addition of 12.5 µL cytochrome c 1 mM and followed by the increase of absorbance at 550 nm due to the reduction of cytochrome c. The baseline activity was measured for 2 minutes and the decrease of absorbance was followed during 2 minutes after starting the reaction. In order to check the specificity of the reaction, negative controls obtained using 2.5 µL of both the complex I and III inhibitors, rotenone (1 mM) and antimycin A (10 $mg.mL^{-1}$), respectively, were performed in separate wells. Linear regression of the experimental values was used to obtain slopes. Complex I+III specific activity was obtained by subtracting the activity of negative controls from the activity of the respective sample. Activity is expressed in enzyme units using the Beer-Lambert law with l = 0.625 cm and $\varepsilon = 18.5\ M^{-1}.cm^{-1}$.

2.7.11 OXPHOS Complex II+III – Succinate dehydrogenase and cytochrome c reductase

The sample preparation was performed as described for the citrate synthase assay. Complex II/III activity was measured according to a previously described protocol[334]. A mix containing 100 µL PB 25 mM pH 7.5, 7.5 µL KCN 10 mM and 6.25 µL succinate 400 mM was added to 15 µL of sample homogenates with 2 mg/mL protein

concentrations. The reaction was started by the addition of 12.5 µL cytochrome c 1 mM and followed by the increase of absorbance at 550 nm due to the reduction of cytochrome c. The baseline activity was measured for 2 minutes and the increase of absorbance was followed during 3 minutes after starting the reaction. In order to check the specificity of the reaction, 2.5 µL of complex II inhibitor, malonate (1 M), was added in separate wells. Sample activities were performed in duplicates and the slope of the negative control was subtracted to the total slope. Linear regression of the experimental values was used to obtain slopes. Activity is expressed in enzyme units (U) using the Beer-Lambert law with $l = 0.331$ cm and $\varepsilon = 18.5\ M^{-1}.cm^{-1}$.

2.7.12 OXPHOS Complex IV – Cytochrome c oxidase

The sample preparation was performed as described for the citrate synthase assay. Complex IV (cytochrome c oxidase) activity was measured according to a previously described protocol[334]. The reaction was started by the addition of 12 µL of the complex IV substrate, reduced cytochrome c 1 mM, to a mix containing 170 µL PB 50 mM pH 7.0 and 37.5 µL sample homogenates with a 2 mg/mL protein concentration. Cytochrome c was reduced using sodium dithionite according to a protocol previously described[334]. Briefly, oxidized cytochrome c was prepared in 20 mM PB pH 7.0. It was reduced, immediately before use, by mixing with a few grains of sodium dithionite in the tip of a pipette. The solution's color changed from brown to red-pink. Cytochrome c reduction was confirmed by measuring the ratio between absorbance values at 550 nm and 565 nm. A ratio greater than 6 indicates that cytochrome c was successfully reduced and that the solution is adequate to be used[334].

The OXPHOS complex IV reaction was followed by the decrease of absorbance at 550 nm due to oxidation of cytochrome c. The baseline activity was measured for 2 minutes and the decrease of absorbance was followed during 3 minutes after starting the reaction. In order to check the specificity of the reaction, 6 µL of the complex IV inhibitor KCN (10 mM) were added in separate wells. Linear regression of the experimental values was used to obtain slopes. All the assays were performed in duplicates and the activity is expressed in enzyme units (U) and was obtained using the Beer-Lambert law with $l = 0.519$ cm and $\varepsilon = 18.5\ M^{-1}.cm^{-1}$.

2.7.13 Superoxide Dismutase

The activity of Superoxide Dismutase (SOD) was measured using a SOD activity kit purchased from Enzo Life Sciences (Farmingdale, New York). This is a colorimetric based assay in which superoxide ions are generated in the presence of molecular oxygen from the conversion of xanthine to uric acid and hydrogen peroxide by the enzyme xanthine oxidase. The generated superoxide anions react with WST-1 converting it to WST-1 formazan, a colored product that absorbs light at 450 nm. When SOD is present the amount of superoxide ion is reduced and consequently the rate of WST-1 formazan

formation decreases (**Figure 2.5**). The relative SOD activities of the hepatic tissue from control and obese ewes were expressed as a percentage of inhibition of the rate of WST-1 formazan formation. The assay was performed according to the kit manufacturer's instructions.

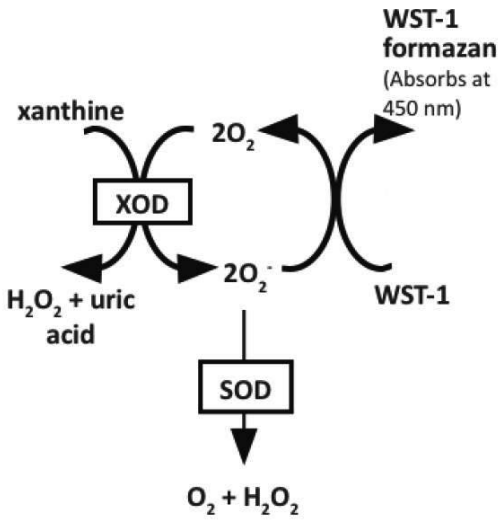

***Figure 2.5**- Schematic representation of the reaction mechanism used in SOD activity assay.*

Briefly, tissue samples were minced and rinsed three times in PBS in order to remove blood clots or other debris. The pelleted decanted fragments were resuspended in 1x extraction buffer supplied with the kit and homogenized during 20 seconds with an UltraTurrax homogenizer from IKA (Staufen, Germany) two times. The homogenates were kept on ice for 30 minutes and periodically vortexed. The disrupted tissue suspension was centrifuged at 10,000xg during 10 minutes at 4ºC to remove insoluble material. The supernatants were recovered, maintained on ice and their protein concentration determined by the BioRad-DC protein assay (Hercules, USA).

SOD activity determination was performed at 25ºC using 200 µl of 1X SOD assay buffer supplemented with WST-1 reagent and xanthine oxidase. The reaction was initiated by the addition of xanthine solution and followed for 10 minutes through absorbance readings at 450 nm every minute using the Cytation 3 multi-mode microplate reader (BioTek Instruments, Inc.). Assays were performed in duplicates and the results are expressed in enzyme units (U). A standard curve obtained with the purified SOD supplied with the kit was used to calculate enzyme activities.

2.8 Molecular Quantifications

2.8.1 GSH levels

Samples' extraction protocol was as previously described for the Glutathione Peroxidase activity determination. Measurements of GSH levels were performed as described previously[332]. The OxisResearch kit (Percipio Biosciences Burlingame, CA,

USA) was used according to manufacturer's instructions. This assay is based on a method that follows absorbance changes at 420 nm due to the formation of a chromophoric thione that occurs proportionally to GSH concentration[335]. Results are expressed as μmol of GSH per L of sample (μM).

2.8.2 MDA levels

Samples were extracted as described for the glutathione peroxidase activity determination. Lipid peroxidation was assessed by quantification of malondialdehyde (MDA) adducts separated by HPLC (Gilson, Lewis Center, Ohio, USA) using the ClinRep complete kit (Recipe, Munich, Germany) as described by the manufacturer. Fluorescence readings with emission at 553 nm and excitation at 515 nm were performed using a Jasco FP-2020/2025 fluorescence detector (Jasco, Tokyo, Japan).

2.8.3 NAD+ and NADH levels

NAD^+ and NADH (oxidized and reduced nicotinamide adenine dinucleotides, respectively) levels and their ratio was measured using NAD/NADH-Glo™ Assay purchased from Promega Corporation (Madison, Wyoming). This assay uses a NAD cycling enzyme which converts NAD^+ to NADH in the presence of a specific substrate provided in the kit. NADH is used by the enzyme reductase to reduce a proluciferin reductase substrate to form luciferin. Luciferin is quantified using Ultra-Glo™ Recombinant Luciferase (rLuciferase), being the light signal produced proportional to the amount of NAD+ or NADH in the sample (**Figure 2.6**).

Samples were homogenized as described for the catalase assay but using a bicarbonate buffer (100 mM sodium carbonate, 20 mM sodium bicarbonate, 10 mM nicotinamide, 0.05% Triton X-100, pH 10) with 1% dodecyltrimethylammonium bromide (DTAB). Samples were centrifuged at 15 700 g for 15 minutes and the pellet discarded. Each sample was split into two eppendorfs in order to measure NAD^+ with one and NADH with the other. In general, oxidized forms are selectively destroyed by heating in a basic solution, while reduced forms are not stable in acidic solutions. To measure NAD^+ levels, 50 μL of samples (0.4 mg of protein/mL) were incubated with 25 μL of 0.4 N HCL and heated at 60ºC for 15 minutes. Samples were left 10 minutes at room temperature before adding 25 μL of 0.5M Trizma base, pH 10.7. For NADH levels measurement, 50 μL of samples (0.4 mg of protein/mL) were heated at 60 ºC for 15 minutes. After cooling down the samples during 10 minutes at room temperature, 50 μL of 0.4 M HCl/ 0.5 M Trizma base were added. Then 20 μL of samples were mixed with 20 μL of the NAD/NADH-Glo™ detection reagent in a Corning 384-well low flange white flat bottom polystyrene not treated microplate. After 1 h incubation, luminescence was measured in a Cytation 3 multi-mode microplate reader (BioTek Instruments, Inc.). NAD^+ and NADH levels were normalized using the control group values, while their ratio was determined directly from the raw data.

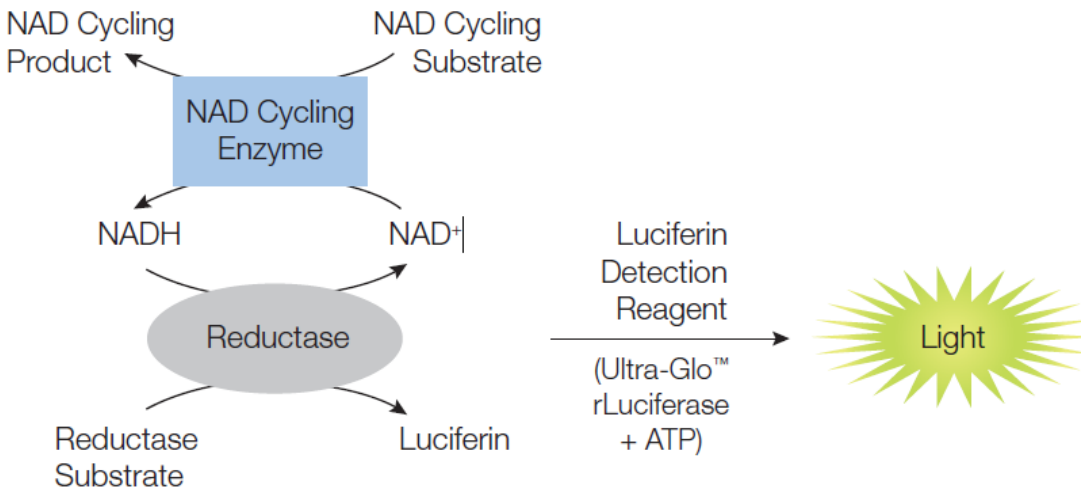

Figure 2.6 *- Schematic diagram of the NAD/NADH-Glo™ Assay technology.*

2.8.4 Vitamin E levels

Samples were homogenized as described for the Glutathione Peroxidase activity assay. Vitamin E levels were quantified by reverse-phase high performance liquid chromatography (HPLC) using an analytic column Spherisorb S10w (250 x 4.6mm). Elution was performed with 0.9% methanol in n-hexane at a flow of 1.5 mL/min. Vitamin E was quantified using absorbance reading at 287 nm and internal standards.

2.9 Western Blot

A piece of tissue with ~30 mg was homogenized two times during 20 seconds with an Ultra-Turrax homogenizer from IKA (Staufen, Germany) in RIPA buffer (50 mM Tris pH 8, 150 mM NaCl, 5 mM EDTA, 15 mM $MgCl_2$, 1% TritonX-100) supplemented with 0.5 mM PMSF, 2.5‰ of a protease inhibitor cocktail (104 mM AEBSF, 80 µM Aprotinin, 4 mM Bestatin, 1.4 mM E-64, 2 mM Leupeptin, and 1.5 mM Pepstatin A), 20 mM NaF, 10 mM NAM, 5 mM Sodium Butyrate, 0.5% DOC and PhosSTOP (phosphatase inhibitor cocktail, Roche, Sigma -Aldrich Quimica) as described by the supplier. After homogenization, samples were centrifuged at 250 g for 2 minutes at 4ºC and the pellet discarded. Protein was quantified and the samples diluted to 2.4 mg/mL with supplemented RIPA buffer. Laemmli buffer 6 times concentrate (375 mM Tris-HCl (pH 6.8), 9% SDS, 50% glycerol, 9% beta-mercaptoethanol, 0.03% bromophenol blue, and 300 mM DTT) was added to each sample to achieve a final protein concentration of 2 mg/mL. Samples were boiled at 95ºC for 5 minutes (except an aliquot which was used

in OXPHOS cocktail protein quantification). Samples were stored at -20ºC until future use.

Samples (25 µg of protein) were loaded in 10% or 12% acrylamide gels (14% was used in LC3B western blot). In each gel Precision Plus Protein Dual Color Standards and a positive control consisting of 25 µg of protein from HepG2 extracts were run in parallel with the samples. Electrophoresis was performed at room temperature with running buffer (25 mM Tris, 192 mM glycine, 0.1% SDS), at constant current intensity (30 mA per gel) in a Mini-PROTEAN tetra Cell (Bio-Rad) for around 75 minutes. Protein was then transferred to PVDF membranes in a Trans-Blot Turbo Transfer System (Bio-Rad). PVDF membranes were activated by incubation for 1 minute in methanol, 5 minutes in ddH_2O and 15 minutes in Trans-Blot Turbo Transfer Buffer (Bio-Rad). Transference occurred for 10 minutes at constant current intensity (2.5 A). Transfer quality was assessed by ponceau staining the membranes.

Membranes were then blocked using 5% free-fat milk, or 5% BSA according to antibodies datasheet, in TBS-T buffer (Tris 20 mM, pH 8.0, NaCl 150 mM, Tween-20 0.1% (w/v)) for 2 hours at room temperature. Membranes were washed 3 times with TBS-T, for at least 5 minutes each time and under agitation, and incubated with primary antibody (**Table 2.5**) overnight, under agitation at 4ºC. Primary antibodies were prepared in 1% free-fat milk in TBS-T buffer, unless stated otherwise in the supplier documentation. Membranes were washed again 3 times as previously described, and incubated with the secondary antibody (**Table 2.6**) prepared in TBS-T buffer, for 2 hours, at room temperature and under agitation.

Table 2.5 *– List of primary antibodies used to perform protein determination by Western blot. 'Accession number' represents the UniProt (The Universal Protein Resource) reference of the protein and 'dilution' corresponds to the dilution used for each antibody during incubation.*

Protein		Accession Number	Manufacture code		Host Specie	MW (kDa)	Dilution
ACO 2	Aconitase 2	Q99798	Cell signaling	6571	Rabbit	85	1:500
ANT 1/2	Adenosine nucleotide translocator 1/2	P12235	Abcam	110322	Mouse	33	1:1000
ATP5a	ATP synthase subunit alpha	P25705	Mito Science	Ab110273	Mouse	54	1:500
Bcl-2	B-cell lymphoma 2	P10415	Cell signaling	2870	Rabbit	26	1:1000
Beclin-1		Q14457	Cell signaling	3495	Rabbit	60	1:500
Cat	Catalase	P04040	Mito Science	Ab14754	Mouse	48	1:1000

COX-II	Cytochrome c oxidase subunit 2	P00403	Mito Science	Ab110258	Mouse	22	1:500
CS	Citrate synthase	O75390	Santa Cruz	390693	Mouse	58	1:1000
CVα	ATP synthase F(o) complex subunit C1	P05496	Mito Science	Ab14748	Mouse	55	1:1000
Cyc D	Cyclophilin D	M5C900	Mito Science	Ab110324	Mouse	21	1:500
Cyt C	Cytochrome c	P99999	Mito Science	Ab110324	Mouse	12	1:500
Fis-1	Mitochondrial fission 1 protein	Q9Y3D6	Santa Cruz	376447	Mouse	17	1:500
GLUT-1	Glucose transporter member 1	P11166	Santa Cruz	377228	Mouse	55	1:500
GPx-1	Glutathione peroxidase 1	P07203	Santa Cruz	133160	Mouse	23	1:500
GPx-4	Glutathione peroxidase 4	P36969	Santa Cruz	166570	Mouse	21	1:500
GR	Glutathione Reductase	P00390	Santa Cruz	133245	Mouse	50	1:1000
LC3B	Microtubule-associated proteins 1A/1B light chain 3B	Q9GZQ8	Cell signaling	3868	Rabbit	14,16	1:500
Mfn-1	Mitofusin-1	Q8IWA4	Santa Cruz	50330	Rabbit	86	1:500
mtCO1	Cytochrome c oxidase subunit 1	P00395	Abcam	14705	Mouse	57	1:1000
Ndufs8	NADH dehydrogenase iron-sulfur protein 8	O00217	Mito Science	Ab110242	Mouse	18	1:1000
OPA-1	Dynamin-like 120 kDa protein	O60313	Santa Cruz	30573	Goat	120	1:250
P62		Q13501	MBL	PM045	Rabbit	62	1:500
p-BCL-2 (Thr56)	B-cell lymphoma 2	P10415	Cell signaling	2875	Rabbit	28	1:500
PGC-1α	Peroxisome proliferator-activated receptor gamma coactivator 1-alpha	Q9UBK2	Santa Cruz	13067	Rabbit	90	1:500
PKA	cAMP-dependent protein kinase catalytic subunit alpha	P17612	Santa Cruz	28892	Rabbit	40	1:1000

PPARγ	Peroxisome proliferator-activated receptor gamma	P37231	abcam	41928	Mouse	58	1:1000
SDHA	Succinate dehydrogenase flavoprotein subunit	P31040	Santa Cruz	59687	Mouse	70	1:1000
SDHB	Succinate dehydrogenase iron-sulfur subunit	P21912	Mito Science	Ab14714	Mouse	29	1:500
Sirt-1	Sirtuin-1	Q96EB6	abcam	110304	Mouse	110	1:500
Tfam	Transcription factor A	Q00059	Santa Cruz	23588	Goat	25	1:500
TOM 20	Mitochondrial import receptor subunit TOM20	Q15388	Santa Cruz	49760	Rabbit	20	1:1000
UQCRC1	Cytochrome b-c1 complex subunit 1	P31930	Mito Science	Ab110252	Mouse	49	1:500
UQCRC2	Cytochrome b-c1 complex subunit 2	P22695	Mito Science	Ab14754	Mouse	48	1:1000
UQCRFS1	Cytochrome b-c1 complex subunit Rieske	P47985	Abcam	Ab14746	Mouse	25	1:500
VDAC	Voltage-dependent anion-selective channel protein 1	P21796	Mito Science	Ab14734	Mouse	39	1:500
β-actin		P68133	Millipore	MAB1501	Mouse	43	1:5000

After the incubation with secondary antibody, membranes were washed 3 times as previously described except that TBS (TBS-T without Tween-20) was used instead of TBS-T. Membranes were then incubated with Clarity Western ECL Substrate (Bio-Rad) for 5 minutes and images collected with a UVP BioSpectrum 500 imaging System (UVP, Upland, California). Images were analyzed with the TotalLab TL120 software (Nonlinear Dynamics, Newcastle, UK), using the background subtraction method 'Rolling Ball' with radius = 50. The volume of the bands was used to compare protein expression between different lanes. Results were normalized by β-actin expression and are reported relatively to the mean of the control group.

Table 2.6 *- List of secondary antibodies used in Western blot. 'Dilution' corresponds to the dilution used for each antibody during incubation.*

Antibody	Description	Manufacture	Code	Host specie	Dilution
Anti-Goat	rabbit@goat	Santa Cruz	2771	Rabbit	1:5000
Anti-Mouse	goat@mouse	Santa Cruz	2008	Goat	1:5000
Anti-Rabbit	goat@rabbit	Santa Cruz	2007	Goat	1:5000

2.10 Data analysis and statistics

The aim of this work is to understand if the hepatic tissue is differently affected by maternal obesity during pregnancy comparing to a control pregnancy. Therefore, two-sided statistical tests were always used. All data were analyzed using GraphPad Prism 6.01 (GraphPad Software, Irvine, CA. USA) and all results are expressed as median, 1st quartile (Q_1) and the 3rd quartile (Q_3) with three significant digits. Each different animal was considered as an experimental unit, although the contribution of each liver lobe was separately taken in account. The number of experiments performed in each assay is described in the respective figure.

To measure differences due to maternal obesity comparisons between ML-C (Maternal Liver – Control) and ML-MO (Maternal Liver – Maternal Obesity), between MLL-C (Maternal Liver Left Lobe – Control) and MLL-MO (Maternal Liver Left Lobe -Maternal Obesity), and between MLR-C (Maternal Liver Right Lobe – Control) and MLR-MO (Maternal Liver Right Lobe – Maternal Obesity) were performed. When $n < 7$ in the group, the data was considered not normal and the nonparametric Mann–Whitney test was performed. Otherwise, the normality of the distribution of the results from each group was measured using Shapiro-Wilk normality test. $\alpha = 0.05$ was considered the threshold to pass normality test. Whenever the data presented a normal distribution, parametric unpaired t-test was performed. Otherwise, the nonparametric Mann–Whitney test was used.

A secondary hypothesis in this work is the existence of a metabolic dichotomy between liver lobes, both originally, in the control group, and also in a situation of maternal obesity during pregnancy. To test this hypothesis, comparisons between MLL-C and MLR-C as well as between MLL-MO and MLR-MO were performed. As liver lobes from the same individual are compared in these cases, paired statistical tests were used. The choice of statistical test to be use according to the type of distribution of the data was as previously described. Nonparametric Wilcoxon test and parametric paired t-test were used.

In all statistical tests values with $p < 0.05$ were considered as statistically significant differences (* $p < 0.05$; ** $p < 0.01$; *** $p < 0.001$; **** $p < 0.001$), and p-value was represented with four significant digits. Statistically significant results were further analyzed to determine the effect size. Cohen's d test with Hedges' g variation,

which is used when there are different sample sizes, allowed to quantify the magnitude of the difference between groups. Values with $g > 0.01$ were considered with a significant effect size and can be further ranked according to magnitudes ($g > 0.01$ very small; s $g > 0.20$ small; $g > 0.50$ medium; $g > 0.80$ large; $g > 1.20$ very large; $g > 2.0$ huge) and g-value was expressed with three significant digits.

Chapter 3 - Results

3.1 Impact of maternal obesity during pregnancy on maternal health

Weight gain is one of the hallmarks of obesity. During this study, maternal weight was measured at three time points: before starting the diet intervention; at the conception; and before the cesarean section. At the beginning of the study no weight differences were observed between the ML-C and ML-MO groups ($p = 0.5744$). However, at the conception, 60 days after starting the diet, a significant difference was measured between ML-C and ML-MO ((ML-C vs ML-MO: median = 69.0, $Q_1 = 57.9$, $Q_3 = 84.0$ vs median = 78.5, $Q_1 = 73.5$, $Q_3 = 94.5$; $p = 0.0471$; effect size $g = 1.07$; **Figure 3.1A**). At 90% of gestation (cesarean section between day 132 and 140), ML-MO live weight was increased compared with ML-C (ML-C vs ML-MO: median = 111, $Q_1 = 105$, $Q_3 = 121$ vs median = 102, $Q_1 = 91.3$, $Q_3 = 115$; $p = 0.0529$; $g = 1.05$).

Subcutaneous fat thickness was also evaluated and a significant increase due to maternal obesity was observed when comparing ML-C with ML-MO (ML-C vs ML-MO: median = 2.00, $Q_1 = 2.00$, $Q_3 = 2.12$ vs median = 3.75, $Q_1 = 3.50$, $Q_3 = 4.50$; $p = 0.0003$; $g = 2.20$, **Figure 3.1B**)). After cesarean section some tissues were also collected and weighted. There are no differences in the measured weights of heart ($p = 0.9028$), liver ($p = 0.1986$) and brain ($p = 0.6207$) between the ML-C and ML-MO groups (**Figure 3.1C**). Significantly higher pituitary's weights were observed in the ML-MO group compared with ML-C ($p = 0.0152$; $g = 1.29$).

3.2 Maternal obesity induced-hepatic metabolic remodeling

Obesity induces several metabolic alterations. In liver, it is associated with lipid accumulation, which induces dysregulations in the hepatic metabolism. With that in mind, Protein Kinase A (PKA) activity and the redox state of liver tissue (**Figure 3.2**), as well as the protein expression of some regulators of hepatic metabolism (**Figure 3.3)** were evaluated in order to assess possible alterations caused by maternal obesity.

Maternal obesity during pregnancy decreased by 40% the hepatic PKA activity (ML-C vs ML-MO: median = 0.945, $Q_1 = 0.775$, $Q_3 = 1.33$ vs median = 0.477, $Q_1 = 0.347$, $Q_3 = 0.832$; $p = 0.0007$; with a large effect size $g = 1.61$; **Figure 3.2A**). This difference is caused essentially by PKA activity alterations in the hepatic right lobe where differences between MLR-C and MLR-MO are more pronounced (MLR-C vs MLR-MO: median = 0.975, $Q_1 = 0.858$, $Q_3 = 1.29$ vs median = 0.434, $Q_1 = 0.328$, $Q_3 = 0.530$; $p < 0.0001$; $g = 1.51$).

The redox state of liver tissue is also modified by maternal obesity (**Figure 3.2B**). The NAD^+/NADH ratio is 35.8% increased in ML-MO (ML-C vs ML-MO: median = 0.640, $Q_1 = 0.595$, $Q_3 = 0.657$ vs median = 0.775, $Q_1 = 0.674$, $Q_3 = 1.07$; $p = 0.0059$), although with a small effect size $g = 0.349$. This alteration caused in NAD^+/NADH ratio

by excessive food intake is mainly due to the effect observed in the right lobe, with a 61.7% rise in MLR-MO (MLT-C vs MLR-MO: median = 0.605, Q_1 = 0.508, Q_3 =0.629 vs median = 0.987, Q_1 = 0.719, Q_3 = 1.10; p = 0.0087; g = 0.541).

Physiologically, the different liver lobes of the control group, MLL-C and MLR-C, already present dissimilar NAD^+/NADH ratios (MLL-C vs MLR-C: median = 0.657, $5Q_1$ = 0.644, Q_3 = 0.717 vs median = 0.605, Q_1 = 0.508, Q_3 = 0.629; p = 0.0625; g = 0.151). The differences in NAD^+/NADH ratios between the experimental groups are caused by a 19.9% decrease in NADH levels (ML-C vs ML-MO: median = 0.977, Q_1 = 0.960, Q_3 = 1.07 vs median = 0.850, Q_1 = 0.769, Q_3 = 0.926; p = 0.0040; g = 1.38; **Figure 3.2D**), while NAD^+ levels remain unchanged (p = 0.796; **Figure 3.2C**). Indeed, NADH levels are also altered by maternal obesity in the liver right lobe (MLR-C vs MLR-MO: median = 1.02, Q_1 = 0.954, Q_3 = 1.08; MLR-MO vs median = 0.806, Q_1 = 0.522, Q_3 = 0.870; p = 0.0070, g = 1.29).

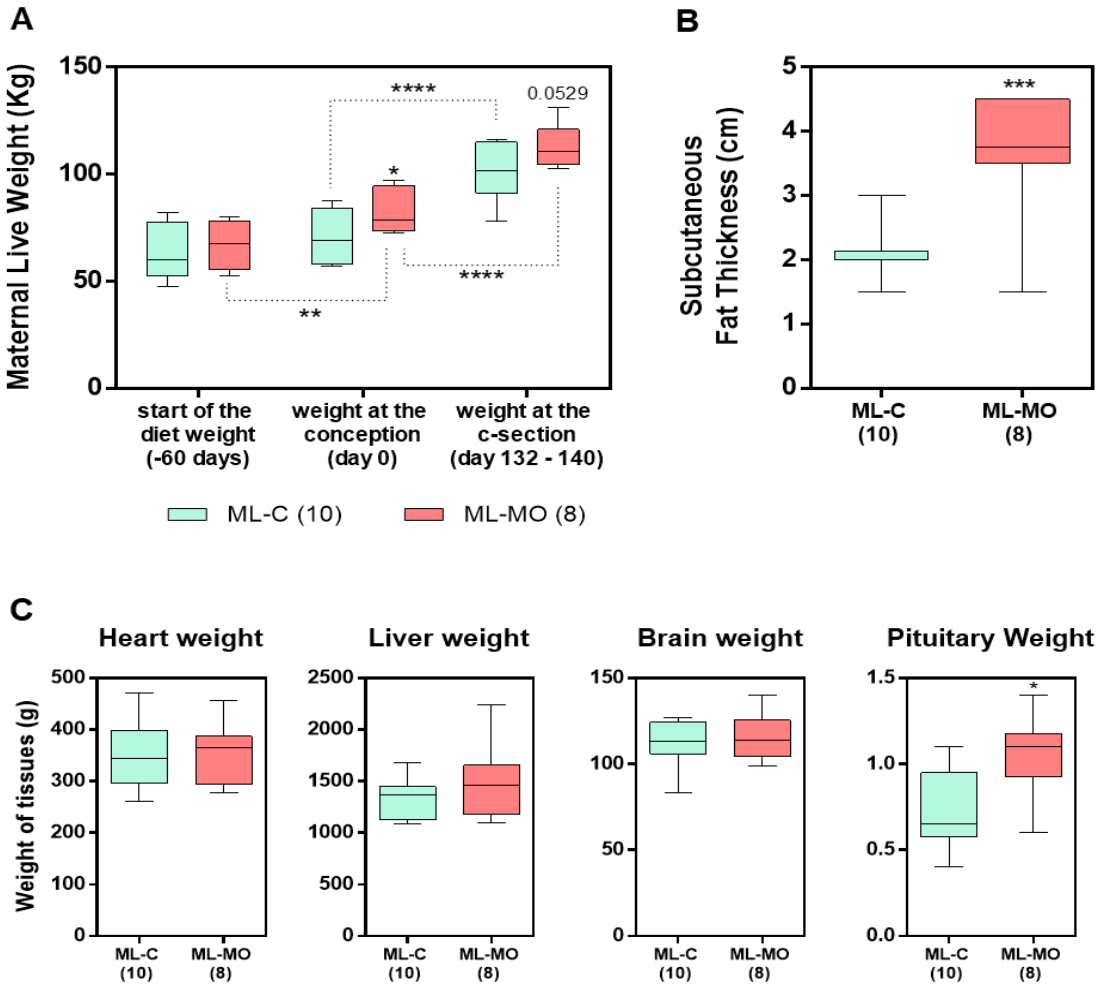

Figure 3.1 *- Maternal morphological parameters from control group (ML-C) and obese group (ML-MO).* ***A:*** *live weight before starting the diet, at the conception and at the c-section.* ***B:*** *subcutaneous fat thickness.* ***C:*** *weight of maternal heart, liver, brain and pituitary gland at the c-section. The number of individuals in each group is indicated in parentheses. Statistical analysis: Comparison between control and maternal obesity groups was performed using unpaired t-test in A (after performing Shapiro-Wilk normality test). P-value lower than 0.05 was considered significant (* $p \leq 0.05$; *** $p \leq 0.001$). Green/light grey bars, ML-C; Red/dark grey bars, ML-MO. Median, interquartile distance, minimum and maximum are depicted.*

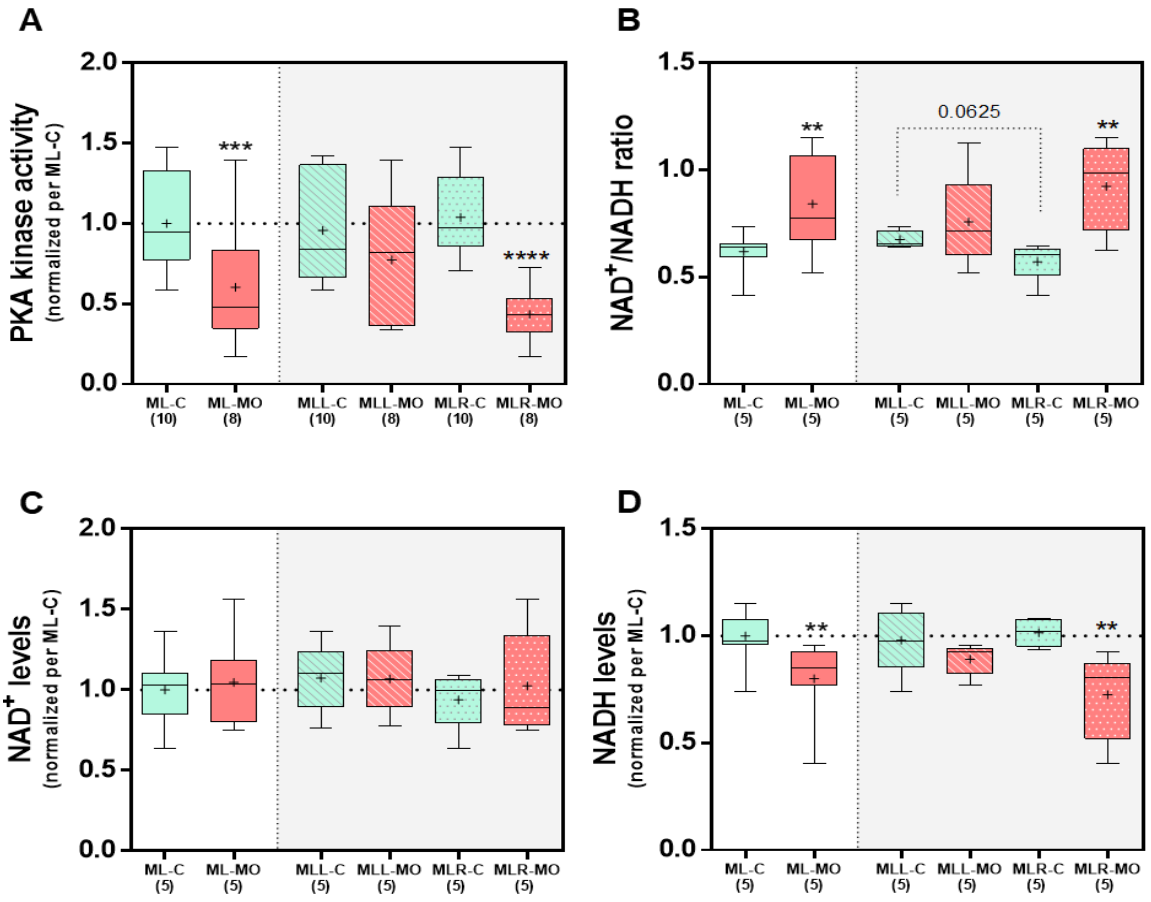

Figure 3.2 *- Metabolic hepatic profile of tissues from control (ML-C) and maternal obesity (ML-MO) ewes. The combined (left white area) or individual (right greyed area) contribution of the left and right liver lobes is depicted.* ***A:*** *Protein Kinase A activity;* ***B:*** *NAD^+ / NADH ratio calculated from* ***C:*** *NAD^+ levels and* ***D:*** *NADH levels. Data is represented relatively to the respective ML-C group mean in A, C, and D. The number of individuals in each group is indicated in parentheses.*
Statistical analysis: Comparison between control and maternal obesity groups was performed using unpaired t-test in A (after performing Shapiro-Wilk normality test) and Mann-Whitney test in B, C, and D. Comparison between lobes was assessed using paired t test in A and Wilcoxon test in B, C, and D. P-value lower than 0.05 was considered significant ($p \leq 0.05$; ** $p \leq 0.01$; *** $p \leq 0.001$; **** $p \leq 0.0001$). Green/light grey bars, ML-C; Red/dark grey bars, ML-MO; diagonal line pattern, left liver lobe (MLL); dot pattern, right liver lobe (MLR). Median, mean (+), interquartile distance, minimum and maximum are depicted.*

Although PKA activity is modified by maternal obesity, PKA protein expression is not affected either in the total liver tissue (p = 0.743) or in any of the lobes (**Figure 3.3**). Hepatic sirtuin-1 protein expression was also evaluated and is similar in both experimental groups (ML-C vs ML-MO, p = 0.829). However, there is a dichotomy in Sirtuin-1 expression if the liver lobes are considered separately (**Figure 3.3B**): no differences in expression are observed in the right lobe (p = 0.180) while there is a small decrease in Sirtuin-1 expression in the left lobe of obese mothers compared with control (MLL-C vs MLL-MO, p = 0.065; g = 0.582).

Peroxisome proliferator-activated receptor gamma (PPAR-γ) protein expression was also analyzed (**Figure 3.3**). In total liver tissue there is a slight decrease in PPAR-γ levels when comparing ML-C with ML-MO (ML-C vs ML-MO: median = 0.952, Q_1 = 0.774, Q_3 = 1.24 vs median = 0.728, Q_1 = 0.519, Q_3 = 1.05; p = 0.0933; g = 0.716). Again, a dichotomy can be observed related with PPAR-γ protein expression in liver lobes

(**Figure 3.3B**): in the left lobe a significant decrease in PPAR-γ levels was measured (p = 0.0022; g = 5.06), while an increase was observed in the right lobe (p = 0.0043; g = 1.96) with excessive food intake compared to controls.

Interestingly, alterations in the protein expression of those regulatory proteins were found originally when comparing right and left lobes of control mothers (PKA: p = 0.0625, g = 1.08; Sirt-1: p = 0.0938, g = 1.10; PPAR-γ: p = 0.0313, g = 2.54; **Figure 3.3B**). Furthermore, these proteins' expression is also different in the right and left lobes of obese mothers (PKA: p = 0.0313, g = 0.432; Sirt-1: p = 0.0313, g = 5.80; PPAR-γ: p = 0.0313, g = 4.87; **Figure 3.3B**).

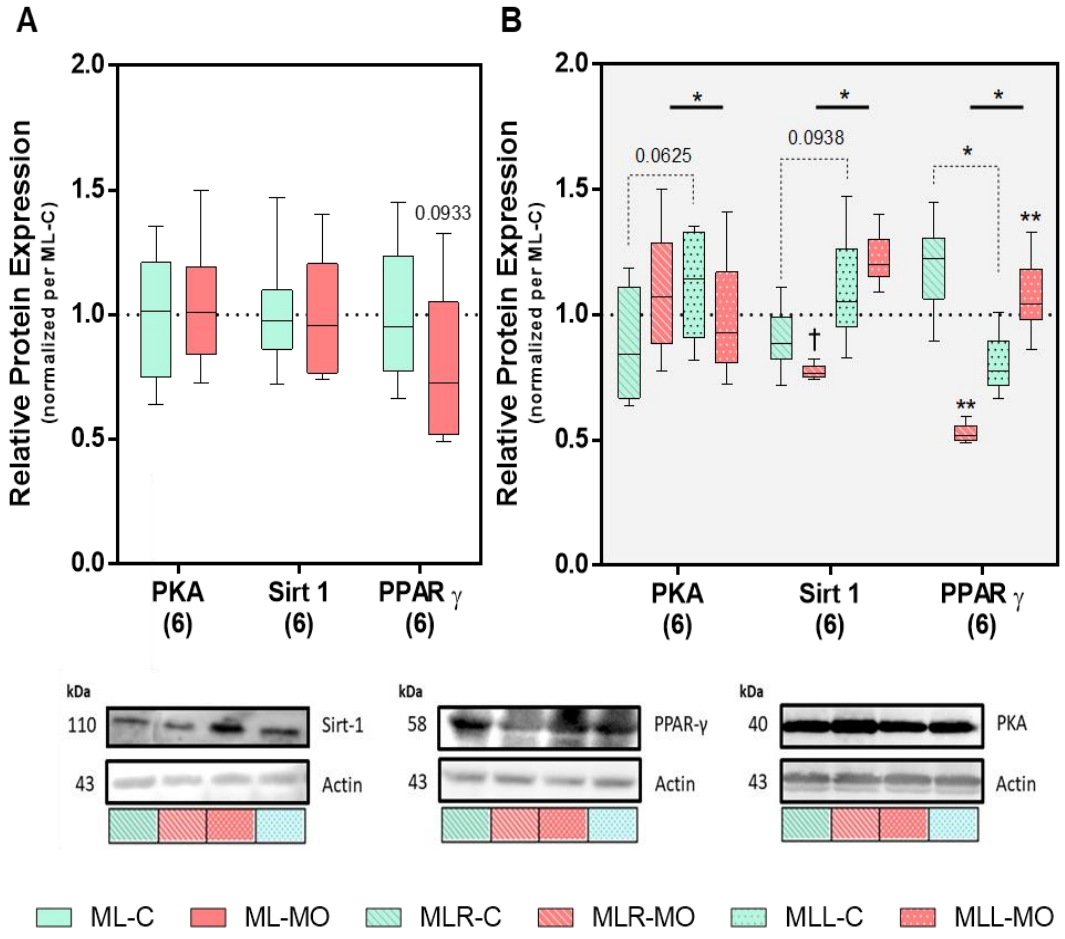

Figure 3.3- *Metabolic remodeling-related protein expression of Protein Kinase A (PKA), Sirtuin-1 (Sirt-1) and Peroxisome proliferator-activated receptor gamma (PPAR-γ), and alterations induced by Maternal Obesity in* ***A:*** *total hepatic tissue from control group (ML-C) and maternal obesity group (ML-MO) and* ***B:*** *the contribution of each liver lobe. Data was normalized using the reference protein β-actin and the protein expression represented relative to ML-C group. The number of individuals in each group is indicated in parentheses.*
Statistical analysis: Comparison between control and maternal obesity groups was performed using Mann-Whitney test in A and B. Comparison between lobes was assessed using Wilcoxon test in B. P-value lower than 0.10 was registered († $p \leq 0.10$) and lower than 0.05 was considered significant ($p \leq 0.05$; ** $p \leq 0.01$). Green/light grey bars, ML-C; Red/dark grey bars, ML-MO; diagonal line pattern, left liver lobe (MLL); dot pattern, right liver lobe (MLR). Median, interquartile distance, minimum and maximum are depicted.*

Since metabolic regulation was changed by maternal obesity it was hypothesized that metabolic proteins expression could also be modified. Therefore, glucose transporter GLUT-1, Adenosine nucleotide translocator (ANT 1/2), as well as Krebs' cycle enzymes aconitase (ACO 2) and citrate synthase protein levels were analyzed. No significant alteration in these proteins expression was found between the experimental groups (ANT 1/2: p = 0.1662; ACO 2: p = 0.1383; citrate synthase: p = 0.3712; GLUT-1: p = 0.2708; Figure **3.4A**).

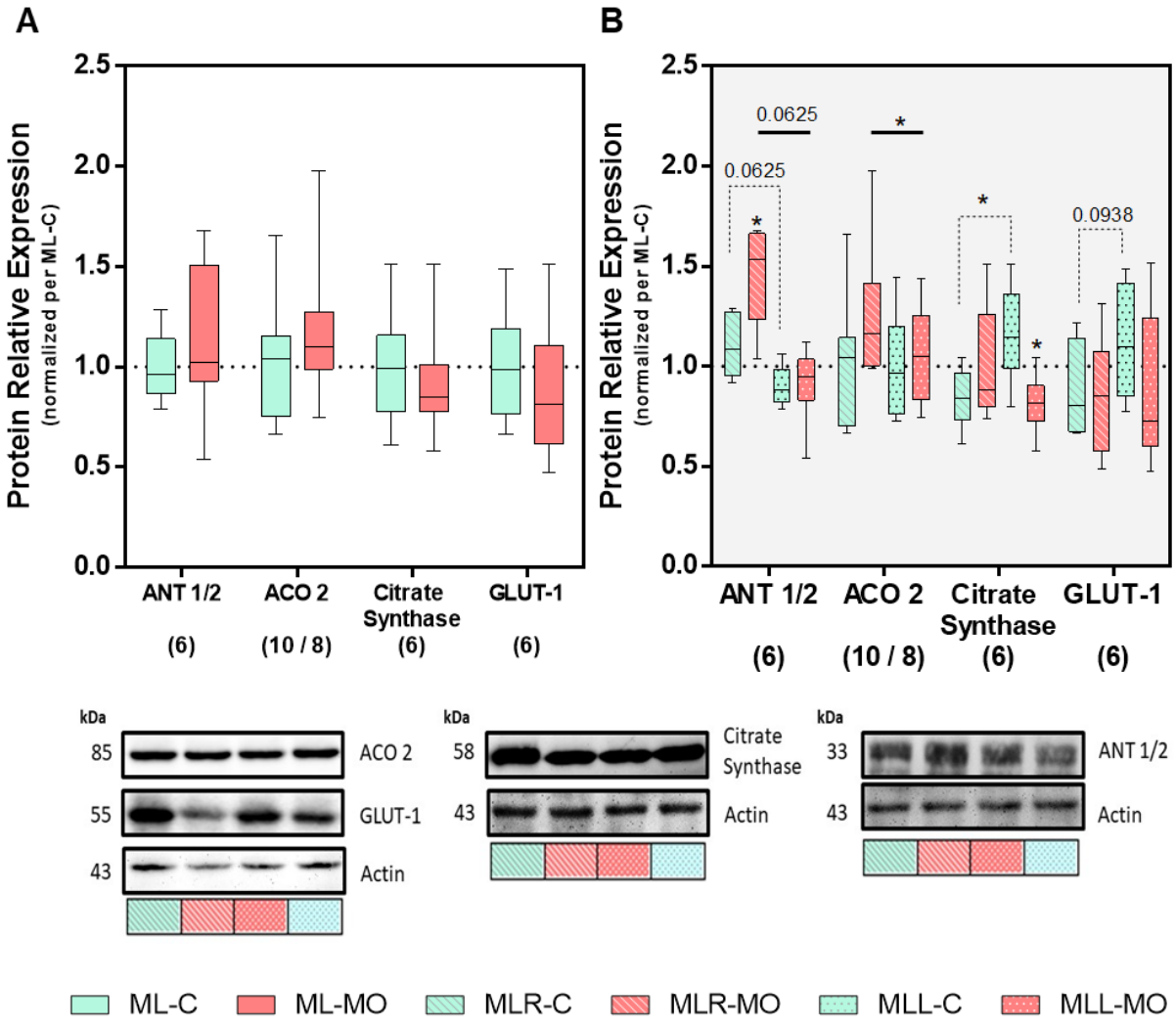

***Figure 3.4**- Metabolism-related protein expression: Adenosine nucleotide translocator 1/2 (ANT 1/2), Aconitase 2 (ACO 2, Citrate Synthase and Glucose transporter 1 (GLUT-1) levels and alterations induced by Maternal Obesity were assessed in **A:** total hepatic tissue from control group (ML-C) and maternal obesity group (ML-MO) and **B:** the contribution of each liver lobe. Data was normalized using the reference protein β-actin and the protein expression represented relative to ML-C group. The number of individuals in each group is indicated in parentheses.*
Statistical analysis: Comparison between control and maternal obesity groups was performed using unpaired t-test in ACO 2 protein expression (after performing Shapiro-Wilk normality test) and Mann-Whitney test in ANT 1/2, Citrate Synthase and GLUT-1. Comparison between lobes was assessed using paired t-test in ACO 2 and Wilcoxon test in ANT 1/2, Citrate Synthase and GLUT-1. P-value lower than 0.05 was considered significant ($p \leq 0.05$). Green/light grey bars, ML-C; Red/dark grey bars, ML-MO; diagonal line pattern, left liver lobe (MLL); dot pattern, right liver lobe (MLR). Median, interquartile distance, minimum and maximum are depicted.*

However, when a lobe-dependent analysis is performed, it is possible to observe a few differences (**Figure 3.4B**). ANT 1/2 protein expression presents a significant increase in the left lobe of obese mothers (MLL-C vs MLL-MO: median = 1.09, Q_1 = 0.954, Q_3 = 1.27 vs median = 1.53, Q_1 = 1.23, Q_3 = 1.66; p = 0.0303; g = 1.70). Citrate synthase protein expression is decreased in the right lobe of obese mothers compared with control (MLR-C vs MLR-MO: median = 1.15, Q_1 = 0.988, Q_3 = 1.36 vs median = 0.818, Q_1 = 0.723, Q_3 = 0.904; p = 0.0152; g = 1.73).

As observed in metabolism regulation-related protein expression, right and left liver lobes of control mothers present a difference in ANT 1/2 (p = 0.0625; g = 1.52), citrate synthase (p = 0.0313; g = 1.59) and GLUT-1 (p = 0.0938; g = 0.939) protein expression. Indeed, there are also differences between the right and left liver lobes of obese mothers in ANT 1/2 (p = 0.0625; g = 2.39) and ACO 2 (p = 0.0499; g = 0.785) protein levels (**Figure 3.4B**).

3.3 Effect of maternal obesity in hepatic mitochondrial function

The protein expression of different components of the mitochondrial oxidative phosphorylation complexes and ATP synthase subunits was measured to realize if the observed maternal obesity-induced metabolic remodeling was also having an effect on mitochondrial function. We observed that, in general, complexes subunits are less expressed while ATP synthase subunits are more expressed in the liver of obese mothers compared with control mothers (**Figure 3.5A**). Hepatic complex I subunit Ndufs8 expression is decreased in obese mothers (ML-C vs ML-MO: median = 0.952, Q_1 = 0.808, Q_3 = 1.20 vs median = 0.882, Q_1 = 0.696, Q_3 = 0.988; p = 0.0658; g = 0.637). This alteration in Ndufs8 expression is a result of the decrease observed notedly in the left lobe of obese mothers (MLL-C vs MLL-MO, p = 0.0245; g = 1.18) with no alterations in the right lobe (MLR-C vs MLR-MO, p = 0.6539; **Figure 3.5B**).

Complex II subunits SDHA (ML-C vs ML-MO: median = 0.841, Q_1 = 0.652, Q_3 = 1.13 vs median = 0.671, Q_1 = 0.588, Q_3 = 0.797; p = 0.0475; g = 0.792) and SDHB (ML-C vs ML-MO: median = 0.957, Q_1 = 0.640, Q_3 = 1.20 vs median = 0.304, Q_1 = 0.202, Q_3 = 0.575; p < 0.0001; g = 1.63) protein expression is also decreased in obese mothers (**Figure 3.5A**). The alteration induced in SDHA protein levels has a greater contribution from the decrease that occurs in the right lobe of obese mothers (MLR-C vs MLR-MO, p = 0.0179; g = 1.25) while the left lobe presents no variation (p = 0.6539; **Figure 3.5B**) between experimental groups. SDHB protein expression presents a decrease in both lobes of obese mothers comparing with their control counterparts (MLL-C vs MLL-MO: p = 0.0002, g = 2.25; MLR-C vs MLR-MO: p = 0.0011, g = 1.92).

Regarding Complex III subunits expression, different behaviors were observed (**Figure 3.5A**). UQCRC1 (p = 0.1302) and UQCRC2 (p = 0.5599) show no alteration in protein levels, either in total liver tissue or when separated by lobes, caused by the

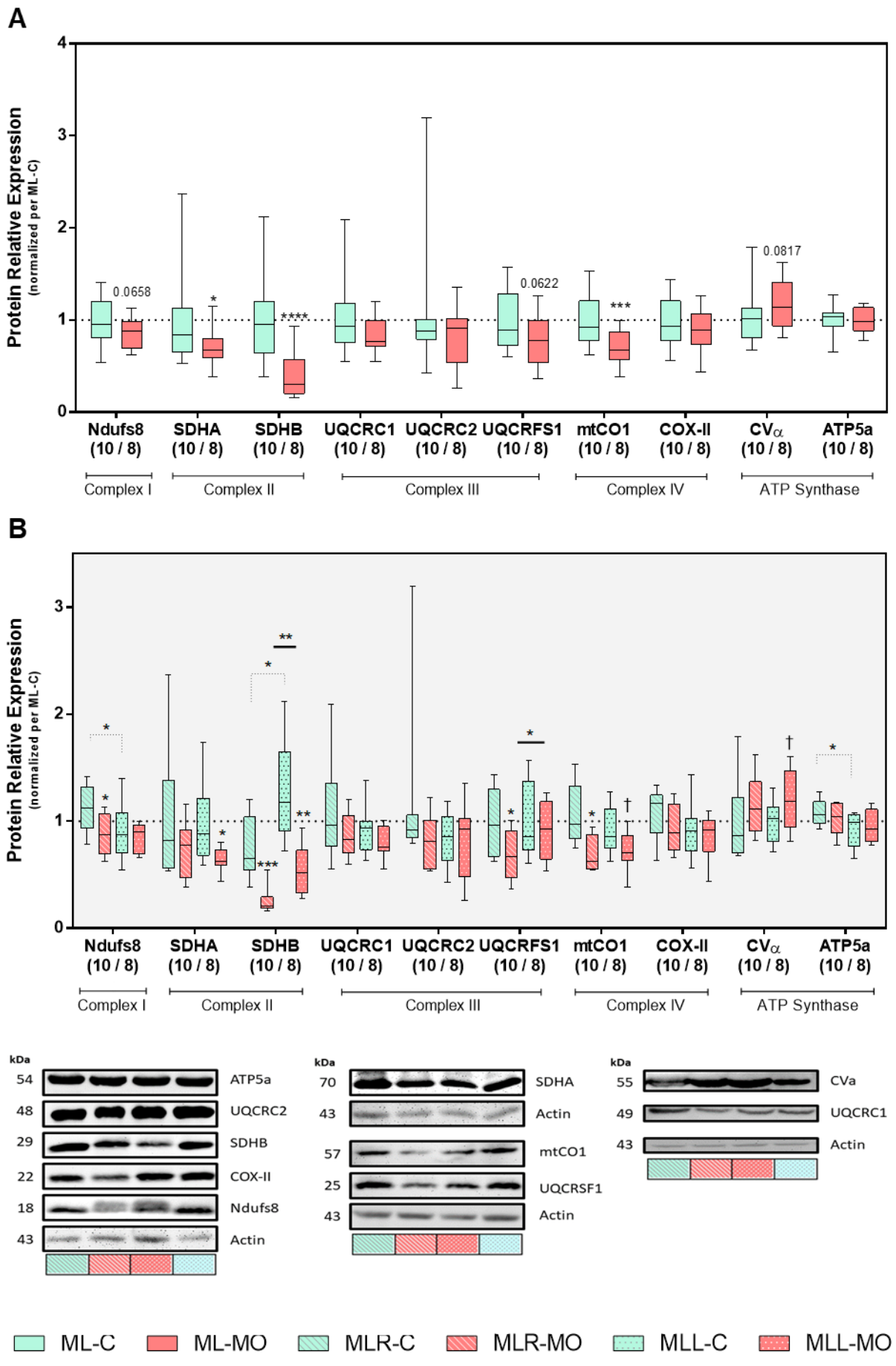
A
Protein Relative Expression
(normalized per ML-C)
0.0658
0.0622
0.0817
Ndufs8 (10 / 8)
SDHA (10 / 8)
SDHB (10 / 8)
UQCRC1 (10 / 8)
UQCRC2 (10 / 8)
UQCRFS1 (10 / 8)
mtCO1 (10 / 8)
COX-II (10 / 8)
CVα (10 / 8)
ATP5a (10 / 8)
Complex I
Complex II
Complex III
Complex IV
ATP Synthase
B
Protein Relative Expression
(normalized per ML-C)
kDa
54 ATP5a
48 UQCRC2
29 SDHB
22 COX-II
18 Ndufs8
43 Actin
70 SDHA
43 Actin
57 mtCO1
25 UQCRSF1
43 Actin
55 CVa
49 UQCRC1
43 Actin
ML-C
ML-MO
MLR-C
MLR-MO
MLL-C
MLL-MO

experimental conditions. UQCRFS1 expression is decreased (ML-C vs ML-MO: median = 0.887, Q_1 = 0.726, Q_3 = 1.28 vs median = 0.777, Q_1 = 0.542, Q_3 = 0.991; p = 0.0622; g = 0.670). These differences in UQCRFS1 expression are a result of the specific decrease in the left lobe of obese mothers (MLL-C vs MLL-MO, p = 0.0385; g = 1.12). This protein expression in the liver right lobe remains constant (MLR-C vs MLR-MO, p = 0.5575; **Figure 3.5B**) in all experimental conditions.

The maternal obesity-induced changes in complex IV are similar to the observed for complex III (**Figure 3.5**). COX-II expression is unaltered between experimental groups, either when total liver tissue is considered (ML-C vs ML-MO, p = 0.1940) or each lobe is measured separately. mtCO1 protein levels are lower in obese mothers than in control mothers (ML-C vs ML-MO: median = 0.924, Q_1 = 0.778, Q_3 = 1.21 vs median = 0.672, Q_1 = 0.569, Q_3 = 0.867; p = 0.0007; g = 1.30). This tendency is also observed when liver lobes are compared separately (MLL-C vs MLL-MO, p = 0.0104, g = 1.62; MLR-C vs MLR-MO, p = 0.0639, g = 0.968).

ATP Synthase subunits expression was also affected by excessive food intake that leads to obesity during pregnancy (**Figure 3.5A**). CVα levels are increased in obese mothers compared with the control ones (ML-C vs ML-MO: median = 1.02, Q_1 = 0.805, Q_3 = 1.13 vs median = 1.14, Q_1 = 0.938, Q_3 = 1.41; p = 0.0817; g = 0.615). However, ATP5a subunit expression is similar in both experimental groups (ML-C vs ML-MO, p = 0.8638). The increased expression of CVα in obese mothers has a greater share of the impact of the maternal obesity on the right lobe of obese mothers (MLR-C vs MLR-MO, p = 0.0841; g = 0.872; **Figure 3.5B**).

The expression of the assessed mitochondrial proteins is different in the right and left liver lobes of control mothers (**Figure 3.5B**). Ndufs8 and ATP5a protein expression is higher in the left lobe when compared with the right lobe (MLL-C vs MLR-C, p = 0.0241, g = 0.987; p = 0.0391, g = 1.11; respectively), while SDHB presents the opposite behavior (MLL-C vs MLR-C, p = 0.0121; g = 1.33). Furthermore, protein expression in both lobes is also different in the excessive food intake group with SDHB and UQCRFS1 expression being higher in the right lobe when compared to the left (MLL-MO vs MLR-MO, p = 0.0078, g = 1.56; p = 0.0477, g = 0.920; respectively).

Figure 3.5 (previous page)- *Oxidative phosphorylation complexes subunits protein expression: Complex I (Ndufs8), Complex II (SDHA, SDHB), Complex III (UQCRC1, UQCRC2, UQCRFS1), complex IV (mtCO1, COX-II), and ATP Synthase (CVα, ATP5a) levels, and alterations induced by Maternal Obesity in* ***A:*** *total hepatic tissue from control group (ML-C) and maternal obesity group (ML-MO) and* ***B:*** *the contribution of each liver lobe. Data was normalized using the reference protein β-actin and the protein expression represented relative to ML-C group. The number of individuals in each group is indicated in parentheses.*
Statistical analysis: Comparison between control and maternal obesity groups was performed using unpaired t-test except for the groups that did not passed Shapiro-Wilk normality test (ML-C: SDHA, UQCRC1, UQCRC2, CVα; ML-MO: SDHB; MLR-C: ATP5a; MLL-C: SDHA, UQCRC2; MLL_MO: SDHB, mtCO1) in which was performed Mann-Whitney test. Comparison between lobes was assessed using paired t-test or Wilcoxon test according to the normality of the groups compared. P-value lower than 0.10 was registered († $p \leq 0.10$) and lower than 0.05 was considered significant ($p \leq 0.05$; ** $p \leq 0.01$; *** $p \leq 0.001$; **** $p \leq 0.0001$). Green/light grey bars, ML-C; Red/dark grey bars, ML-MO; diagonal line pattern, left liver lobe (MLL); dot pattern, right liver lobe (MLR). Median, interquartile distance, minimum and maximum are depicted.*

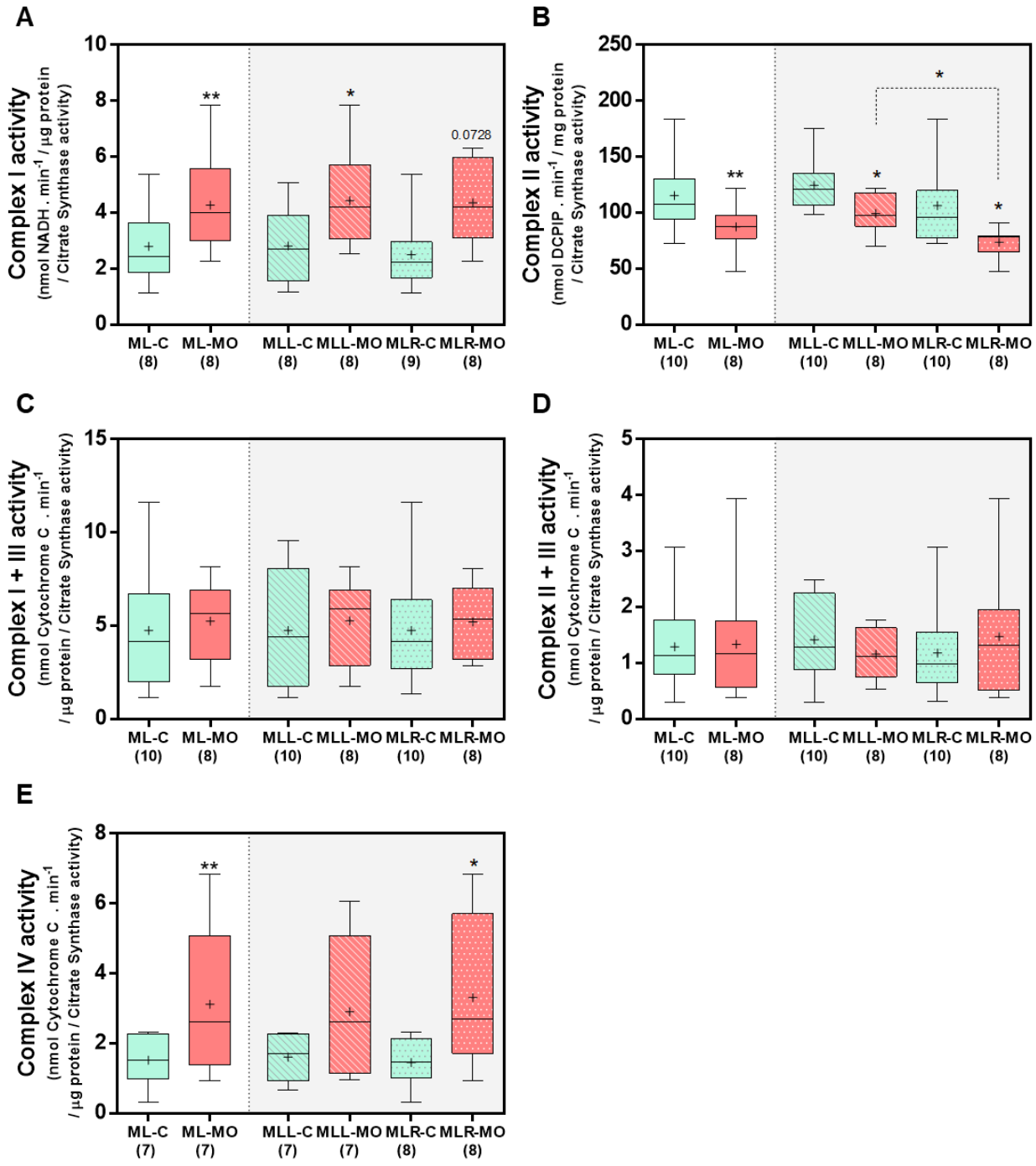

***Figure 3.6**- Oxidative phosphorylation complexes activities: **A**: Complex I, **B**: Complex II, **C**: Complex I+III, **D**: Complex II+III, and **E**: Complex IV activities in total hepatic tissue from control group (ML-C) and maternal obesity group (ML-MO) and the contribution of each liver lobe. Data is represented in Units normalized per mass of protein used in each assay and by the mitochondrial mass marker citrate synthase. The number of individuals in each group is indicated in parentheses.*
Statistical analysis: Comparison between control and maternal obesity groups was performed using unpaired t-test in A, B, C, and D (after performing Shapiro-Wilk normality test) and Mann-Whitney test in E. Comparison between lobes was assessed using paired t-test or Wilcoxon test according to the normality of the groups compared. P-value lower than 0.05 was considered significant ($p \leq 0.05$; ** $p \leq 0.01$). Green/light grey bars, ML-C; Red/dark grey bars, ML-MO; diagonal line pattern, left liver lobe (MLL); dot pattern, right liver lobe (MLR). Median, mean (+), interquartile distance, minimum and maximum are depicted.*

Since OXPHOS proteins expression is affected by maternal obesity their activity might also be altered. Therefore, each complexes' maximal activity was determined (**Figure 3.6**). Complex I activity was increased by maternal obesity (ML-C vs ML-MO: median = 2.43, Q_1 = 1.84, Q_3 = 3.62 vs median = 3.99, Q_1 = 3.00, Q_3 = 5.59; p = 0.0072; g = 0.992; **Figure 3.6A**). This behavior is consistent in liver lobes, with a significant increase in both left (MLL-C vs MLL-MO: median = 2.71, Q_1 = 1.55, Q_3 = 3.91 vs median = 4.19, Q_1 = 3.05, Q_3 = 5.70; p = 0.0139; g = 0.998) and right lobe (MLR-C vs MLR-MO: median = 2.22, Q_1 = 1.67, Q_3 = 2.96 vs median = 4.20, Q_1 = 3.10, Q_3 = 5.97; p = 0.0728; g = 1.35).

Complex II activity is also different in the two experimental groups (**Figure 3.6B**). In total liver tissue complex II activity was 20% decreased by maternal obesity (ML.C vs ML-MO: median = 108, Q_1 = 94.1, Q_3 = 130 vs median = 87.1, Q_1 = 77.1, Q_3 = 97.7; p = 0.0048; g = 1.04). Indeed, decreased complex II activity is equally observed in left (MLL-C vs MLL-MO: median = 121, Q_1 = 106, Q_3 = 135 vs median = 97.3, Q_1 = 87.5, Q_3 = 118; p = 0.0234; g = 1.19) and right (MLR-C vs MLR-MO: median = 95.9, Q_1 = 77.4, Q_3 = 120 vs median = 78.6, Q_1 = 64.8, Q_3 = 79.0; p = 0.0401; g = 1.13) liver lobes. There are also differences between the right and the left liver lobes complex II activity in the ML-MO group (MLL-MO vs MLR-MO, p = 0.0105; g = 1.60).

The combined activity of complex I and complex III was evaluated (**Figure 3.6C**). No alterations were found due to excessive food intake either in total liver tissue (ML-C vs ML-MO, p = 0.5729) or when each lobe was considered separately. The combined activity of complex III and complex II was also measured (**Figure 3.6D**) again with no difference between the experimental groups (ML-C vs ML-MO, p = 0.8711).

Regarding complex IV, an increased activity was observed in in maternal obesity group (ML-C vs ML-MO: median = 1.50, Q_1 = 0.981, Q_3 = 2.27 vs median = 2.62, Q_1 = 1.38, Q_3 = 5.07; p = 0.0093; g = 1.06; **Figure 3.6E**), mainly due to the increased complex IV activity on right lobe of obese mothers (MLR-C vs MLR-MO: median = 1.46, Q_1 = 0.997, Q_3 = 2.12 vs: median = 2.71, Q_1 = 1.71, Q_3 = 5.71; p = 0.0207; g = 1.14).

The hypothesis was raised that the observed differences between complexes subunits expression and their activity might be caused by mitochondrial mass alterations. Since there is no single method completely reliable to measure mitochondrial mass in frozen tissue, three different approaches were used: mtDNA copy number determination; citrate synthase activity measurement; and mitochondria-related protein expression quantification.

No differences were observed between ML-C and ML-MO in the mtDNA copy number (p = 0.6935) or in citrate synthase activity (p = 0.4635), either considering the liver as a whole or each lobe individually (**Figure 3.7A, B**). Accordingly, the same protein expression levels were observed for the mitochondrial Cyclophilin D (Cyc D; p = 0.1506), Cytochrome C (Cyt C; p = 0.6928), TOM 20 – translocase of outer mitochondrial membrane 20 (p = 0.1957) and VDAC – voltage dependent anion channel (p = 0.8715; **Figure 3.7C**) in ML-C and ML-MO experimental groups.

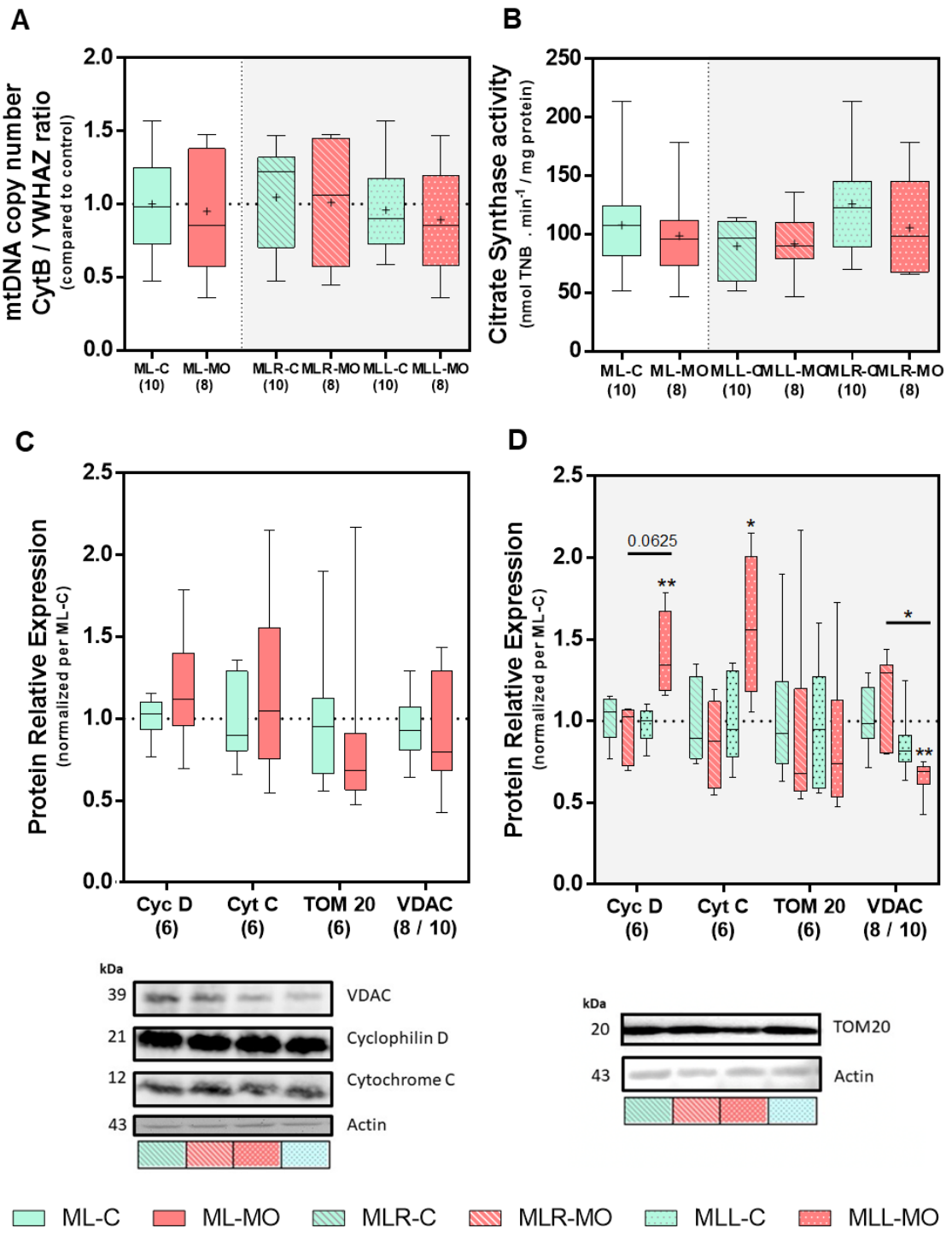

Figure 3.7 *- Mitochondrial mass indicators modulation in maternal obesity measured by* ***A:*** *mtDNA copy number,* ***B:*** *Citrate synthase activity and mitochondrial specific-protein expression (Cyc C, Cyt C, TOM20, VDAC) in* ***C:*** *total hepatic tissue from control group (ML-C) and maternal obesity group (ML-MO) and* ***D:*** *the contribution of each liver lobe. Data from western blot was normalized using the reference protein β-actin or normalized per mass of protein in Citrate synthase activity. On* ***B****, data is represented relative to ML-C group. The number of individuals in each group is indicated in parentheses.*

Statistical analysis: Comparison between control and maternal obesity groups was performed using unpaired t-test except for the groups that did not passed Shapiro-Wilk normality test (ML-MO: TOM20) in which was performed Mann-Whitney test. Comparison between lobes was assessed using Wilcoxon test. P-value lower than 0.10 was registered and lower than 0.05 was considered significant ($p \leq 0.05$; ** $p \leq 0.01$). Green/light grey bars, ML-C; Red/dark grey bars, ML-MO; diagonal line pattern, left liver lobe (MLL); dot pattern, right liver lobe (MLR). Median, mean (+), interquartile distance, minimum and maximum are depicted.*

However, when only the liver right lobe is considered, an increased expression of Cyc D (MLR-C vs MLR-MO, p = 0.0043; g = 2.19) and Cyt C (MLR-C vs MLR-MO, p = 0.0381; g = 1.56), and a decreased expression of VDAC (MLR-C vs MLR-MO, p = 0.0046; g = 1.42) were observed in the maternal obese group (**Figure 3.7D**). Indeed, these results reveal a mitochondrial dichotomy between both lobes and were corroborated by the differences in the ML-MO group in Cyc D (MLL-MO vs MLR-MO, p = 0.0625; g = 2.21) and VDAC (MLL-MO vs MLR-MO, p = 0.0156; g = 2.64) expression.

Since no alterations in mitochondrial mass were observed between ML-C and ML-MO we evaluated also mitochondrial dynamics. An increase in Mitofusin-1 (Mfn-1) protein expression was observed in ML-MO (ML-C vs ML-MO: median = 1.00, Q_1 = 0.793, Q_3 = 1.11 vs median = 1.22, Q_1 = 0.899, Q_3 = 1.33; p = 0.0775; g = 0.768; **Figure 3.8A**). This result is mainly driven by significant differences of Mfn-1 expression in the liver left lobe (MLL-C vs MLL-MO; p = 0.0022; g = 2.57; **Figure 3.8A, B**). Surprisingly, OPA-1 protein expression was decreased in the liver of obese mothers (ML-C vs ML-MO: median = 0.875, Q_1 = 0.728, Q_3 = 1.11; ML-MO vs median = 0.393, Q_1 = 0.265, Q_3 = 0.523; p = 0.0011; g = 1.39). This behavior was observed both in the left (MLL-C vs MLL-MO, p = 0.0556; g = 1.48) and right (MLR-C vs MLR-MO, p = 0.0022; g = 3.71) liver lobes (**Figure 3.8A, B**). Moreover, in hepatic tissue of obese mothers, OPA-1 expression is lower in the liver right lobe than in the left lobe (MLL-MO vs MLR-MO, p = 0.0625; g = 2.10).

On the other hand, Fis-1 protein expression was increased in the liver of obese mothers (ML-C vs ML-MO: median = 1.03, Q_1 = 0.818, Q_3 = 1.13 vs median = 1.03, Q_1 = 0.965, Q_3 = 1.69; p = 0.0490; g = 0.693). This is mostly caused by differences in Fis-1 expression in the liver left lobe (MLL-C vs MLL-MO, p = 0.0918; g = 0.858; **Figure 3.8A, B**). The balance between mitochondrial fusion and fission is indeed affected by excessive food intake during pregnancy, as assessed by the OPA-1/Fis-1 protein expression ratio (**Figure 3.8C**). This ratio is decreased in the hepatic tissue of obese mothers (ML-C vs ML-MO: median = 0.785, Q_1 = 0.616, Q_3 = 1.42 vs median = 0.256, Q_1 = 0.195, Q_3 = 0.464; p < 0.0001; g = 1.61) and the same is observed when left (MLL-C vs MLL-MO, p = 0.0043; g = 1.47) or right (MLR-C vs MLR-MO, p = 0.0043; g = 2.26) liver lobes are considered.

Mitochondrial Biogenesis was also assessed and no differences in PGC-1α (ML-C vs ML-MO, p = 0.2328) and TFAM (ML-C vs ML-MO, p = 0.8353) protein expression were found between experimental groups when both liver lobes were considered together (Figure 3.8A). However, both proteins present an increased protein expression specifically in the liver left lobe when comparing MLL-MO with MLL-C (MLL-C vs, MLL-MO, PGC-1α: p = 0.0190, g = 1.91; TFAM: p = 0.0519, g = 1.19; **Figure 3.8B**).

3.4 Maternal obesity induces oxidative stress

Excessive nutrient consumption is related with an increase in metabolism rate, e.g. mitochondrial oxidative phosphorylation. During this process an increase in ROS

production might occur. ROS can react with biomolecules causing damage, such as lipid peroxidation. An increase in lipid peroxidation, indicated by MDA levels, was observed in the hepatic tissue of obese mothers (ML-C vs ML-MO: median = 8.22, Q_1 =6.73, Q_3 = 9.53 vs median = 12.1, Q_1 = 9.23, Q_3 = 14.2; p = 0.0015; g = 1.31; **Figure 3.9A**). This alteration is similar in both left (MLL-C vs MLL-MO, p = 0.0165; g = 1.559) and right (MLR-C vs MLR-MO, p = 0.0449; g = 1.03) liver lobes (**Figure 3.9A**).

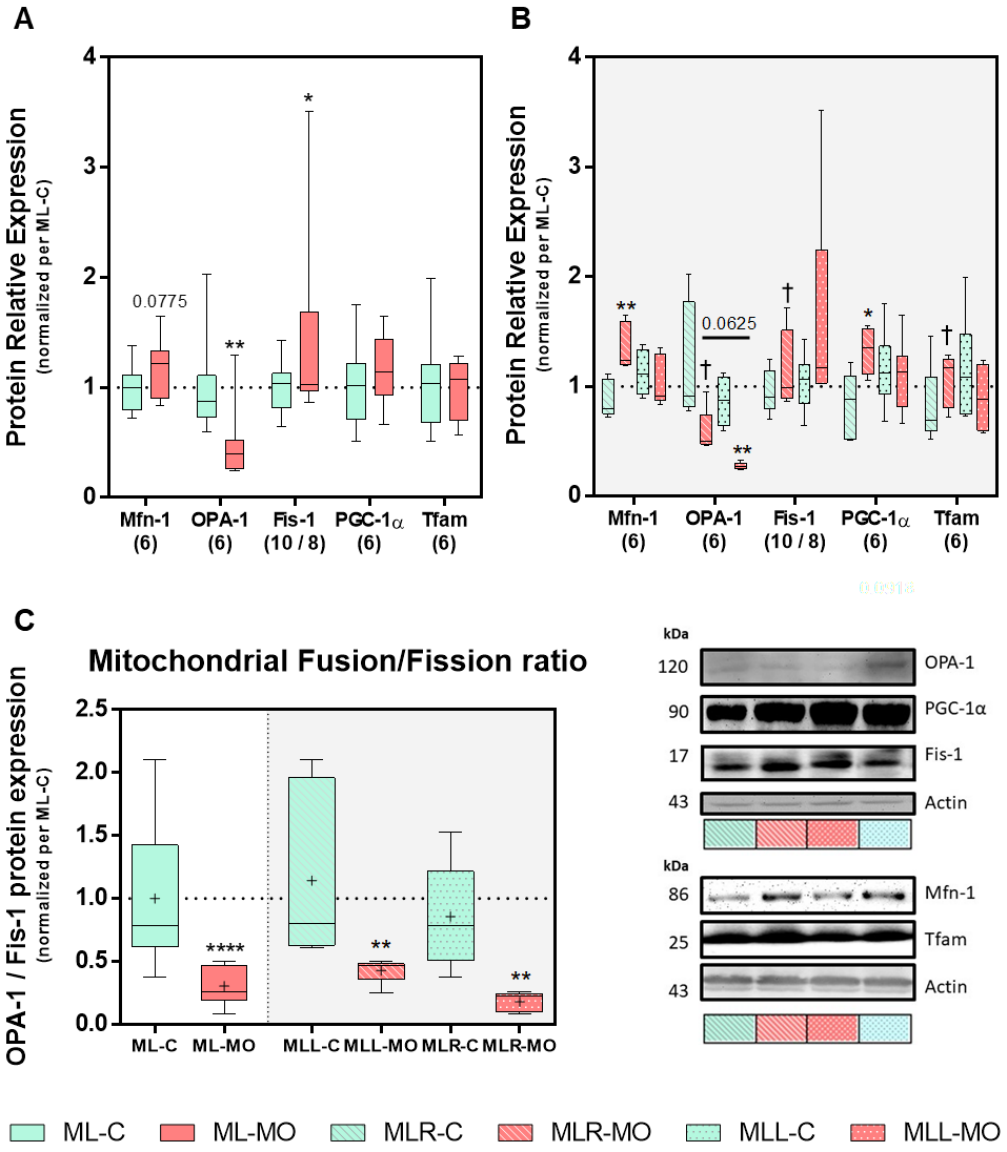

***Figure 3.8**- Mitochondrial dynamics alterations induced by Maternal Obesity by protein expression **A:** in total liver tissue from control group (ML-C) and maternal obesity group (ML-MO), and **B:** the contribution of each lobe, and **C:** mitochondrial fusion/fission ratio. Data was normalized using the reference protein β-actin and the protein expression represented relative to ML-C group. The number of individuals in each group is indicated in parentheses.*
Statistical analysis: Comparison between control and maternal obesity groups was performed using Mann-Whitney test except for Fis-1 in which was used unpaired t-test after passed Shapiro-Wilk normality test. Comparison between lobes was assessed using Wilcoxon test except for Fis-1 in which was performed the unpaired t-test. P-value lower than 0.10 was registered († $p \leq 0.10$) and lower than 0.05 was considered significant ($p \leq 0.05$; ** $p \leq 0.01$; **** $p \leq 0.0001$). Green/light grey bars, ML-C; Red/dark grey bars, ML-MO; diagonal line pattern, left liver lobe (MLL); dot pattern, right liver lobe (MLR). Median, mean (+), interquartile distance, minimum and maximum are depicted.*

When exposed to increased levels of ROS, cells activated several mechanisms, such as GSH oxidation to GSSG, in order to prevent oxidative stress. A decrease in the GSH/GSSG ratio was found in the hepatic tissue of obese mothers (ML-C vs ML-MO: median = 4.99, Q_1 = 3.08, Q_3 = 34.5 vs median = 2.21, Q_1 = 1.71, Q_3 = 5.42; p = 0.0685; g = 0.931; **Figure 3.9B**).This difference is mainly caused by an increase in GSSG levels in ML-MO (ML-C vs ML-MO: median = 8.53, Q_1 = 2.82, Q_3 = 13.2 vs median = 13.4, Q_1 = 8.81, Q_3 = 23.6; p = 0.0903; g = 0.740; **Figure 3.9D**) without alterations in hepatic GSH levels due to maternal nutrition (ML-C vs ML-MO, p = 0.2432; **Figure 3.9C**).

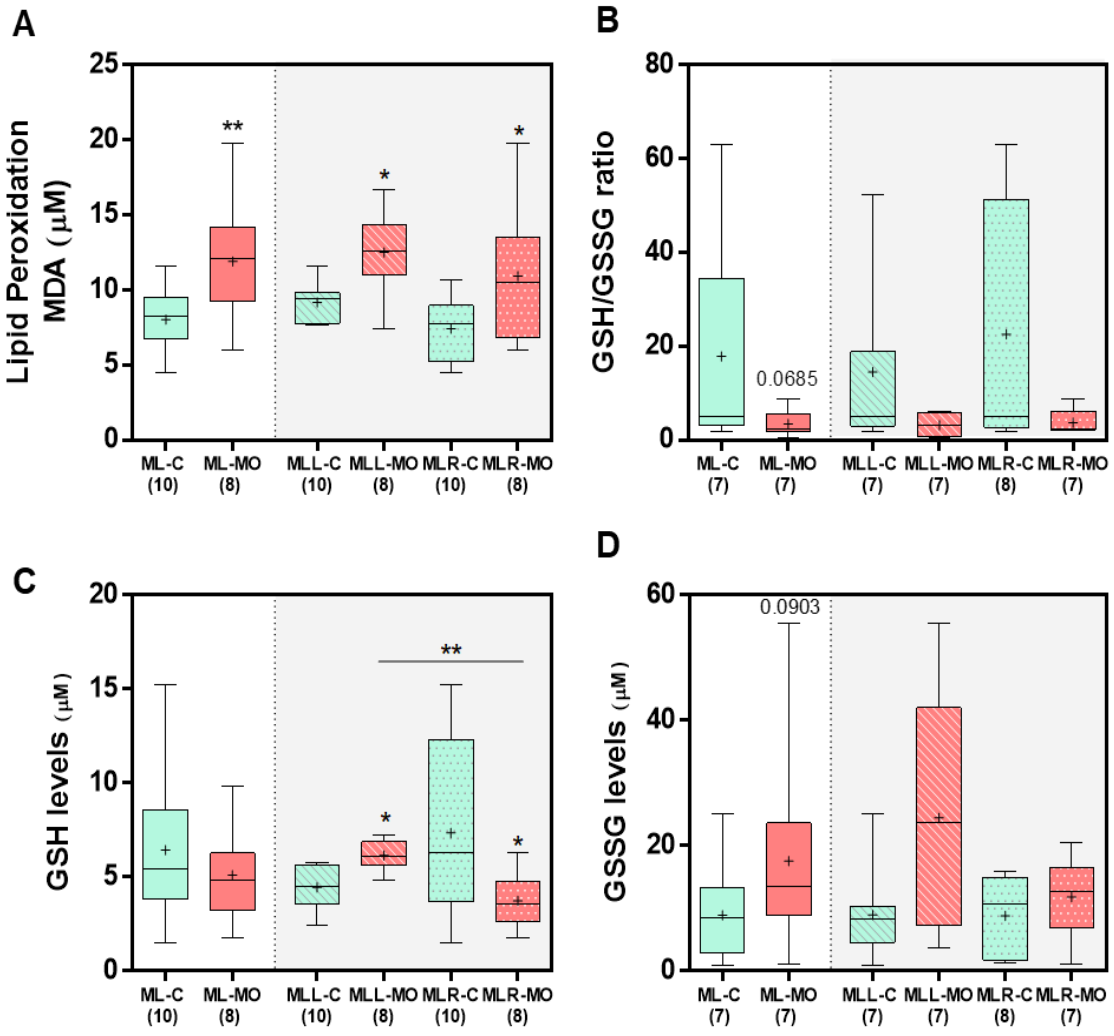

Figure 3.9 *– Maternal obesity increase ROS formation measured by* ***A:*** *lipid peroxidation levels and* ***B:*** *GSH/GSSG ratio obtained from* ***C:*** *GSH and* ***D:*** *GSSG levels. Data is represented in absolute concentrations. The number of individuals in each group is indicated in parentheses.*
Statistical analysis: comparison between control and maternal obesity groups was performed using unpaired t-test after passed Shapiro-Wilk normality test in ***A*** *and* ***C*** *and using Mann-Whitney test in* ***B*** *and* ***D****. Comparison between lobes was assessed using unpaired t-test or Wilcoxon test according to normality of the results. P-value lower than 0.10 was registered and lower than 0.05 was considered significant (* $p \leq 0.05$; ** $p \leq 0.01$). Green/light grey bars, ML-C; Red/dark grey bars, ML-MO; diagonal line pattern, left liver lobe (MLL); dot pattern, right liver lobe (MLR). Median, mean (+), interquartile distance, minimum and maximum are depicted.*

Interestingly, a contrasting behavior is observed in GSH levels when the comparison is performed in a lobe-dependent manner (**Figure 3.9C)**. In the left lobe GSH levels are increased (MLL-C vs MLL-MO, p = 0.0176; g = 1.60) in obese mothers, while in the right lobe they are decreased (MLR-C vs MLR-MO, p = 0.0494; g = 1.01) comparing with the respective lobes of control mothers. A statistically significant difference was also observed between MLL-MO and MLR-MO (MLL-MO vs MLR-MO, p = 0.0025; g = 2.04).

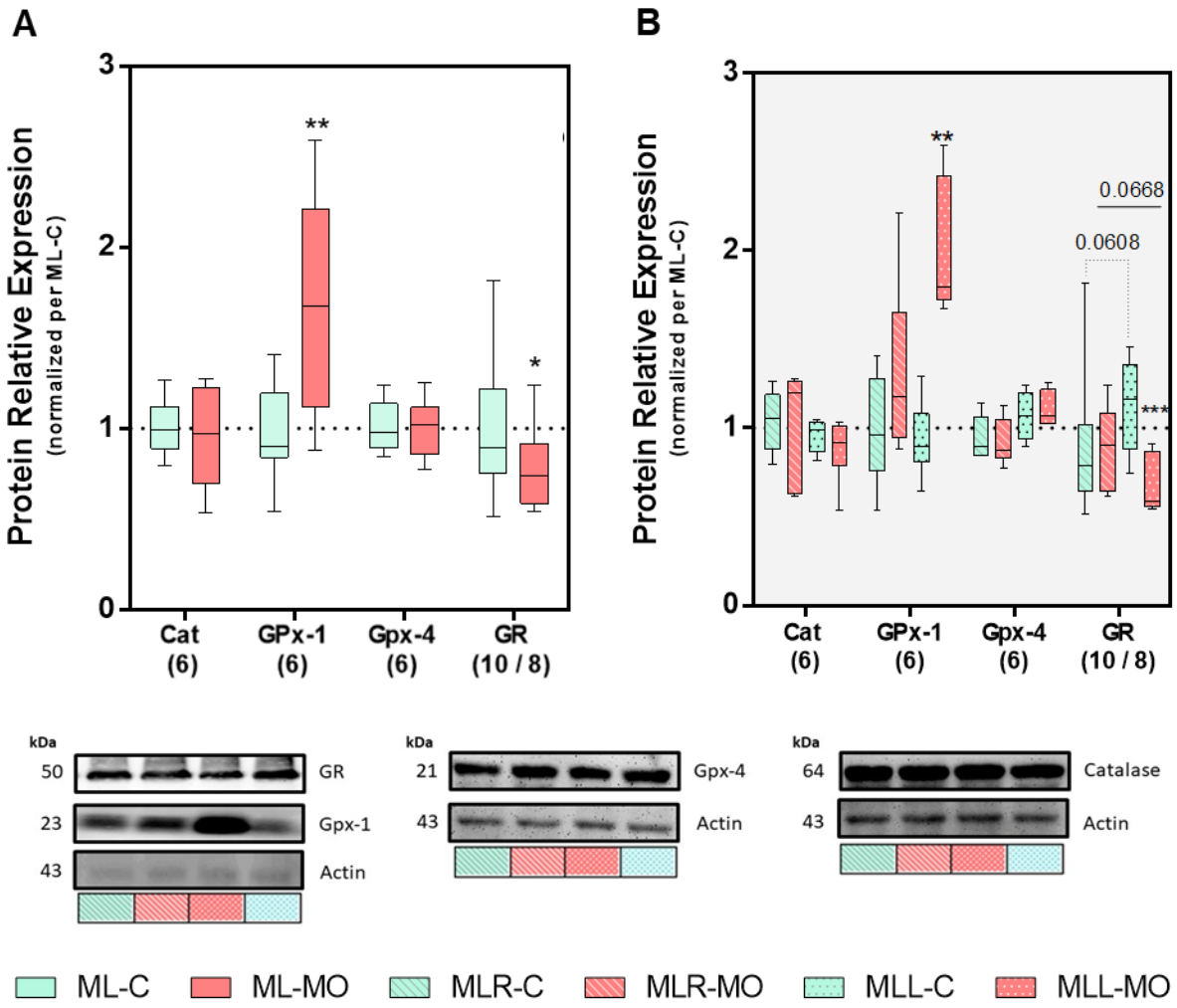

Figure 3.10 *– Antioxidant defense enzymes protein expression in maternal obesity* ***A:*** *in total liver tissue from control group (ML-C) and maternal obesity group (ML-MO), and* ***B:*** *the contribution of each lobe. Data was normalized using the reference protein β-actin and the protein expression represented relative to ML-C group. The number of individuals in each group is indicated in parentheses.*
Statistical analysis: Comparison between control and maternal obesity groups was performed using Mann-Whitney test except for GR in which was used unpaired t-test after passed Shapiro-Wilk normality test. Comparison between lobes was assessed using Wilcoxon test except for GR in which was performed the unpaired t-test. P-value lower than 0.10 was registered and lower than 0.05 was considered significant ($p \leq 0.05$; ** $p \leq 0.01$; *** $p \leq 0.001$). Green/light grey bars, ML-C; Red/dark grey bars, ML-MO; diagonal line pattern, left liver lobe (MLL); dot pattern, right liver lobe (MLR). Median, interquartile distance, minimum and maximum are depicted.*

Hepatic antioxidant defense enzymes protein expression is also modified by maternal obesity (**Figure 3.10**). Glutathione peroxidase 1 hepatic expression is increased in maternal obesity (ML-C vs ML-MO: median = 0.897, Q_1 = 0.840, Q_3 = 1.20 vs median = 1.67, Q_1 = 1.12, Q_3 = 2.21; p = 0.0017; g = 1.54; **Figure 3.10**). This variation is mainly caused by the increase in protein expression in the right lobe (MLR-C vs MLR-MO, p = 0.0043; g = 3.46). In opposition, glutathione reductase protein expression is decreased in ML-MO (ML-C vs ML-MO: median = 0.894, Q_1 = 0.754, Q_3 = 1.22 vs median = 0.739, Q_1 = 0.585, Q_3 = 0.918; p = 0.0335; g = 0.742) compared with ML-C. Again, the variation is mainly due to a decrease in protein expression in the right lobe (MLR-C vs MLR-MO, p = 0.0007; g = 1.99). Moreover, glutathione reductase protein levels are already different between both lobes of control mothers (MLL-C vs MLR-C, p = 0.0608; g = 0.724), a variation that is also observed after maternal obesity stimulus (MLL-MO vs MLR-MO, p = 0.0668; g = 1.02). Hepatic catalase (ML-C vs ML-MO, p = 0.7857) and glutathione peroxidase 4 (ML-C vs ML-MO, p = 0.7917) expression are not altered by excessive food consumption, either when liver lobes are considered together or separately.

An increase in liver SOD activity was observed in ML-MO compared with ML-C (ML-C vs ML-MO: median = 0.650, Q_1 = 0.310, Q_3 = 0.874 vs median = 0.908, Q_1 = 0.631, Q_3 = 1.06; p = 0.0347; g = 0.894; **Figure 3.11A**), mainly resulting from the variation observed in the liver right lobe (MLR-C vs MLR-MO, p = 0.0825; g = 1.04). Catalase activity is decreased in ML-MO compared with ML-C (ML-C vs ML-MO: median = 1708, Q_1 = 1457, Q_3 = 1973 vs median = 1458, Q_1 = 875, Q_3 = 1755; p = 0.0281; g = 0.770; **Figure 3.11B**) when considering both liver lobes. The decrease in the left lobe has the greater impact in this variation (MLL-C vs MLL-MO, p = 0.0428; g = 1.05). Concerning catalase activity, obesity during pregnancy had a more pronounced effect in the hepatic left lobe with (MLL-MO vs MLR-MO, p = 0.0526; g = 0.945).

The liver glutathione system is also compromised by maternal obesity. Glutathione peroxidase (ML-C vs ML-MO: median = 105, Q_1 = 90.3, Q_3 = 133 vs median = 89.0, Q_1 = 75.9, Q_3 = 110; p = 0.0843; g = 0.803; **Figure 3.11C**) and glutathione reductase (ML-C vs ML-MO: median = 100, Q_1 = 86.8, Q_3 = 119 vs median = 75.6, Q_1 = 70.9, Q_3 = 88.9; p = 0.0666; g = 0.602; **Figure 3.11D**) activities are decreased in ML-MO compared with ML-C. In the case of glutathione reductase, the observed effect is mostly a result of the decreased activity in the right lobe induced by maternal obesity (MLR-C vs MLR-MO, p = 0.0023; g = 0.935). The non-enzymatic antioxidant defense Vitamin E concentrations present no hepatic alteration in the experimental groups (ML-C vs ML-MO, p = 0.8143).

3.5 Maternal obesity changes hepatic autophagy

Cellular oxidative stress is associated with increased cellular damage, mostly in mitochondria, the main source of ROS. When damaged biomolecules start to accumulate, cells try to degrade them in order to maintain homeostasis. One of the processes responsible for controlled cellular biomolecules degradation is autophagy.

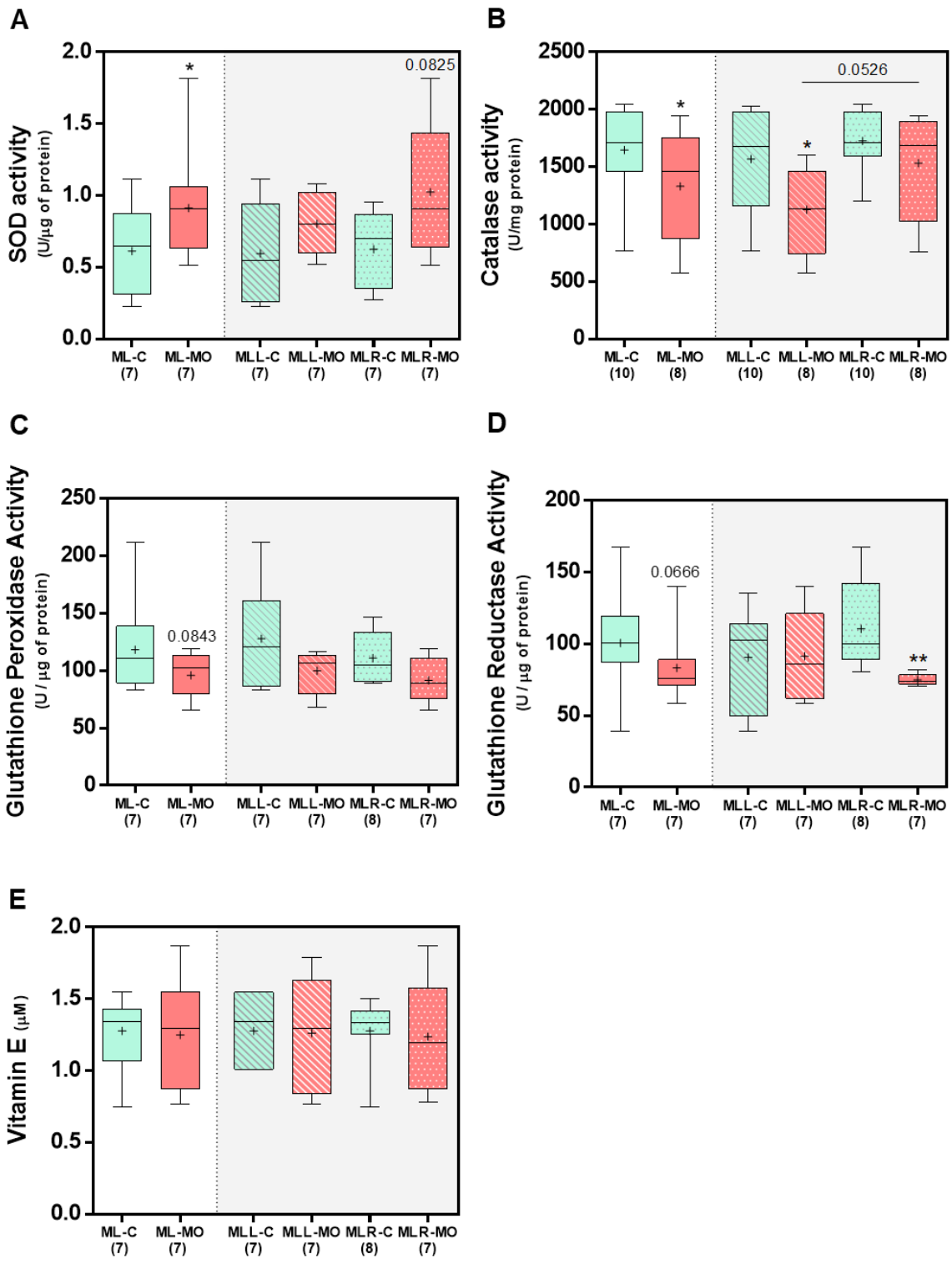

***Figure 3.11**- Maternal obesity induces alterations in antioxidant defense both enzymatic **A:** SOD; **B:** Catalase, **C:** Glutathione Peroxidase, and **D** Glutathione Reductase activities, and non-enzymatic **E:** Vitamin E levels. Data is represented in Units normalized per mass of protein used in each assay in enzymatic protein and in absolute concentration in **E**. The number of individuals in each group is indicated in parentheses.*
*Statistical analysis: comparison between control and maternal obesity groups was performed using Mann-Whitney test except for **A** and **B** in which was used unpaired t-test after passed Shapiro-Wilk normality test. Comparison between lobes was assessed using Wilcoxon test except for **A** and **B** in which was performed the unpaired t-test. P-value lower than 0.10 was registered and lower than 0.05 was considered significant (* $p \leq 0.05$; ** $p \leq 0.01$). Green/light grey bars, ML-C; Red/dark grey bars, ML-MO; diagonal line pattern, left liver lobe (MLL); dot pattern, right liver lobe (MLR). Median, mean (+), interquartile distance, minimum and maximum are depicted.*

An increase in the LC3-II/LC3-I ratio was observed in the hepatic tissue of obese mothers (ML-C vs ML-MO: median = 0.864, Q_1 = 0.632, Q_3 = 1.50 vs median = 3.15, Q_1 = 2.54, Q_3 = 4.85; $p < 0.0001$; g = 2.48; **Figure 3.12C**). This difference is equally observed in the left (MLL-C vs MLL-MO, $p < 0.0001$; g = 3.29) and right (MLR-C vs MLR-MO, p = 0.0005; g = 2.14) liver lobes. No alteration was observed in LC3-I expression (ML-C vs ML-MO, p = 0.1842; **Figure 3.12A**) due to maternal nutrition. Increase LC3-II levels are responsible for the observed changes in the LC3-II/LC3-I ratio (ML-C vs ML-MO: median = 0.946, Q_1 = 0.687, Q_3 = 1.36; vs median = 3.17, Q_1 = 2.50,

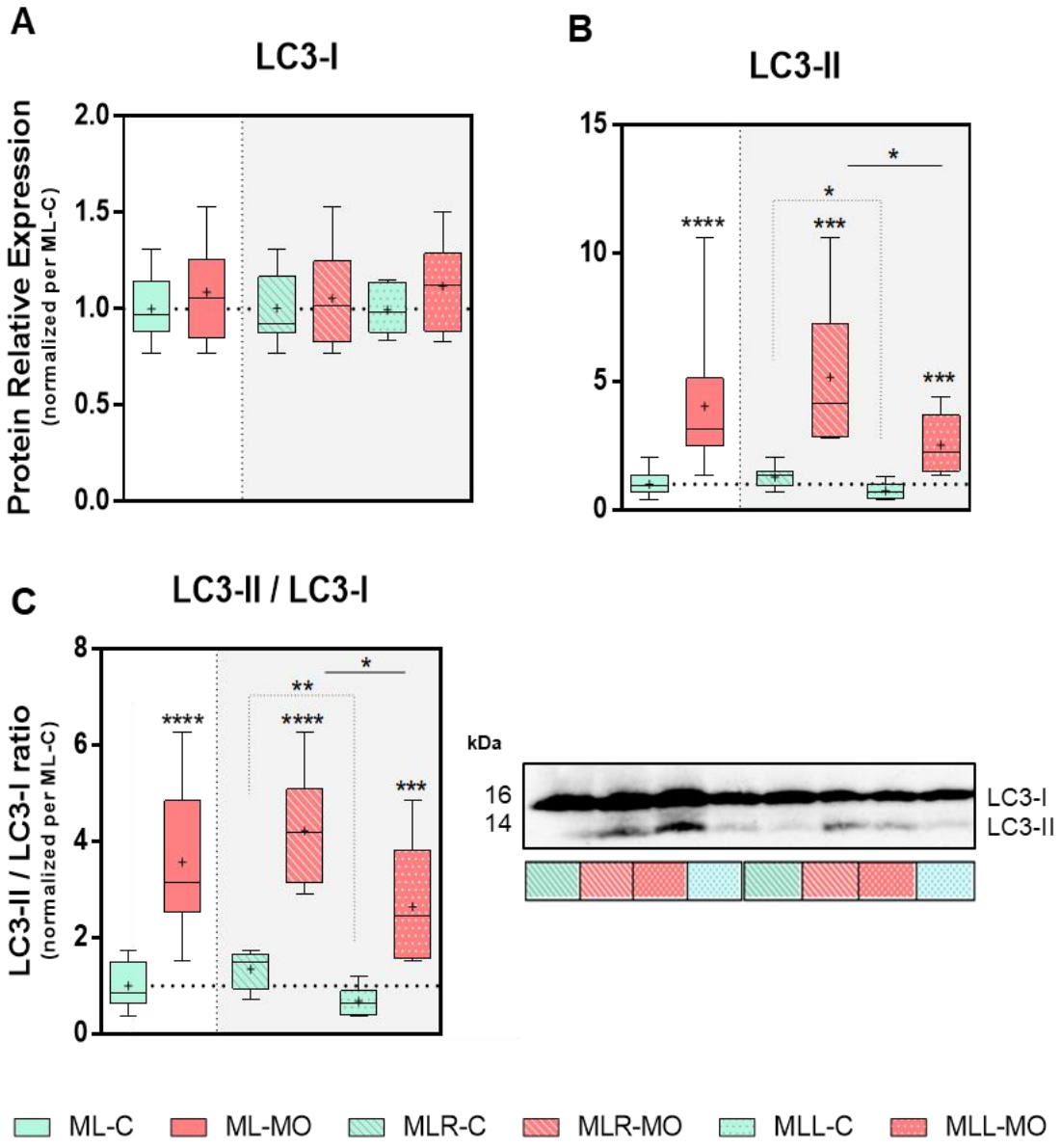

***Figure 3.12**- Autophagy in maternal obesity **A:** LC3-I form levels, **B:** LC3-II form levels, and **C:** LC3-II / LC3-I ratio in total liver tissue from control group (ML-C) and maternal obesity group (ML-MO) and the contribution of each lobe. Data was normalized using the reference protein β-actin and the protein expression represented relative to ML-C group. The number of individuals is 10 in control groups and 8 in maternal obesity groups.*
Statistical analysis: Comparison between control and maternal obesity groups was performed using unpaired t-test after passed Shapiro-Wilk normality test. Comparison between lobes was assessed using unpaired t-test. P-value lower than 0.05 was considered significant ($p \leq 0.05$; ** $p \leq 0.01$; *** $p \leq 0.001$; **** $p \leq 0.0001$). Green/light grey bars, ML-C; Red/dark grey bars, ML-MO; diagonal line pattern, left liver lobe (MLL); dot pattern, right liver lobe (MLR). Median, mean (+), interquartile distance, minimum and maximum are depicted.*

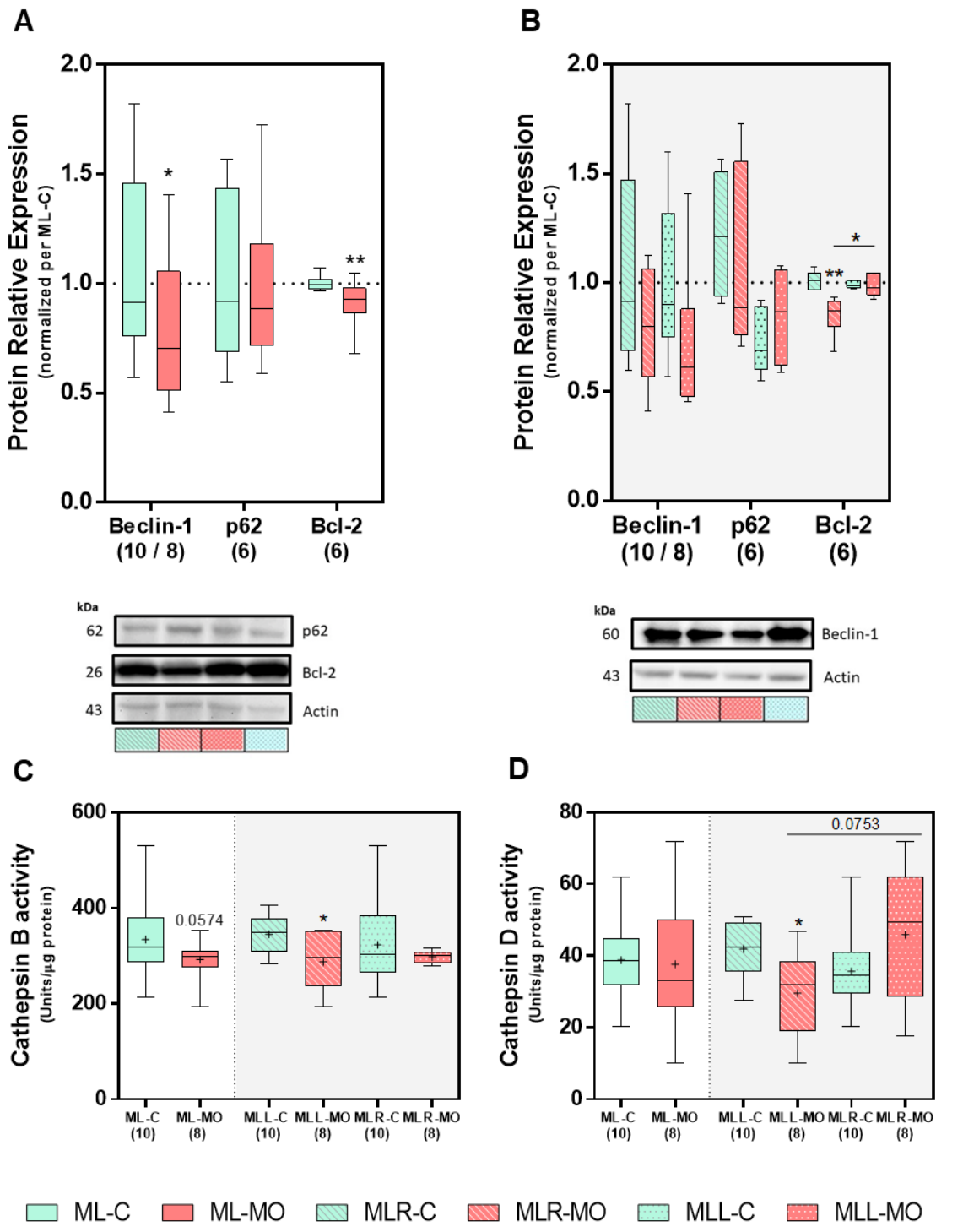

Figure 3.13 *- Autophagy and lysosomal activity in maternal obesity. Protein expression of Beclin-1, p62 and Bcl-2 in* ***A:*** *total liver tissue from control group (ML-C) and maternal obesity group (ML-MO), and* ***B:*** *the contribution of each lobe. Lysosomal activity measured by* ***C:*** *Cathepsin B and* ***D:*** *Cathepsin D activity. Data in* ***A*** *and* ***B*** *was normalized using the reference protein β-actin and the protein expression represented relative to ML-C group and in* ***C*** *and* ***D*** *represented in Units normalized per mass used in the assay. The number of individuals in each group is indicated in parentheses.*

Statistical analysis: Comparison between control and maternal obesity groups was performed using Mann-Whitney test in ***A*** *and* ***B*** *except for Beclin-1 protein expression in which, as well as in* ***C*** *and* ***D*** *was, used unpaired t-test after passed Shapiro-Wilk normality test. Comparison between lobes was assessed using Wilcoxon test or unpaired t-test according to the normality of the results. P-value lower than 0.10 was registered and lower than 0.05 was considered significant (* $p \leq 0.05$; ** $p \leq 0.01$). Green/light grey bars, ML-C; Red/dark grey bars, ML-MO; diagonal line pattern, left liver lobe (MLL); dot pattern, right liver lobe (MLR). Median, mean (+), interquartile distance, minimum and maximum are depicted.*

Q_3 = 5.14; p < 0.0001; g = 1.74; **Figure 3.12B**). LC3-II increased levels are observed both in the left (MLL-C vs MLL-MO, p = 0.0368; g = 2.05) and right (MLR-C vs MLR-MO, p = 0.0005; g = 2.12) liver lobes. Interestingly, LC3-II levels are originally different in both lobes of control mothers (MLL-C vs MLR-C, p = 0.0368, g =1.49), they are higher in the left lobe, leading to differences in the LC3-II/LC3-I ratio between both lobes (MLL-C vs MLR-C, p = 0.0074; g = 1.94). The same is observed between both liver lobes of obese mothers (MLL-MO vs MLR-MO, LC3-II levels: p = 0.0120; g = 1.21; LC3-II/LC3-I ratio: p = 0.0235; g = 1.22).

In addition, Beclin-1 (ML-C vs ML-MO: median = 0.915, Q_1 = 0.762, Q_3 = 1.46 vs median = 0.704, Q_1 = 0.514, Q_3 = 1.06; p = 0.0470; g = 0.744; **Figure 3.13A**) as well as Bcl-2 (ML-C vs ML-MO: median = 0.915, Q_1 = 0.762, Q_3 = 1.46 vs median = 0.704, Q_1 = 0.514, Q_3 = 1.06; p = 0.0083; g = 0.290; **Figure 3.13A**) protein expression are decreased in ML-MO compared with ML-C. The decrease in Bcl-2 protein expression is mostly caused by differences in the left lobe (MLL-C vs MLL-MO, p = 0.0022; g = 2.28) and the excess of maternal diet induced a differential expression Bcl-2 protein in the liver lobes (MLL-Mo vs MLR-MO, p = 0.0313; g = 1.84; **Figure 3.13B**). No differences in p62 levels were observed (ML-C vs ML-MO, p = 0.9596).

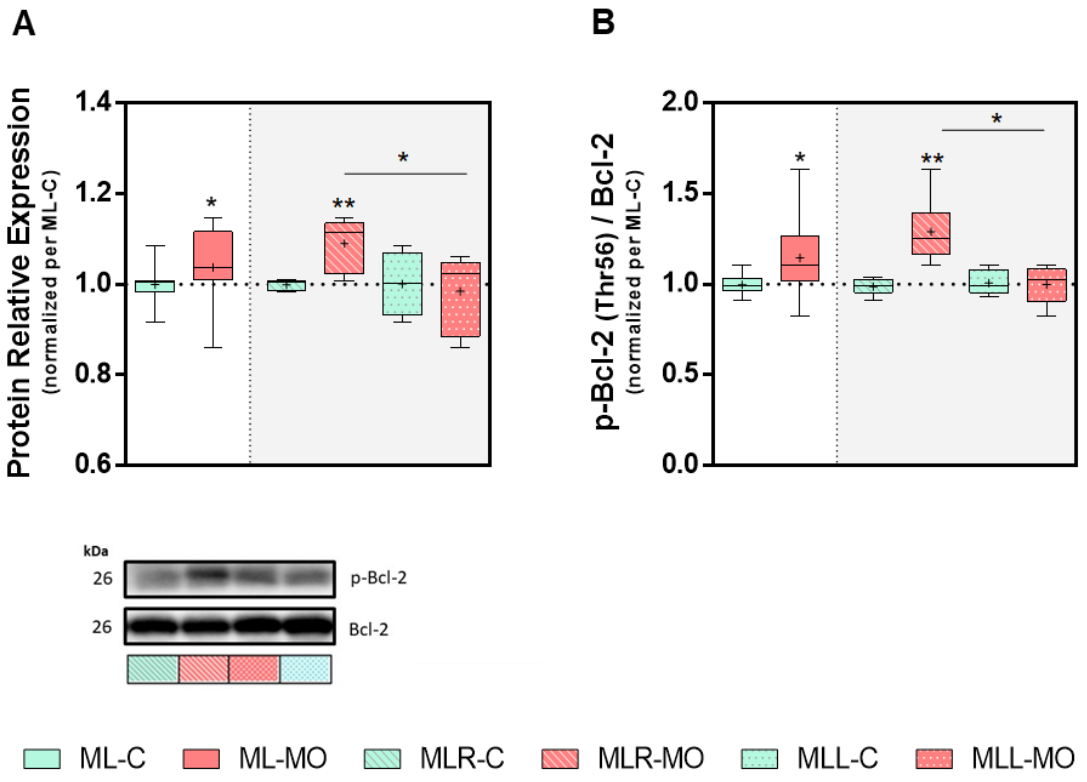

Figure 3.14 *– Bcl-2 phosphorylation levels in maternal obesity.* ***A:*** *p-Bcl-2 protein levels in total liver tissue from control group (ML-C) and maternal obesity group (ML-MO) and the contribution of each lobe, and* ***B:*** *phosphorylation ratio of Bcl-2. Data was normalized using the reference protein β-actin and the protein expression represented relative to ML-C group. The number of individuals is 6 in both experimental groups.*
Statistical analysis: Comparison between control and maternal obesity groups was performed using Mann-Whitney test and comparison between lobes was assessed using Wilcoxon test. P-value lower than 0.05 was considered significant (p ≤ 0.05; ** p ≤ 0.01). Green/light grey bars, ML-C; Red/dark grey bars, ML-MO; diagonal line pattern, left liver lobe (MLL); dot pattern, right liver lobe (MLR). Median, mean (+), interquartile distance, minimum and maximum are depicted.*

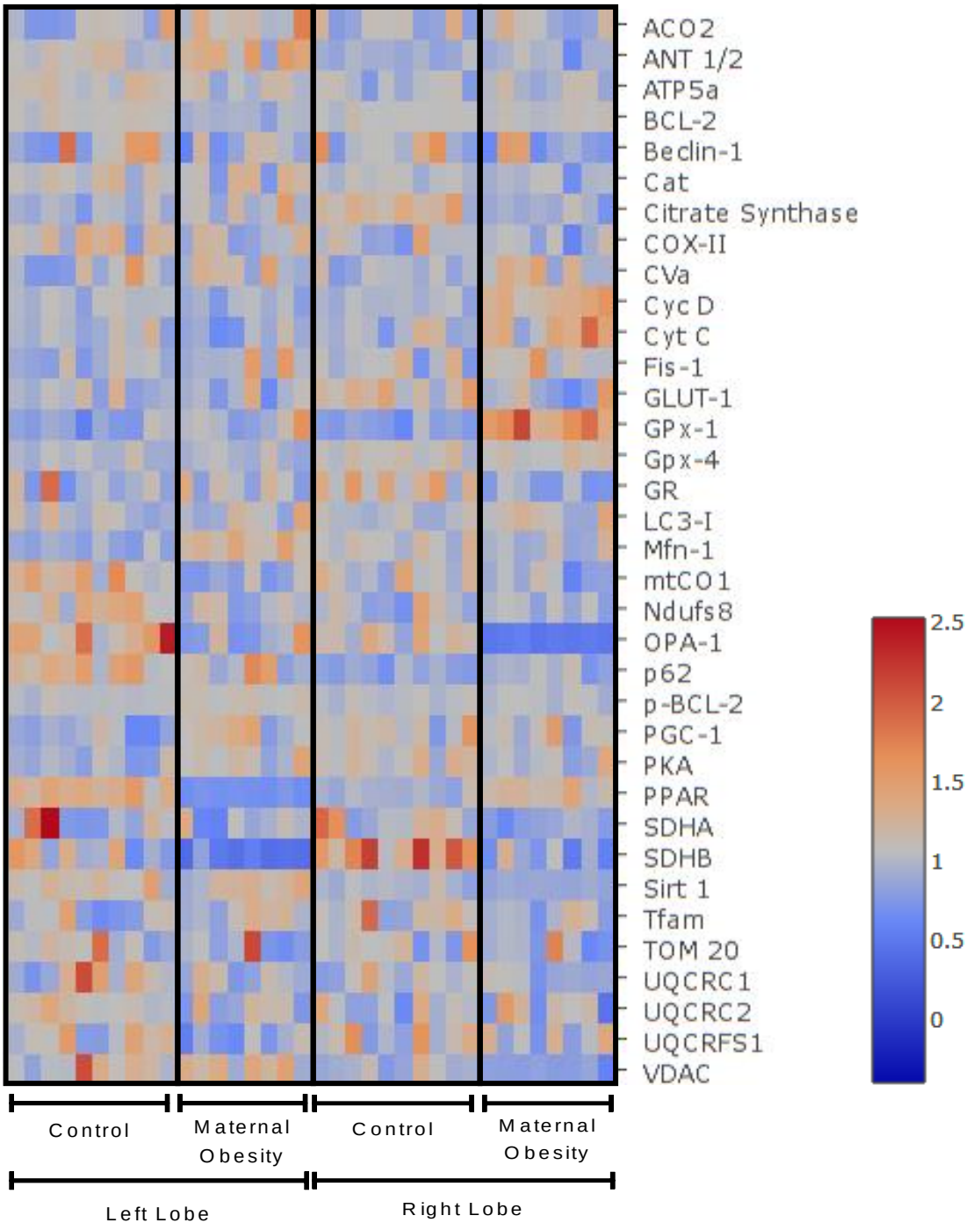

Figure 3.15 *– Protein expression variations due to maternal obesity in left and right liver lobes.*

Hepatic cathepsins activity is also affected by maternal obesity. Cathepsin B activity is decreased in the liver of obese mothers (ML-C vs ML-MO: median = 318, Q_1 = 286, Q_3 = 380 vs median = 298, Q_1 = 276, Q_3 = 310; p = 0.0574; g = 0.718; **Figure 3.13C**) mainly due to decreased activity that occurs in the left lobe (MLL-C vs MLL-MO, p = 0.0285; g = 1.18; **Figure 3.13C**). Cathepsin D activity in total liver tissue is similar between both experimental groups (ML-C vs ML-MO, p = 0.8119). However, there is a specific decrease in cathepsin D activity in the liver left lobe of obese mothers (MLL-C vs MLL-MO, p = 0.0157; g = 1.28). However, a difference between lobes emerge for the obese mothers group (MLL-MO vs MLR-MO, p = 0.0753; g = 1.04; **Figure 3.13D**).

Threonine 56 phosphorylated Bcl-2 (p-Bcl-2) levels were also measured in the hepatic tissues, being increased in the maternal obese group (ML-C vs ML-MO: median = 1.00, Q_1 = 0.984, Q_3 = 1.00 vs median = 1.04, Q_1 = 1.01, Q_3 = 1.12; p = 0.0447; g = 0.539; **Figure 3.14A**). These differences are a reflection of the increased p-Bcl-2 levels induced by over-nutrition in the hepatic left lobe (MLL-C vs MLL-MO, p= 0.0043; g =2.20). In the livers of the obese individuals, p-Bcl-2 expression is higher in the left lobe than in the right one (MLL-MO, MLR-MO, p = 0.0313; g = 1.45; **Figure 3.14A**). Considering the observed differences in total Bcl-2levels, the hepatic Bcl-2 phosphorylation ratio is increased in the maternal obese group (ML-C vs ML-MO: median = 0.991, Q_1 = 0.962, Q_3 = 1.04) vs median = 1.10, Q_1 = 1.02, Q_3 = 1.24; p = 0.0145; g = 0.967). Once more, this is a specific effect due to the effect of maternal diet on the liver left lobe (MLL-C vs MLL-MO, p = 0.0022; g = 2.28), since differential hepatic adaptations were observed between the left and right lobes of obese mothers (MLL-MO vs MLR-MO, p = 0.0313; g = 1.96).

Interestingly, taking all results together, striking differences were found in the protein expression profile between the left and right liver lobes of individuals of the same experimental group (Figure **II.1**). Moreover, it was observed that excessive food intake prior and during pregnancy induces several alterations in the protein expression profile (**Figure 3.15**), and that these changes are not equal in the left and right liver lobes (**Figure II.2**).

Chapter 4 - Discussion

Maternal obesity during pregnancy represents a huge metabolic burden for the female organism because of the metabolic impairment caused by obesity itself and the physiological increase in nutrient and energy requirements characteristic of a healthy pregnancy. Epidemiological studies associated maternal obesity with increased disease development during and after the gestation. However, the cellular and molecular mechanisms underlying this association are poorly understood or unknown. Most scientific research focus on maternal obesity consequences to offspring's health. To the best of our knowledge, this is the first report scrutinizing the consequences of being obese during pregnancy on the maternal hepatic mitochondrial physiology.

4.1 The morphological maternal impact of being obese during pregnancy

In this work, a previously validated sheep model of maternal obesity was used. It consists of overfeeding ewes with 150% of the NRC nutrient recommendations for 60 days and during pregnancy. It has already been reported that this strategy induces an increase in total body weight as well as in body fat percentage[329]. In the present work, an increase in total body weight at the conception and at the c-section, as well as an increase in subcutaneous fat thickness, the predominant place of fat accumulation[336], were also observed.

Liver weight increase is a common consequence of fatty liver diseases[337–339] and, in rodents, it is also a common feature during pregnancy, named gestational hepatomegaly, in order to meet the increased metabolic demands on the maternal liver[340]. However, in the present work, no alterations in the maternal liver, heart and brain weights were found at the c-section. In contrast, an increased pituitary weight was observed in ovine obese mothers. It has been previously reported that the adult offspring of obese ewes has an impaired leptin signaling in the pituitary that can impact their adiposity regulation[341]. It is possible that the observed increase in pituitary weight might somehow be related to an endocrine dysregulation due to maternal obesity.

All these morphological alterations lead to, and concomitantly can be caused by, alterations in body homeostasis regulation and cellular signaling. In fact, due to the metabolic burden of both obesity and pregnancy, liver seems to be one of the most challenged tissues during maternal obesity gestation.

4.2 Maternal obesity and hepatic metabolic remodeling

One of the hallmarks of obesity in hepatic tissue is the metabolic dysregulation. Excessive nutrient consumption propels the liver to modulate metabolic pathways by increasing anabolism in order to deal with the excess of energy[175]. This process entails a shift in the metabolism by which *de novo* lipogenesis is increased leading to the synthesis of lipids such as fatty acids and triglycerides[182]. When the excessive nutrient consumption

is prolonged, newly formed lipids start to accumulate in hepatocytes, a characteristic phenotype of NAFLD.

Protein Kinase A is one of the metabolic master-regulators kinases. It is responsible for the phosphorylation of several enzymes that modulate hepatic metabolism[342–344]. When PKA is activated it stimulates glycogenolysis (by activating glycogen phosphorylase and inhibiting acetyl-CoA carboxylase), inhibits glycogenesis (through glycogen synthase inhibition), stimulates gluconeogenesis, and inhibits glycolysis (via phosphofructokinase-2 inactivation, pyruvate kinase inhibition, and fructose 2,6 – bisphosphatase stimulation)[345–350]. PKA can also negatively regulate SREBP-1c through phosphorylation, therefore controlling hepatic lipogenesis[351].

A lower PKA activity was observed in obese pregnant ewes. Thus, carbohydrate consumption and storage are being promoted in these animals, while glycogenolysis and gluconeogenesis are less stimulated. Decreased gluconeogenesis is associated with a decrease in PPAR γ levels[352], which were found to be lower in the maternal obesity experimental group. Therefore, the obtained results regarding PKA activity and PPAR γ levels are highly concordant towards the development of the above-mentioned metabolic shift.

As outlined in the Introduction section 1.4.4.2.3, Acetyl-CoA carboxylase (ACC) is an enzyme fundamental to the *de novo* lipogenesis whose activity is inhibited by PKA phosphorylation. Indeed, it has been previously reported that the decrease in acetyl-CoA carboxylase phosphorylation by PKA stimulates *de novo* lipogenesis[353]. Moreover, decreased PPAR γ levels are also associated with insulin resistance and lower lipid droplets formation, and consequently with a decrease in steatosis, due to the export of newly formed lipids from hepatocytes[354]. Facing the obtained results regarding PKA activity and PPAR γ levels, it is plausible to assume a similar scenario in the liver of the ewes from the maternal obesity group.

The observed alterations of the hepatic NAD^+/NADH ratio due to a decrease in NADH levels in obese mothers might as well be a consequence of this metabolic shift. NADH deprivation is associated with both an increase in nutrient consumption and OXPHOS, and an increase in fatty acids synthesis. Together with the observed decrease in GSH/GSSG ratio, the results obtained in the present study clearly show that maternal obesity during pregnancy induces an alteration in the hepatic redox state, which might share similarities with NAFLD progression[355].

PKA activity also affects mitochondrial function, regulating OXPHOS activity, mitochondrial dynamics and apoptosis[344]. Several studies have shown that PKA can be translocated to the mitochondrial matrix and phosphorylate numerous PKA substrates inside mitochondria. The process that governs PKA translocation across mitochondrial membranes is still not understood[356,357]. PKA phosphorylates complex I and complex IV, thereby impacting OXPHOS rate. The phosphorylation of complex I subunit NDUFS4 by PKA facilitates its interaction with the chaperone Hsp70 and with mitochondrial proteases leading, therefore, to its degradation[358]. Similarly, complex IV subunits I, IV1,

and Vb phosphorylation by PKA also induces their degradation and the consequent decrease in complex IV activity, putatively through the compromising of complex IV stability[359,360]. Indeed, an increase in liver complex I and IV activities were observed in the obese pregnant ewes' experimental group. This result might as well be a consequence of the observed decrease in PKA activity.

The dynamic nature of mitochondria is essential in cells' metabolism, homeostasis and function. Mitochondrial fusion and fission rates are maintained in a delicate equilibrium that is crucial to prevent mitochondrial damage and dysfunction, to respond to substrates availability, metabolic state and energetic demands, and to modulate the mitochondrial network[361]. PKA can also interfere with this mitochondrial balance by phosphorylating and inhibiting Dynamin-1-like protein (Drp1). This GTPase is a fundamental component of mitochondrial fission and its inhibition leaves mitochondrial fusion unopposed leading to severe physiological alterations that can culminate in cell death[362]. In fact, a decrease in mitochondrial fusion (lower OPA-1 protein levels) and an increase in mitochondrial fission (higher Fis-1 protein levels) were observed in the hepatic tissue of maternal obesity group. These results are in agreement with the decreased PKA activity determined in the same experimental group.

As previously described in section 1.5.2, mitophagy is usually preceded by mitochondrial fission to facilitate encapsulation by the autophagosome[267]. Since PKA can inhibit mitochondrial fission through Drp1 phosphorylation, it can also affect mitophagy. Additionally, PKA can also phosphorylate MIC60 and MIC19, reducing PINK1 levels in the OMM and, consequently, preventing Parkin recruitment and mitophagy progression[363,364]. In the present work, the observed increase in mitochondrial fission and in the formation of autophagosomes (based on the LC3-II/LC3-I ratio) suggest that mitophagy might be increased in the liver of maternal obesity group. Again, the regulation of PKA may be linked to these observations. However, additional experiments are necessary to confirm these assumptions.

Finally, PKA can also regulate apoptosis through the phosphorylation, and hence inactivation, of the pro-apoptotic protein BCL2 Associated Agonist Of Cell Death (Bad)[365–367]. Bad is a protein that counteracts the anti-apoptotic effects of Bcl-2. Therefore, the decreased hepatic PKA kinase activity observed in the maternal obesity group suggests an increased hepatocytes' apoptosis in the liver of these animals. The results obtained regarding Bcl-2 Thr56 phosphorylation strengthen this hypothesis. Bcl-2 has numerous phosphorylation sites whose post translational modification by different kinases can lead to distinct outcomes. This particularity has led to some controversy regarding the precise role played by Bcl-2 phosphorylation in apoptosis regulation. However, Thr 56 has been identified as a residue prone to phosphorylation by mitogen activated protein kinases (MAPK) and whose modification is crucial to apoptosis triggered by different stimuli. The exact mechanism by which this happens is unknown, since this residue phosphorylation does not induce a significant proteosomal degradation of Bcl-2 [368–372]. An increased level of Bcl-2 Thr56 phosphorylation (p-Bcl-2), and a consequent increase in the p-Bcl-2/total Bcl-2 ratio, was observed in the hepatic tissue of

obese pregnant ewes, suggesting that the decrease in PKA activity also observed in this experimental group might be truly leading to apoptosis stimulation. However, this statement needs further experimental work to be taken as certain. Interestingly, Bcl-2 Thr56 phosphorylation dependent apoptosis has been observed with stimuli that induce oxidative stress[370].

4.3 Hepatic mitochondrial adaptation to maternal obesity during pregnancy

Mitochondrial OXPHOS protein expression and activities were measured. Alterations at this level might constitute a possible mechanism by which the hepatic redox state is altered justifying, for example, the increase in NAD^+/NADH ratio measured in obese pregnant ewes' livers. Excessive nutrient uptake stimulates hepatocytes to increase their catabolic rate, prompting Krebs' cycle. Reduced forms of NADH and succinate will be produced as a consequence and, on their turn, will stimulate OXPHOS and lead to ATP production. However, increases in OXPHOS also rise the production of ROS which can damage the OXPHOS enzymatic complexes and turn this process dysfunctional[228].

Nevertheless, no significant differences were detected for ANT 1/2, ACO 2, citrate synthase and GLUT-1 protein expression induced by maternal obesity, meaning that glucose uptake, Krebs' cycle rate and adenosine nucleotide translocation through mitochondria are not affected in the liver of this model of maternal obesity. However, decreased levels of complex I subunit Ndufs8, complex II subunits SDHA and SDHB, complex III subunit UQCRFS1 and complex IV subunit mtCO1 were measured in the hepatic homogenates of the maternal obesity group. This general decrease in ETC complexes subunits protein expression might be a result of damage accumulation which perturbs proteins' stability targeting them to degradation[373]. Another possible mechanism justifying this observation might be increased mtDNA damage. This scenario would lead to the expression of dysfunctional OXPHOS proteins or to impairment of the mitochondrial protein import mechanisms and the compromising of OXPHOS proteins transport to mitochondria[374–376]. The putative mtDNA damage can as well lead to stoichiometric imbalances between mtDNA- and nuclear-encoded OXPHOS subunits, which might jeopardize complexes' assembly and decrease subunits' protein levels[376].

The decreased expression of the complex II subunits SDHA and SDHB in livers from obese pregnant ewes is in agreement with the lower complex II activity measured in the same hepatic homogenates. On the contrary, increased complex I and complex IV activities were observed, contrasting with their decreased protein expression in liver homogenates from the maternal obesity group. The observed unaltered activities of combined complexes activities I + III and II + III are probably a reflex of an experimental limitation related to the cellular quinone pool, what compromises complex III ideal stimulation. In fact, complex I and II present, by themselves, different impacts in complex III activity[377].

One hypothesis to explain these results consists of the decrease in OXPHOS subunits expression being a consequence of a lower mitochondrial number/mass. Should this happen, the measured complexes' activity would be affected since it is normalized per mitochondrial mass. However, no mitochondrial number differences were observed between the experimental groups, as measured by mtDNA copy number, citrate synthase activity, and TOM20 and VDAC protein expression levels. This dichotomy in the results might also be caused by the formation of supercomplexes that comprise complex I and IV. The increased enzymatic activity concomitant with lower protein expression would be explained by a higher efficiency due to supercomplexes' formation. Indeed, the formation of supercomplexes containing complex I, III and/or IV, but not complex II, and their physical association with enzymes involved in mitochondrial fatty acid β-oxidation have been observed[378]. It has also been proposed that these molecular associations may modulate the subtle energy metabolism dysfunction characteristic of pathologies with increased cellular fatty acids levels, such as obesity and type 2 diabetes[378]. This mechanism, however, fails to explain the observed absence of alterations in complexes I + III activity. In summary, more data is required to better understand the relation between complexes subunits expression and activities observed in this work.

Although there is no difference in mitochondrial mass, hepatic mitochondrial dynamics are affected by maternal obesity. While mitochondrial fusion is decreased (measured by OPA-1 protein levels), mitochondrial fission is increased (taken by Fis-1 levels) and no variation in mitochondrial biogenesis was found (measured by PGC-1α and TFAM protein expression). This means that hepatic mitochondria are more divided, rather than forming an elongated and interconnected network, in maternal obesity. This scenario seems to favor an increased activity of mitochondrial quality control pathways, since mitochondrial fission allows the elimination of damaged mitochondria[267]. Surprisingly, a contrasting behavior was found in the alterations induced by maternal obesity in protein expression levels of Mfn-1 and OPA-1. Both these proteins take part in the mitochondrial fusion machinery. While OPA-1 is responsible for the fusion of the IMM, Mfn-1 is responsible for connecting OMM with other membranes. The observed Mfn-1 increased levels in hepatic homogenates of obese pregnant ewes might be associated with the establishment of connections between mitochondria and endoplasmic reticulum. These inter-organelle contact points are usual and important in conditions with increased phospholipid metabolism, as consequence of an increase in fatty acid synthesis, and to avoid lipotoxicity[379].

Another possible explanation for the observed Mfn-1 increased protein expression in the livers of maternal obesity group is protein ubiquitination. Mfn-1 ubiquitination is a usual mechanism to target mitochondria to degradation[276]. It is plausible to conceive that ubiquitin-conjugated Mfn-1 removal be impaired, however the ubiquitin target activates compensatory mechanisms to restore its unconjugated normal form would result in an increase of Mfn-1 levels. The increased rate in fission without alteration in mitochondrial number and the increase in LC3-II / LC3-I ratio also observed, are in agreement with the suggested mechanism.

4.4 Maternal obesity and hepatic oxidative stress

Mitochondria damage might occur associated with oxidative stress[228]. An increase in lipid peroxidation and GSSG levels was observed in the hepatic tissue of maternal obesity experimental group, probably as a result of an increase in ROS production[380]. In fact, OXPHOS is one of the major cellular processes contributing to ROS generation, almost exclusively at the level of complex I and complex III. Since complex I activity was found to be increased in the same experimental group, it is very likely that ROS production by this OXPHOS complex is a main cause of the rise in ROS-related damage[232].

The ROS formed in OXPHOS are superoxide anion, which is degraded by the SOD activity. Accordingly, an increased SOD activity was observed in the liver of obese pregnant ewes. Superoxide anion dismutation by SOD leads to H_2O_2 production. Two enzymatic systems are responsible for H_2O_2 degradation: catalase and the glutathione system[381]. A lower hepatic catalase activity was observed as a consequence of maternal obesity, although no alterations in protein expression were detected. This might be a consequence of catalase phosphorylation, which impairs its activity and occurs in intense oxidative stress cases[382].

Furthermore, the glutathione system is also impaired in hepatic homogenates from the maternal obesity group. GSH/GSSG ratios are decreased as a consequence of oxidized glutathione accumulation in this experimental condition. This alteration is most probably due to the determined lower glutathione reductase protein expression levels and enzymatic activity, which compromise the ability to restore GSH levels[383]. Concomitantly, glutathione peroxidase activity was also found to be decreased in hepatic tissue of the maternal obesity group. This general context paves the way to a seriously compromised hepatic H_2O_2 degradation system in the obese ewes. Consequently, the tendency of homeostatic dysregulation towards oxidative stress is significantly raised. Interestingly, glutathione peroxidase 1 protein expression is increased in hepatic homogenates from the maternal obesity group, contrasting with the observed in its enzymatic activity. In fact, glutathione peroxidase 1 activity is regulated by oxidative stress itself. Therefore, high levels of H_2O_2 induce irreversible modifications in this enzyme active site that inhibit its activity[384].

4.5 Maternal obesity and hepatic autophagy

Oxidative stress in hepatic cells due to maternal obesity leads to oxidative damage accumulation. One way to deal with it is by stimulating macroautophagy and, therefore, degrade damaged molecules[385].Indeed, an increase in the LC3-II/LC3-I ratio was observed in the livers of pregnant obese ewes at c-section. This result suggests that there is more autophagosomes formation and that damaged molecules and mitochondria are being targeted to autophagy in consequence[386]. In contrast to this, no decrease in p62 protein levels was observed.

Usually, an increase in autophagy is associated with a decrease in p62 levels. Whenever this is not observed, autophagic flux is probably impaired at the level of the fusion process between the autophagosomes and lysosomes or at the level of autolysosome degradative processes themselves (see section 1.5.2 for further details). The decrease in cathepsin B activity suggests that lysosomal activity is indeed compromised in the hepatic tissue of obese pregnant ewes. However, p62 accumulation was not observed. Therefore, it is not possible to affirm that the autophagy flux is stopped in the hepatic tissue of obese pregnant ewes[387,388]. An additional result further suggests that autophagy is impaired in this experimental group, the observed decrease in Beclin-1 protein levels probably means that phagophore formation is also reduced[291,389,390].

Beclin-1, together with Bcl-2, balance the autophagy and apoptosis fluxes through the formation and breaking of the Beclin-1: Bcl-2 complex. When complexed with Bcl-2, Beclin-1 is inactivated and autophagy inhibited. However, when Bcl-2 is connected to other proteins harboring a BH3 domain or when it is phosphorylated, Beclin-1 is activated[389]. A decrease in liver Bcl-2 protein expression as well as an increase in Bcl-2 phosphorylation ratio was observed in the livers of the maternal obesity group. This result suggests that, in this experimental condition, there is less Bcl-2 available to interact with Beclin-1 and, therefore, that the autophagic flux should be enhanced. It is fairly clear that additional data is necessary to completely understand the repercussions of maternal obesity in the hepatic autophagic flux.

.

4.6 Can maternal obesity during pregnancy cause hepatic lobe-dependent effects?

The mechanism of response to maternal obesity during pregnancy in both liver lobes seems to be different. While right lobe tries to adapt to excessive nutrient consumption by shifting the metabolism, the left lobe follows a more drastic response by impairing autophagy and possibly inducing apoptosis.

The idea that different cells perform different functions in liver has been reported recently in a mechanism called zonation[391]. Briefly, hepatocytes function varies according to their distance to the closest blood supply, a consequence of a variation in local oxygen tension.

Interestingly, the blood supply during fetal development is different between left and right lobe[392]. The right lobe presents lower pO_2 when compared to the left lobe, resulting in functional cellular differences[393]. Other studies show that hypoxia during fetal development results in epigenetic alterations which change liver susceptibility to metabolic diseases in adult age[394–398]. Together, these reports suggest a possible lobe-dependent functional difference in adult liver, contrasting with the prevailing idea of the liver as a homogeneous functional and parenchymal tissue.

Moreover, radiopharmacological studies show differences in the uptake of various agents between liver lobes. Both ^{99m}Tc-HIDA and ^{111}Inpentetreotide showed increased

uptake levels in the right liver lobe compared to the left one in SPECT analysis of healthy subjects[84]. Using MRI, a greater Gd-EOB-DTPA-enhanced distribution in the right lobe uptake was observed, suggesting an overestimation of function in this liver lobe in cirrhosis[83].

Other factors, such as increased levels of catecholamines and higher sympathetic nerve density in the left lobe, can also be responsible for differences of the cellular function between lobes[84]. Furthermore, in liver living donor, right lobe transplantations present a higher rate of complications compared with the left lobe[82,399,400]. Interestingly, 3 months after hepatic transplantation increased rate in liver regeneration is observed when the left lobe was donated[401].

In the present work it seems that there is a common hepatic impact of excessive nutrient consumption in both lobes. Diet starts by inducing an increase in complex I and complex IV activities, possibly caused by β-oxidation stimulation, which lead to overproduction of ROS and molecular damage, as observed by lipid peroxidation, which in turn decrease OXPHOS subunits expression. Hepatocytes also change mitochondrial fusion/fission balance and start to stimulate autophagy and then they reach a point where each lobe answers by different ways.

In the right lobe we observed the activation of mechanisms as decreased PKA activation and increased PPAR-γ levels that are associated with the biogenesis of lipid droplets. The shift in metabolism is supported by the increase in NAD^+/NADH, which is associated with an increase in OXPHOS function and *de novo* lipogenesis, to deal with the nutrient excess. At the same time, antioxidant mechanisms are activated. SOD activity and glutathione peroxidase expression are both increased. Concomitantly, they also seem to be partially compromised. Glutathione reductase levels and activity are decreased, compromising GSH levels restore and, consequently, decreasing its levels, as observed. The unaltered Beclin-1 and Bcl-2 levels as well as unchanged cathepsins' activity support the idea of an increase in the autophagic flux.

In contrast, the metabolic shift promoted by obesity during pregnancy is not so pronounced in the indicators measured in the hepatic left lobe. Only a decrease in PPAR-γ and Sirt-1 protein expression is apparent. As a mechanism to compensate mitophagy stimulation, mitochondrial biogenesis is being stimulated, observed by both PGC-1α and TFAM increased protein expression. However, the mitophagic process is impaired in the left lobe due to cathepsin decreased activity and Beclin-1 and Bcl-2 decreased protein levels. Moreover, the increase in Bcl-2 phosphorylation in Thr56 might contribute to Bcl-2 degradation, stimulating apoptosis.

From these results it is possible to conclude that maternal obesity stimulates OXPHOS, changes mitochondrial dynamics and induces an increase in ROS formation. The liver right lobe seems to have increased metabolic plasticity, reacting to maternal obesity stimulus by inducing steatosis and mitochondrial network remodeling. On the other hand, in the liver left lobe effects are more severe, impairing autophagy and possibly

stimulating apoptosis. This might be related with the increased regeneration capability observed in the left lobe.

Chapter 5 - Conclusions and Future Perspectives

Obesity is a worldwide epidemic that is responsible for the development of numerous metabolic diseases. More and more women in reproductive age are overweight or obese when became pregnant, that condition can impact fetal and maternal health and jeopardize pregnancy. Indeed, more than 50% of the actual pregnancies are characterized by maternal obesity.

In this work we characterize for the first time, to our knowledge, the hepatic outcome of maternal obesity during pregnancy with special focus in mitochondrial pathophysiology. We found that excessive nutrient consumption and obesity lead to a hepatic stimulation of OXPHOS what induces oxidative stress, which is exacerbated by a dysfunctional enzymatic antioxidant defense. Moreover, hepatic mitochondrial regulation by PKA is affected by maternal obesity during pregnancy. Mitochondrial dynamics are also affected being observed a stimulation of mitochondrial fission and decreasing fusion. Macroautophagy is also increased however, maternal obesity might lead to the impairment of the mechanism (Figure 5.1).

Further complementary results are needed to completely understand the impact of maternal obesity during pregnancy in the hepatic metabolism and function. The role of mitophagy and apoptosis must be better understood since it might offer a pharmaceutical approach to the hepatic negative outcomes of maternal obesity. As well, better characterize the metabolic shift might be important to understand the mechanisms that are stimulating both macroautophagy and apoptosis.

Despite the actual idea of liver as a parenchymal tissue, our data suggest that maternal obesity during pregnancy impacts the liver function in a lobe-dependent manner. Again, more information is required to confirm these results, with more animal models and with different metabolic approaches. However, the validation of these findings could affect the actual knowledge and perception about hepatic activity as will stimulate more precise liver biopsies.

In conclusion, this work can be interpreted as beginning of a new area of research to support a new clinical approach to prevent the perpetuation of liver and metabolic diseases triggered by maternal obesity during pregnancy.

It is mandatory to understand the maternal immediately and long-term implications of being obese during pregnancy. A better understanding of the underlying pathogenesis of maternal obesity during pregnancy and the cellular mechanisms responsible for programmed predisposition to metabolic and hepatic disease will allow development of early biomarkers for diagnosis and an opportunity to offer more timely interventions to improve life course health.

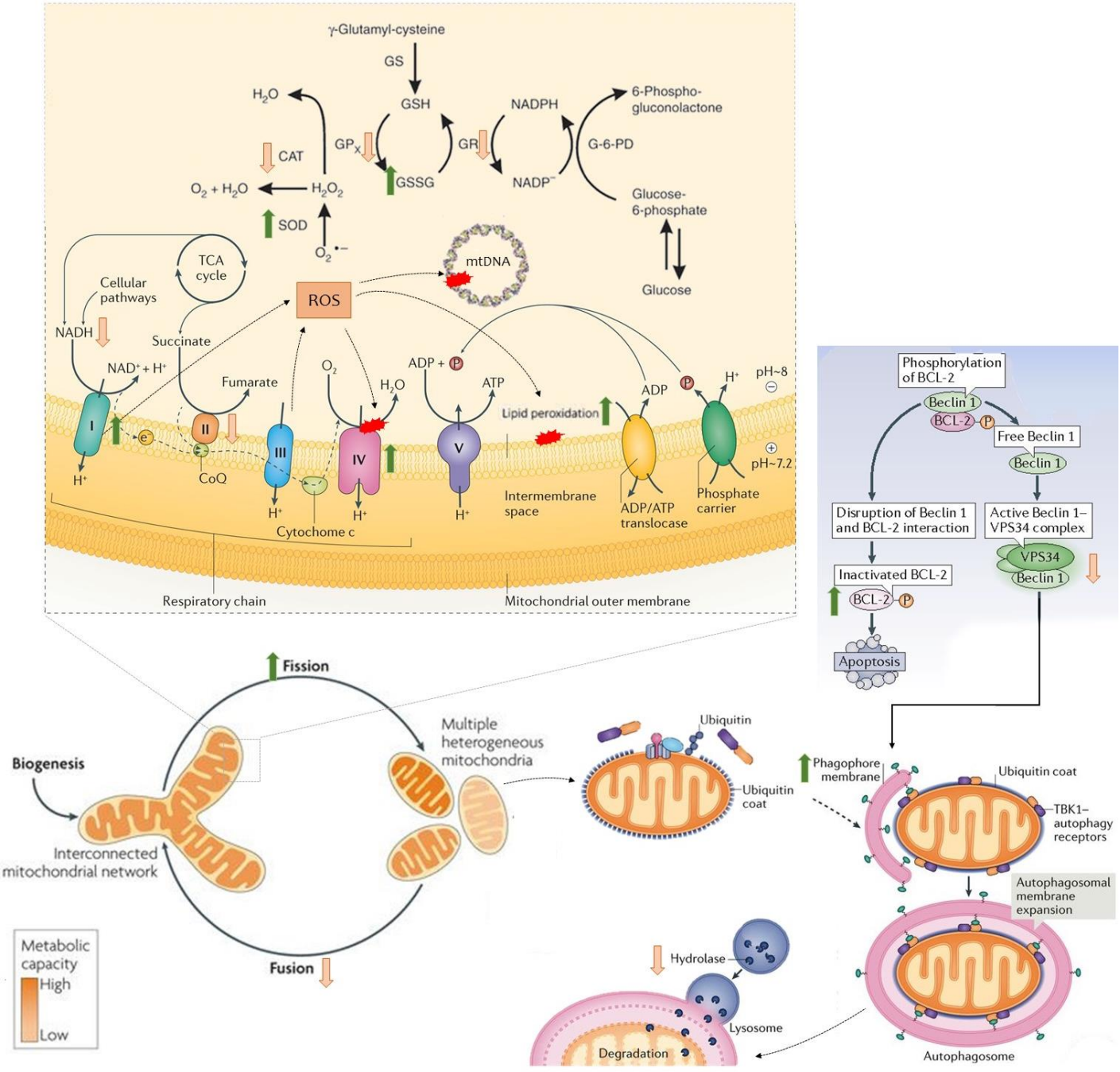

Figure 5.1 *- Schematic representation of Maternal Obesity effect in hepatic tissue.*

Appendix I- Obesity Prevalence

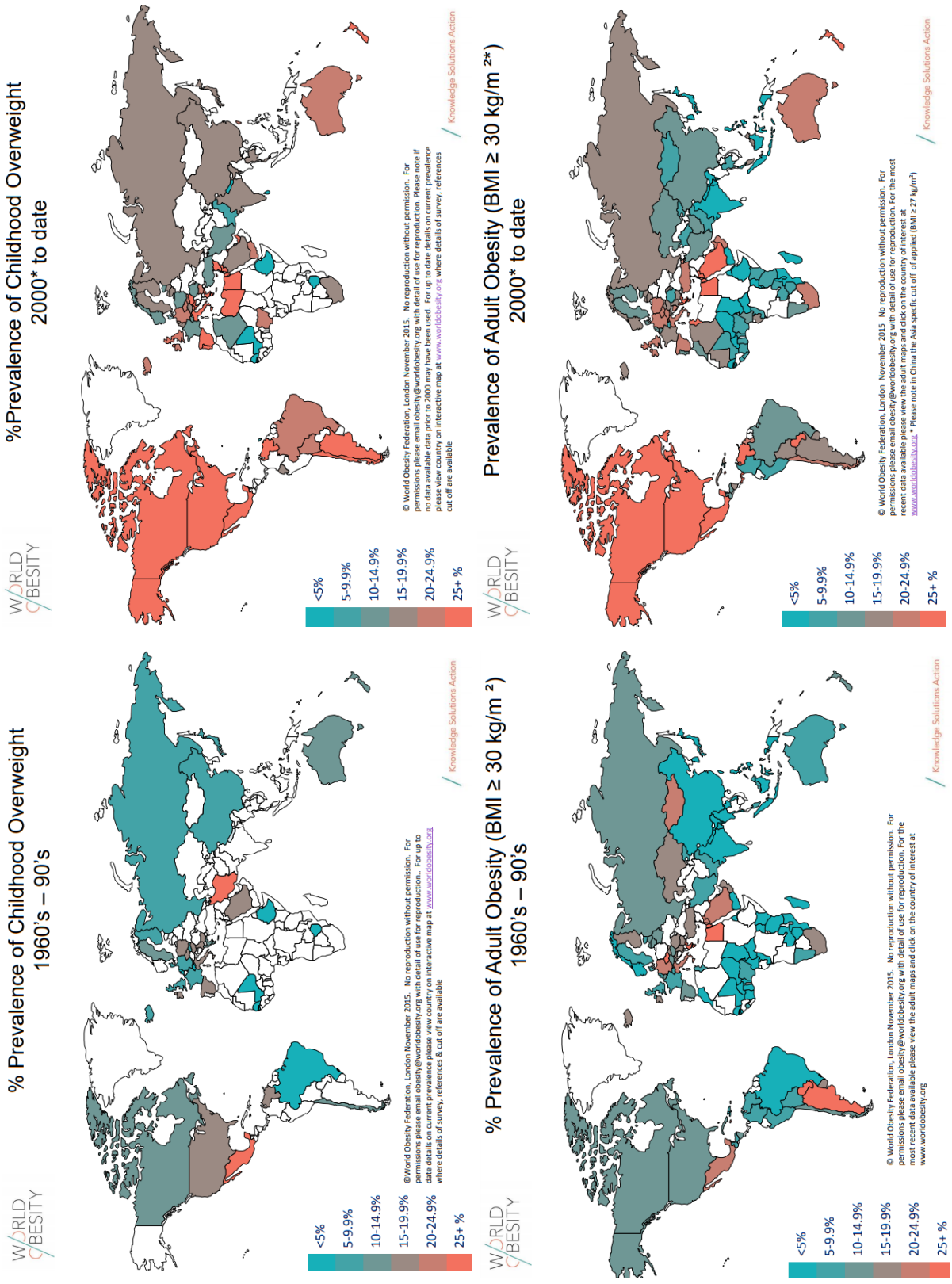

***Figure I.1**- Evolution of the prevalence of childhood overweight and adult obesity. Source: World Obesity*[21] .

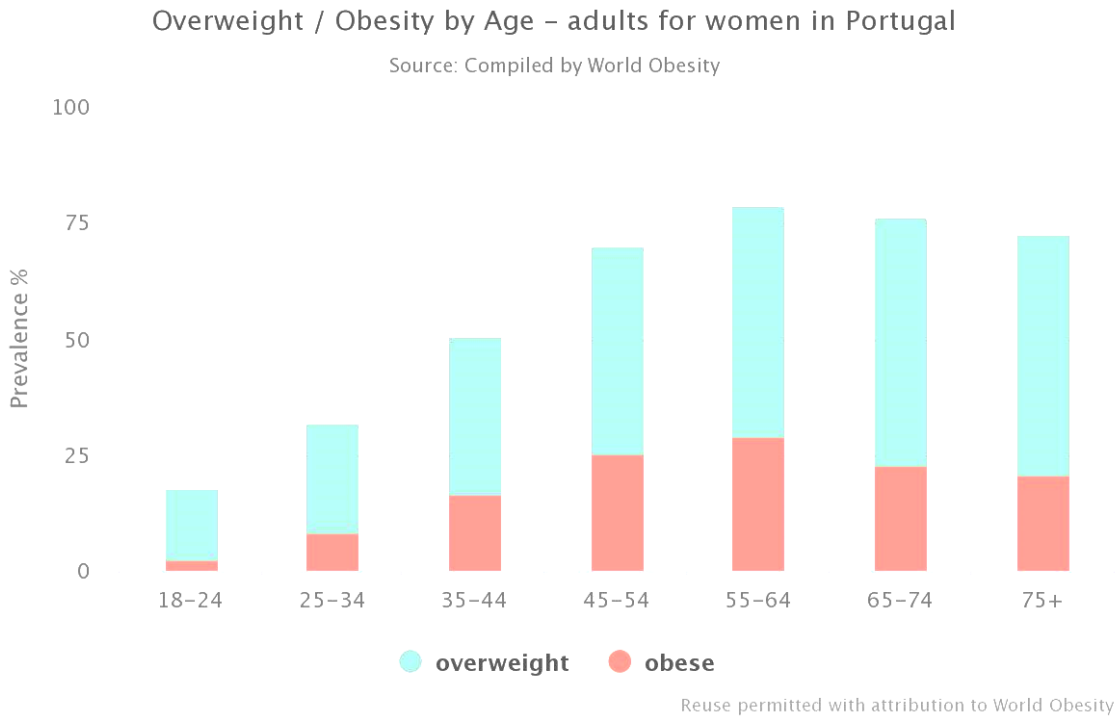

Figure I.2 *– Prevalence of Overweight and Obesity in adult women in Portugal by age. Source: World Obesity*[21] *(Sample Size: 9447).*

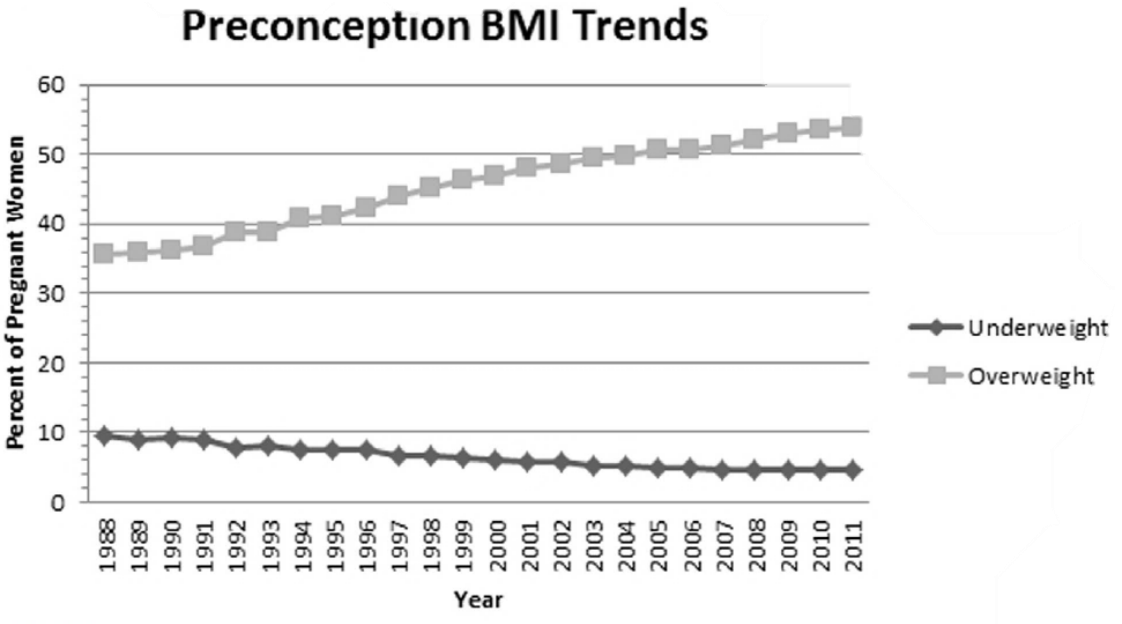

Figure I.3 *- Original condition of women that get pregnant and its trend in the last 30 years. Source: Gilmore et. al, 2015*[18].

Appendix II- Comparison of protein expression in liver lobes

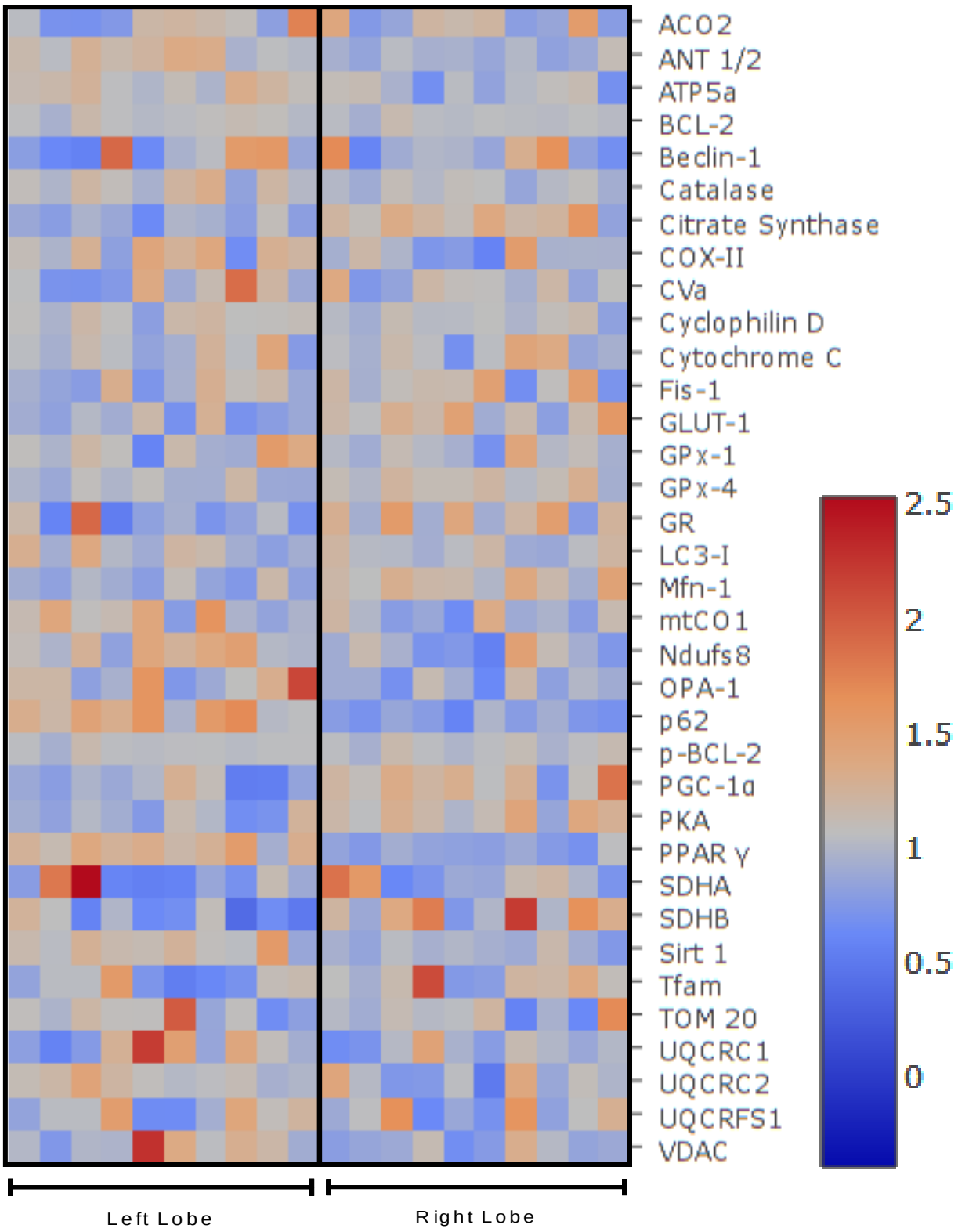

Figure II.1 *– Protein expression profile in left and right liver lobes of the control group.*

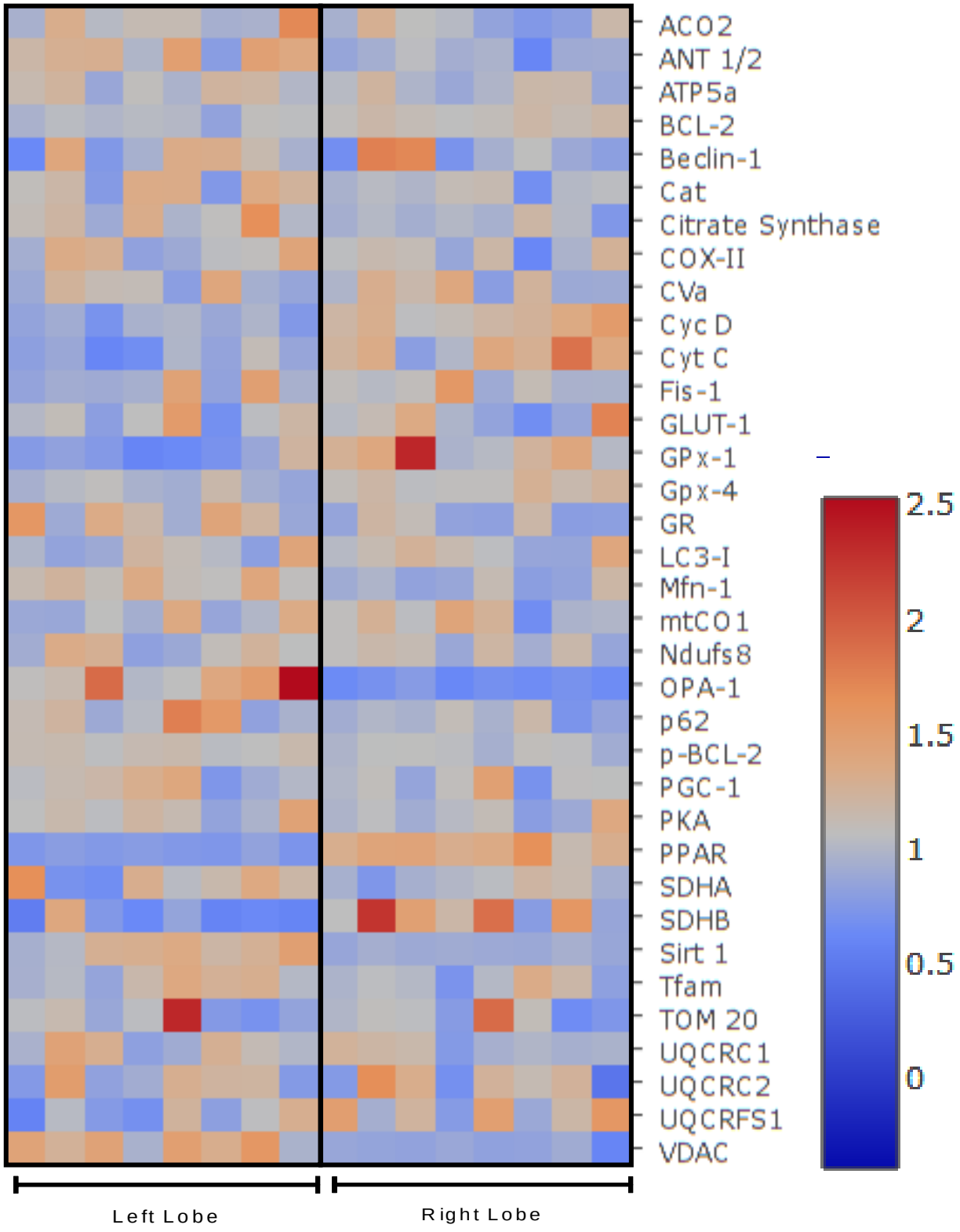

Figure II.2 *- Protein expression profile in left and right liver lobes of the maternal obesity group.*

References

1. Sikaris, K. A. The clinical biochemistry of obesity. *Clin. Biochem. Rev.* **25**, 165–181 (2004).
2. Fernández-Sánchez, A. *et al.* Inflammation, oxidative stress, and obesity. *Int. J. Mol. Sci.* **12**, 3117–3132 (2011).
3. Mission, J. F., Marshall, N. E. & Caughey, A. B. Obesity in Pregnancy. *Obstet. Gynecol. Surv.* **68**, 389–399 (2013).
4. Williams, E. P., Mesidor, M., Winters, K., Dubbert, P. M. & Wyatt, S. B. Overweight and Obesity: Prevalence, Consequences, and Causes of a Growing Public Health Problem. *Curr. Obes. Rep.* **4**, 363–370 (2015).
5. World Health Organization. WHO, Obesity and overweight. (2013).
6. World Health Organization. WHO, Preventing andmanaging the global epidemic. (2000).
7. Dulloo, A. G., Jacquet, J., Solinas, G., Montani, J. P. & Schutz, Y. Body composition phenotypes in pathways to obesity and the metabolic syndrome. *Int. J. Obes.* **34**, S4–S17 (2010).
8. Deng, Y. & Scherer, P. E. Adipokines as novel biomarkers and regulators of the metabolic syndrome. *Ann. N. Y. Acad. Sci.* **1212**, E1–E19 (2010).
9. Abel, E. D. Free fatty acid oxidation in insulin resistance and obesity. *Heart Metab.* **48**, 5–10 (2010).
10. Bajzer, M. & Seeley, R. J. Obesity and gut flora. *Nature* **444**, 1009–1010 (2006).
11. Ley, R. E., Turnbaugh, P. J., Klein, S. & Gordon, J. I. Human gut microbes associated with obesity. *Nature* **444**, 1022–1023 (2006).
12. Turnbaugh, P. J. *et al.* An obesity-associated gut microbiome with increased capacity for energy harvest. *Nature* **444**, 1027–1031 (2006).
13. Locke, A. E. *et al.* Genetic studies of body mass index yield new insights for obesity biology. *Nature* **518**, 197–206 (2015).
14. Neri, C. & Edlow, A. G. Effects of Maternal Obesity on Fetal Programming : Molecular Approaches. 1–21 (2015).
15. Wu, G., Bazer, F. W., Cudd, T. A., Meininger, C. J. & Spencer, T. E. Maternal Nutrition and Fetal Development. *J. Nutr.* **134**, 2169–2172 (2004).
16. Marchi, J., Berg, M., Dencker, A., Olander, E. K. & Begley, C. Maternal Obesity / Pediatric Health Risks associated with obesity in pregnancy , for the mother and baby : a systematic review of reviews. 621–638 (2015). doi:10.1111/obr.12288
17. Kriebs, J. M. Obesity in Pregnancy - Addressing Risks to Improve Outcomes. **28**, 32–40 (2014).
18. Gilmore, L. A., Klempel-donchenko, M. & Redman, L. M. Pregnancy as a window to future health : Excessive gestational weight gain and obesity. *Semin. Perinatol.* 1–8 (2015). doi:10.1053/j.semperi.2015.05.009
19. IOM, S. N. Nutrition DuringPregnancy:PartI:Weight Gain, PartII: Nutrient Supplements: Institute of Medicine (US), National Research Council (US), National Academy of Engineering (US), and National Academy of Sciences (US), Committee on Nutrition Status During Pregna. (1990).
20. IOM. Weight Gain During Pregnancy: Reexaming the Guidelines: Institute of Medicine (US), National Research Council (US), Committee to Reexamine IOM Pregnancy Weight Guidelines. (2009).
21. World Obesity. No Title. Available at: https://www.worldobesitydata.org/. (Accessed: 14th January 2019)

22. Oliveira, A. *et al.* Prevalence of general and abdominal obesity in Portugal: Comprehensive results from the National Food, nutrition and physical activity survey 2015-2016. *BMC Public Health* **18**, 1–9 (2018).

23. World Health Organization. WHO Global Health Observatory Data Repository. (2013). Available at: http://apps.who.int/gho/data/view.main. (Accessed: 14th January 2019)

24. Whitaker, R. C. Predicting Preschooler Obesity at Birth: The Role of Maternal Obesity in Early Pregnancy. *Pediatrics* **114**, e29–e36 (2004).

25. Mouzon, S. H. & Lassance, L. Endocrine and metabolic adaptations to pregnancy ; impact of obesity. **24**, 65–72 (2015).

26. Salihu, H. M., De La Cruz, C., Rahman, S. & August, E. M. Does maternal obesity cause preeclampsia? A systematic review of the evidence. *Minerva Ginecol.* **64**, 259–80 (2012).

27. Bodnar, L. M., Catov, J. M., Klebanoff, M. A., Ness, R. B. & Roberts, J. M. Prepregnancy body mass index and the occurrence of severe hypertensive disorders of pregnancy. *Epidemiology* **18**, 234–239 (2007).

28. Biering, K. *et al.* Pregnancy-related pelvic pain is more frequent in women with increased body mass index. *Acta Obstet. Gynecol. Scand.* **90**, 1132–1139 (2011).

29. Torloni, M. R. *et al.* Prepregnancy BMI and the risk of gestational diabetes: A systematic review of the literature with meta-analysis: Diagnostic in Obesity and Complications. *Obes. Rev.* **10**, 194–203 (2009).

30. Callaghan, W. M., Chu, S. Y., Kim, Y. S., Schmid, C. H., Lau, J., England, J. L. & & Dietz, M. P. Maternal Obesity and Risk of Gestational. *Diabetes Care* **30**, 2070–2076 (2007).

31. Solomon, C. G. A Prospective Study of Pregravid Determinants of Gestational Diabetes Mellitus. *JAMA J. Am. Med. Assoc.* **278**, 1078 (1997).

32. Chu, S. Y. *et al.* Maternal obesity and risk of cesarean delivery: A meta-analysis. *Obes. Rev.* **8**, 385–394 (2007).

33. S., C. *et al.* Maternal obesity and risk of preterm delivery. *JAMA - J. Am. Med. Assoc.* **309**, 2362–2370 (2013).

34. E.A., N. *et al.* Maternal obesity and neonatal mortality according to subtypes of preterm birth. *Obstet. Gynecol.* **110**, 1083–1090 (2007).

35. Butte, N. F. & King, J. C. Energy requirements during pregnancy and lactation. **8**, 1010–1027 (2005).

36. Westbrook, R. H., Dusheiko, G. & Williamson, C. Pregnancy and liver disease. *J. Hepatol.* **64**, 933–945 (2016).

37. Einstein, F. H. *et al.* Accretion of visceral fat and hepatic insulin resistance in pregnant rats. 451–456 (2008). doi:10.1152/ajpendo.00570.2007.

38. Martin, A. M. *et al.* Abdominal Visceral Adiposity in the First Trimester Predicts Glucose Intolerance in Later Pregnancy. *Diabetes Care* **32**, 1308–1310 (2009).

39. Butte, N. F., Wong, W. W., Treuth, M. S., Ellis, K. J. & Smith, E. O. B. expenditure and energy deposition 1 – 4. 1078–1087 (2018).

40. Davis, E. M., Stange, K. C. & Horwitz, R. I. Childbearing, stress and obesity disparities in women: a public health perspective. *Matern. Child Health J.* **16**, 109–18 (2012).

41. Lassance, L., Haghiac, M., Minium, J., Catalano, P. & Hauguel-de Mouzon, S. Obesity-Induced Down-Regulation of the Mitochondrial Translocator Protein (TSPO) Impairs Placental Steroid Production. *J. Clin. Endocrinol. Metab.* **100**, E11–E18 (2015).

42. Moog-Lutz, C. *et al.* MLN64 exhibits homology with the steroidogenic acute regulatory protein (STAR) and is over-expressed in human breast carcinomas. *Int. J. cancer* **71**, 183–91 (1997).

43. Fan, J., Lindemann, P., Feuilloley, M. G. J. & Papadopoulos, V. Structural and functional evolution of the translocator protein (18 kDa). *Curr. Mol. Med.* **12**, 369–86 (2012).

44. Meyer, B. J. *et al.* Maternal Obesity Is Associated With the Formation of Small Dense LDL and Hypoadiponectinemia in the Third Trimester. *J. Clin. Endocrinol. Metab.* **98**, 643–652 (2013).

45. Perley, M. & Kipnis, D. M. Effect of Glucocorticoids on Plasma Insulin. *N. Engl. J. Med.* **274**, 1237–1241 (1966).

46. Metzger, B. E., Ravnikar, V., Vileisis, R. A. & Freinkel, N. 'Accelerated starvation' and the skipped breakfast in late normal pregnancy. *Lancet (London, England)* **1**, 588–92 (1982).

47. Hauguel-de Mouzon, S. & Guerre-Millo, M. The Placenta Cytokine Network and Inflammatory Signals. *Placenta* **27**, 794–798 (2006).

48. Shi, H. *et al.* TLR4 links innate immunity and fatty acid–induced insulin resistance. *J. Clin. Invest.* **116**, 3015–3025 (2006).

49. Petersen, M. C., Vatner, D. F. & Shulman, G. I. Regulation of hepatic glucose metabolism in health and disease. *Nat. Rev. Endocrinol.* **13**, 572–587 (2017).

50. Petta, S. *et al.* Pathophysiology of non alcoholic fatty liver disease. *Int. J. Mol. Sci.* **17**, (2016).

51. Okereke, N. C., Huston-Presley, L., Amini, S. B., Kalhan, S. & Catalano, P. M. Longitudinal changes in energy expenditure and body composition in obese women with normal and impaired glucose tolerance. *Am. J. Physiol. Metab.* **287**, E472–E479 (2004).

52. Sivan, E., Homko, C. J., Chen, X., Reece, E. A. & Boden, G. Effect of insulin on fat metabolism during and after normal pregnancy. *Diabetes* **48**, 834–8 (1999).

53. Hyötyläinen, T. *et al.* Genome-scale study reveals reduced metabolic adaptability in patients with non-alcoholic fatty liver disease. *Nat. Commun.* **7**, 1–9 (2016).

54. Boden, G., Chen, X., Rosner, J. & Barton, M. Effects of a 48-h fat infusion on insulin secretion and glucose utilization. *Diabetes* **44**, 1239–42 (1995).

55. Gastaldelli, A. *et al.* Influence of Obesity and Type 2 Diabetes on Gluconeogenesis and Glucose Output in Humans. *Diabetes* **49**, 1367 (2000).

56. Paradis, V. *et al.* High glucose and hyperinsulinemia stimulate connective tissue growth factor expression: A potential mechanism involved in progression to fibrosis in nonalcoholic steatohepatitis. *Hepatology* **34**, 738–744 (2001).

57. Donnelly, K. L., Smith, C. I., Schwarzenberg, S. J., Jessurun, J., Boldt, M. D. & Parks, E. J. Sources of fatty acids stored in liver and secreted via lipoproteins in patients with nonalcoholic fatty liver disease. *J. Clin. Invest.* **115**, 1343–1351 (2005).

58. Wewer Albrechtsen, N. J., Kuhre, R. E., Pedersen, J., Knop, F. K. & Holst, J. J. The biology of glucagon and the consequences of hyperglucagonemia. *Biomark. Med.* **10**, 1141–1151 (2016).

59. Junker, A. E., Gluud, L., Holst, J. J., Knop, F. K. & Vilsbøll, T. Diabetic and nondiabetic patients with nonalcoholic fatty liver disease have an impaired incretin effect and fasting hyperglucagonaemia. *J. Intern. Med.* **279**, 485–493 (2016).

60. Fantuzzi, G. Adiponectin and inflammation: Consensus and controversy. *J. Allergy Clin. Immunol.* **121**, 326–330 (2008).

61. Kamari, Y. *et al.* Metabolic stress with a high carbohydrate diet increases adiponectin levels. *Horm. Metab. Res.* **39**, 384–388 (2007).

62. Scherer, P. E. The multifaceted roles of adipose tissue - Therapeutic targets for diabetes and beyond: The 2015 banting lecture. *Diabetes* **65**, 1452–1461 (2016).

63. Haghiac, M. *et al.* Patterns of Adiponectin Expression in Term Pregnancy: Impact of Obesity. *J. Clin. Endocrinol. Metab.* **99**, 3427–3434 (2014).

64. Bugianesi, E. *et al.* Plasma Adiponectin in nonalcoholic fatty liver is related to hepatic insulin

resistance and hepatic fat content, not to liver disease severity. *J. Clin. Endocrinol. Metab.* **90**, 3498–3504 (2005).

65. Catalano, P. M. *et al.* Adiponectin in human pregnancy: implications for regulation of glucose and lipid metabolism. *Diabetologia* **49**, 1677–1685 (2006).

66. Izadi, V., Saraf-Bank, S. & Azadbakht, L. Dietary intakes and leptin concentrations. *ARYA Atheroscler.* **10**, (2014).

67. Fonseca-Alaniz, M. H., Takada, J., Alonso-Vale, M. I. C. & Lima, F. B. Adipose tissue as an endocrine organ: from theory to practice. *J. Pediatr. (Rio. J).* **83**, S192-203 (2007).

68. Martin, L. J. M. *et al.* Postprandial response of plasma insulin, amylin and acylated ghrelin to various test meals in lean and obese cats. *Br. J. Nutr.* **103**, 1610–1619 (2010).

69. Highman, T. J., Friedman, J. E., Huston, L. P., Wong, W. W. & Catalano, P. M. Longitudinal changes in maternal serum leptin concentrations, body composition, and resting metabolic rate in pregnancy. *Am. J. Obstet. Gynecol.* **178**, 1010–5 (1998).

70. Polyzos, S. A. *et al.* Circulating leptin in non-alcoholic fatty liver disease: a systematic review and meta-analysis. *Diabetologia* **59**, 30–43 (2016).

71. Steffes, M. W., Gross, M. D., Lee, D.-H., Schreiner, P. J. & Jacobs, D. R. Adiponectin, Visceral Fat, Oxidative Stress, and Early Macrovascular Disease: The Coronary Artery Risk Development in Young Adults Study*. *Obesity* **14**, 319–326 (2006).

72. Pyrzak, B., Ruminska, M., Popko, K. & Demkow, U. Adiponectin as a biomarker of the metabolic syndrome in children and adolescents. *Eur. J. Med. Res.* **15 Suppl 2**, 147–51 (2010).

73. Hotamisligil, G. S., Shargill, N. S. & Spiegelman, B. M. Adipose expression of tumor necrosis factor-alpha: direct role in obesity-linked insulin resistance. *Science* **259**, 87–91 (1993).

74. Hotamisligil, G. S. Inflammation and metabolic disorders. *Nature* **444**, 860–867 (2006).

75. Challier, J. C. *et al.* Obesity in Pregnancy Stimulates Macrophage Accumulation and Inflammation in the Placenta. *Placenta* **29**, 274–281 (2008).

76. Ramsay, J. E. *et al.* Maternal Obesity Is Associated with Dysregulation of Metabolic, Vascular, and Inflammatory Pathways. *J. Clin. Endocrinol. Metab.* **87**, 4231–4237 (2002).

77. Lastra, G., Manrique, C. M. & Hayden, M. R. The role of beta-cell dysfunction in the cardiometabolic syndrome. *J. Cardiometab. Syndr.* **1**, 41–6 (2006).

78. Steppan, C. M. *et al.* The hormone resistin links obesity to diabetes. *Nature* **409**, 307–312 (2001).

79. Abdel-Misih, Sherif R. Z.; Bloomston, M. Liver Anatomy. *Surg Clin North Am* **90**, 643–653 (2014).

80. Corey, K. E. & Kaplan, L. M. Obesity and liver disease. The epidemic of the twenty-first century. *Clin. Liver Dis.* **18**, 1–18 (2014).

81. Al Sharif, M., Alov, P., Vitcheva, V., Pajeva, I. & Tsakovska, I. Modes-of-action related to repeated dose toxicity: Tissue-specific biological roles of PPAR γ ligand-dependent dysregulation in nonalcoholic fatty liver disease. *PPAR Res.* **2014**, (2014).

82. Steinbrück, K. *et al.* Is there any difference between right hepatectomy and left lateral sectionectomy for living donors? As much you cut, as much you hurt? *Hpb* **12**, 684–687 (2010).

83. Nilsson, H., Karlgren, S., Blomqvist, L. & Jonas, E. The inhomogeneous distribution of liver function: Possible impact on the prediction of post-operative remnant liver function. *Hpb* **17**, 272–277 (2015).

84. Jacobsson, H., Jonas, E., Hellström, P. M. & Larsson, S. A. Different concentrations of various radiopharmaceuticals in the two main liver lobes: A preliminary study in clinical patients. *J. Gastroenterol.* **40**, 733–738 (2005).

85. Joshi, D., James, A., Quaglia, A., Westbrook, R. H. & Heneghan, M. A. Liver disease in

pregnancy. *Lancet* **375**, 594–605 (2010).

86. Martin, J. N., Rose, C. H. & Briery, C. M. Understanding and managing HELLP syndrome: The integral role of aggressive glucocorticoids for mother and child. *Am. J. Obstet. Gynecol.* **195**, 914–934 (2006).

87. Walker, I., Chappell, L. C. & Williamson, C. Abnormal liver function tests in pregnancy. *BMJ* **347**, f6055–f6055 (2013).

88. Natarajan, S. K. *et al.* Acute fatty liver of pregnancy: an update on mechanisms. *Obstet. Med.* **4**, 99–103 (2011).

89. Papafragkakis, H., Singhal, S. & Anand, S. Acute fatty liver of pregnancy. *South. Med. J.* **106**, 588–593 (2013).

90. Goel, A., Jamwal, K. D., Ramachandran, A., Balasubramanian, K. A. & Eapen, C. E. Pregnancy-related liver disorders. *J. Clin. Exp. Hepatol.* **4**, 151–162 (2014).

91. Langhans, W., Grossmann, F. & Geary, N. Intrameal hepatic-portal infusion of glucose reduces spontaneous meal size in rats. *Physiol. Behav.* **73**, 499–507 (2001).

92. Rolland, V. *et al.* Body weight, body composition, and energy metabolism in lean and obese Zucker rats fed soybean oil or butter. *Am. J. Clin. Nutr.* **75**, 21–30 (2002).

93. Varadarajan, R. *et al.* Nitric oxide in early ischaemia reperfusion injury during human orthotopic liver transplantation. *Transplantation* **78**, 250–6 (2004).

94. Giannini, E. G., Testa, R. & Savarino, V. Liver enzyme alteration: a guide for clinicians. *CMAJ* **172**, 367–79 (2005).

95. Sarwar, R., Pierce, N. & Koppe, S. Obesity and nonalcoholic fatty liver disease: current perspectives. *Diabetes. Metab. Syndr. Obes.* **11**, 533–542 (2018).

96. Nassir, F. & Ibdah, J. Role of Mitochondria in Nonalcoholic Fatty Liver Disease. *Int. J. Mol. Sci.* **15**, 8713–8742 (2014).

97. Byrne, C. D. & Targher, G. NAFLD: A multisystem disease. *J. Hepatol.* **62**, S47–S64 (2015).

98. Mofrad, P. *et al.* Clinical and histologic spectrum of nonalcoholic fatty liver disease associated with normal ALT values. *Hepatology* **37**, 1286–1292 (2003).

99. Neuschwander-Tetri, B. A. Non-alcoholic fatty liver disease. *BMC Med.* **15**, 1–6 (2017).

100. Blachier, M., Leleu, H., Peck-Radosavljevic, M., Valla, D. C. & Roudot-Thoraval, F. The burden of liver disease in Europe: A review of available epidemiological data. *J. Hepatol.* **58**, 593–608 (2013).

101. Williams, C. D. *et al.* Prevalence of nonalcoholic fatty liver disease and nonalcoholic steatohepatitis among a largely middle-aged population utilizing ultrasound and liver biopsy: A prospective study. *Gastroenterology* **140**, 124–131 (2011).

102. Brunello, G., Michaud, P.-C. & Sanz-de-Galdeano, A. The Rise in Obesity across the Atlantic: An Economic Perspective. (2008). doi:10.1111/j.0042-7092.2007.00700.x

103. Bedogni, G. *et al.* Incidence and natural course of fatty liver in the general population: The dionysos study. *Hepatology* **46**, 1387–1391 (2007).

104. Fazel, Y., Koenig, A. B., Sayiner, M., Goodman, Z. D. & Younossi, Z. M. Epidemiology and natural history of non-alcoholic fatty liver disease. *Metabolism.* **65**, 1017–1025 (2016).

105. Maglio, C., Pirazzi, C., Pujia, A., Valenti, L. & Romeo, S. The PNPLA3 I148M variant and chronic liver disease: When a genetic mutation meets nutrients. *Food Res. Int.* **63**, 239–243 (2014).

106. Liu, Y. L. *et al.* TM6SF2 rs58542926 influences hepatic fibrosis progression in patients with non-alcoholic fatty liver disease. *Nat. Commun.* **5**, 1–6 (2014).

107. Dongiovanni, P., Anstee, Q. & Valenti, L. Genetic Predisposition in NAFLD and NASH: Impact on Severity of Liver Disease and Response to Treatment. *Curr. Pharm. Des.* **19**, 5219–5238 (2013).

108. McPherson, S., Stewart, S. F., Henderson, E., Burt, A. D. & Day, C. P. Simple non-invasive fibrosis scoring systems can reliably exclude advanced fibrosis in patients with non-alcoholic fatty liver disease. *Gut* **59**, 1265–1269 (2010).

109. Yang, J. D. *et al.* Gender and menopause impact severity of fibrosis among patients with nonalcoholic steatohepatitis. *Hepatology* **59**, 1406–1414 (2014).

110. Adams, L. A. *et al.* The natural history of nonalcoholic fatty liver disease: A population-based cohort study. *Gastroenterology* **129**, 113–121 (2005).

111. Bambha, K. *et al.* Ethnicity and nonalcoholic fatty liver disease. *Hepatology* **55**, 769–780 (2012).

112. Lomonaco, R. *et al.* Role of ethnicity in overweight and obese patients with nonalcoholic steatohepatitis. *Hepatology* **54**, 837–845 (2011).

113. Mohanty, S. R. *et al.* Influence of ethnicity on histological differences in non-alcoholic fatty liver disease. *J. Hepatol.* **50**, 797–804 (2009).

114. Kallwitz, E. R. *et al.* The histologic spectrum of liver disease in african-american, non-hispanic white, and hispanic obesity surgery patients. *Am. J. Gastroenterol.* **104**, 64–69 (2009).

115. Younossi, Z. M. *et al.* Association of nonalcoholic fatty liver disease (NAFLD) with hepatocellular carcinoma (HCC) in the United States from 2004 to 2009. *Hepatology* **62**, 1723–1730 (2015).

116. Hossain, N. *et al.* Independent Predictors of Fibrosis in Patients With Nonalcoholic Fatty Liver Disease. *Clin. Gastroenterol. Hepatol.* **7**, 1224–1229.e2 (2009).

117. Yasui, K. *et al.* Characteristics of Patients With Nonalcoholic Steatohepatitis Who Develop Hepatocellular Carcinoma. *Clin. Gastroenterol. Hepatol.* **9**, 428–433 (2011).

118. Lu, Z. Y., Shao, Z., Li, Y. L., Wulasihan, M. & Chen, X. H. Prevalence of and risk factors for non-alcoholic fatty liver disease in a Chinese population: An 8-year follow-up study. *World J. Gastroenterol.* **22**, 3663–3669 (2016).

119. Baffy, G., Brunt, E. M. & Caldwell, S. H. Hepatocellular carcinoma in non-alcoholic fatty liver disease: An emerging menace. *J. Hepatol.* **56**, 1384–1391 (2012).

120. Bertot, L. C. & Adams, L. A. The natural course of non-alcoholic fatty liver disease. *Int. J. Mol. Sci.* **17**, (2016).

121. Kim, D., Kim, W. R., Kim, H. J. & Therneau, T. M. Association between noninvasive fibrosis markers and mortality among adults with nonalcoholic fatty liver disease in the United States. *Hepatology* **57**, 1357–1365 (2013).

122. Haring, R. *et al.* Ultrasonographic hepatic steatosis increases prediction of mortality risk from elevated serum gamma-glutamyl transpeptidase levels. *Hepatology* **50**, 1403–1411 (2009).

123. Wong, V. W. S. *et al.* Disease progression of non-alcoholic fatty liver disease: A prospective study with paired liver biopsies at 3 years. *Gut* **59**, 969–974 (2010).

124. Pais, R. *et al.* A systematic review of follow-up biopsies reveals disease progression in patients with non-alcoholic fatty liver. *J. Hepatol.* **59**, 550–556 (2013).

125. Singh, S. *et al.* Fibrosis Progression in Nonalcoholic Fatty Liver vs Nonalcoholic Steatohepatitis: A Systematic Review and Meta-analysis of Paired-Biopsy Studies. *Clin. Gastroenterol. Hepatol.* **13**, 643–654 (2015).

126. McPherson, S. *et al.* Evidence of NAFLD progression from steatosis to fibrosing-steatohepatitis using paired biopsies: Implications for prognosis and clinical management. *J. Hepatol.* **62**, 1148–1155 (2015).

127. Angulo, P. *et al.* The NAFLD fibrosis score: A noninvasive system that identifies liver fibrosis in patients with NAFLD. *Hepatology* **45**, 846–854 (2007).

128. Singal, A. K. *et al.* Evolving frequency and outcomes of liver transplantation based on etiology of liver disease. *Transplantation* **95**, 755–760 (2013).

129. Agopian, V. G. *et al.* Liver transplantation for nonalcoholic steatohepatitis: The new epidemic. *Ann. Surg.* **256**, 624–633 (2012).

130. Moore, J. B. Non-alcoholic fatty liver disease: the hepatic consequence of obesity and the metabolic syndrome. *Proc. Nutr. Soc.* **69**, 211–220 (2010).

131. Neuschwander-Tetri, B. A. Hepatic lipotoxicity and the pathogenesis of nonalcoholic steatohepatitis: The central role of nontriglyceride fatty acid metabolites. *Hepatology* **52**, 774–788 (2010).

132. Ioannou, G. N. The Role of Cholesterol in the Pathogenesis of NASH. *Trends Endocrinol. Metab.* **27**, 84–95 (2016).

133. Puri, P. *et al.* A lipidomic analysis of nonalcoholic fatty liver disease. *Hepatology* **46**, 1081–1090 (2007).

134. Li, Y. *et al.* Free Cholesterol-loaded Macrophages Are an Abundant Source of Tumor Necrosis Factor-α and Interleukin-6. *J. Biol. Chem.* **23**, 21763–21772 (2005).

135. Zámbó, V. *et al.* Lipotoxicity in the liver. **5**, 550–557 (2013).

136. Ponziani, F. R., Pecere, S., Gasbarrini, A. & Ojetti, V. Physiology and pathophysiology of liver lipid metabolism. *Expert Rev. Gastroenterol. Hepatol.* **9**, 1055–1067 (2015).

137. Grey, N. J., Karl, I. & Kipnis, D. M. Physiologic mechanisms in the development of starvation ketosis in man. *Diabetes* **24**, 10–16 (1975).

138. Kazantzis, M. & Stahl, A. Fatty acid transport proteins, implications in physiology and disease. *Biochim. Biophys. Acta - Mol. Cell Biol. Lipids* **1821**, 852–857 (2012).

139. Su, X. & Abumrad, N. A. Cellular fatty acid uptake: a pathway under construction. *Trends Endocrinol. Metab.* **20**, 72–77 (2009).

140. Bremer, J. O. N. Carnitine-Metabolism. **63**, (1983).

141. Zhu, L. *et al.* Lipid in the livers of adolescents with nonalcoholic steatohepatitis: Combined effects of pathways on steatosis. *Metabolism.* **60**, 1001–1011 (2011).

142. van Rossum, D. B. & Patterson, R. L. PKC and PLA2: Probing the complexities of the calcium network. *Cell Calcium* **45**, 535–545 (2009).

143. Fantino, M. Role of lipids in the control of food intake. *Curr. Opin. Clin. Nutr. Metab. Care* **14**, 138–144 (2011).

144. Kohan, A. B., Qing, Y., Cyphert, H. A., Tso, P., & Salati, L. M. Chylomicron Remnants and Nonesterified Fatty Acids Differ in Their Ability to Inhibit Genes Involved in Lipogenesis in Rats. *J. Nutr.* **141(2)**, 171–176 (2010).

145. Jump, D. B. Fatty acid regulation of hepatic lipid metabolism. *Curr. Opin. Clin. Nutr. Metab. Care* **14(2)**, 115–120 (2011).

146. Vallim, T. & Salter, A. M. Regulation of hepatic gene expression by saturated fatty acids. *Prostaglandins Leukot. Essent. Fat. Acids* **82**, 211–218 (2010).

147. Guan, M., Qu, L., Tan, W., Chen, L. & Wong, C. W. Hepatocyte nuclear factor-4 alpha regulates liver triglyceride metabolism in part through secreted phospholipase A2GXIIB. *Hepatology* **53**, 458–466 (2011).

148. Kennedy, A., Martinez, K., Chuang, C.-C., LaPoint, K. & McIntosh, M. Saturated Fatty Acid-Mediated Inflammation and Insulin Resistance in Adipose Tissue: Mechanisms of Action and Implications. *J. Nutr.* **139**, 1–4 (2008).

149. Stahl, A., Evans, J. G., Pattel, S., Hirsch, D. & Lodish, H. F. Translocation and Enhanced Fatty Acid Uptake in Adipocytes. **2**, 477–488 (2002).

150. Stump, D. D., Zhou, S. L. & Berk, P. D. Comparison of plasma membrane FABP and mitochondrial isoform of aspartate aminotransferase from rat liver. *Am J Physiol* **265**, G894-902 (1993).

151. Clarke, D. C. Overexpression of membrane-associated fatty acid binding protein (FABPpm) in vivo increases fatty acid sarcolemmal transport and metabolism. *Physiol. Genomics* **17**, 31–37 (2004).

152. Bradbury, M. W. & Berk, P. D. with two distinct functions to two subcellular sites does not require alternative splicing of the mRNA. *Society* **427**, 423–427 (2000).

153. Chabowski, A., Górski, J., Luiken, J. J. F. P., Glatz, J. F. C. & Bonen, A. Evidence for concerted action of FAT/CD36 and FABPpm to increase fatty acid transport across the plasma membrane. *Prostaglandins Leukot. Essent. Fat. Acids* **77**, 345–353 (2007).

154. Han, X.-X. *et al.* Metabolic challenges reveal impaired fatty acid metabolism and translocation of FAT/CD36 but not FABPpm in obese Zucker rat muscle. *AJP Endocrinol. Metab.* **293**, E566–E575 (2007).

155. Chabowski, A. *et al.* The subcellular compartmentation of fatty acid transporters is regulated differently by insulin and by AICAR. *FEBS Lett.* **579**, 2428–2432 (2005).

156. Chabowski, A., Górski, J., Calles-Escandon, J., Tandon, N. N. & Bonen, A. Hypoxia-induced fatty acid transporter translocation increases fatty acid transport and contributes to lipid accumulation in the heart. *FEBS Lett.* **580**, 3617–3623 (2006).

157. Huang, H., Starodub, O., McIntosh, A., Kier, A. B. & Schroeder, F. Liver fatty acid-binding protein targets fatty acids to the nucleus. Real time confocal and multiphoton fluorescence imaging in living cells. *J. Biol. Chem.* **277**, 29139–29151 (2002).

158. Coburn, C. T., Hajri, T., Ibrahimi, A. & Abumrad, N. A. Role of CD36 in membrane transport and utilization of long-chain fatty acids by different tissues. *J. Mol. Neurosci.* **16**, 117–121 (2001).

159. He, J., Lee, J. H., Febbraio, M. & Xie, W. The emerging roles of fatty acid translocase/CD36 and the aryl hydrocarbon receptor in fatty liver disease. *Exp. Biol. Med.* **236**, 1116–1121 (2011).

160. Ehehalt, R. *et al.* Uptake of long chain fatty acids is regulated by dynamic interaction of FAT/CD36 with cholesterol/sphingolipid enriched microdomains (lipid rafts). *BMC Cell Biol.* **9**, 1–12 (2008).

161. Handberg, A. *et al.* Plasma sCD36 is associated with markers of atherosclerosis, insulin resistance and fatty liver in a nondiabetic healthy population. *J. Intern. Med.* **271**, 294–304 (2012).

162. Choi, Y. J. *et al.* Activation of AMPK by berberine induces hepatic lipid accumulation by upregulation of fatty acid translocase CD36 in mice. *Toxicol. Appl. Pharmacol.* **316**, 74–82 (2017).

163. Sheedfar, F. *et al.* Increased hepatic CD36 expression with age is associated with enhanced susceptibility to nonalcoholic fatty liver disease. *Aging (Albany. NY).* **6**, 281–295 (2014).

164. Wilson, C. G. *et al.* Hepatocyte-specific disruption of CD36 attenuates fatty liver and improves insulin sensitivity in HFD-fed mice. *Endocrinology* **157**, 570–585 (2016).

165. Koonen, D. P. Y., Jacobs, L., Febbraio, M., Young, M. E. & Soltys, C. M. Increased Hepatic CD36 Expression Contributes to Dyslipidemia Associated With Diet-Induced Obesity. *Diabetes* **56**, 2863–2871 (2007).

166. Stahl, A., Gimeno, R. E., Tartaglia, L. A. & Lodish, H. F. Fatty acid transport proteins: A current view of a growing family. *Trends Endocrinol. Metab.* **12**, 266–273 (2001).

167. Richards, M. R. *et al.* Oligomerization of the murine fatty acid transport protein 1. *J. Biol. Chem.* **278**, 10477–10483 (2003).

168. Richards, M. R., Harp, J. D., Ory, D. S. & Schaffer, J. E. Fatty acid transport protein 1 and long-chain acyl coenzyme A synthetase 1 interact in adipocytes. *J. Lipid Res.* **47**, 665–672 (2006).

169. Falcon, A., Doege, H., Fluitt, A., Tsang, B., Watson, N., Kay, M. A., & Stahl, A. FATP2 is a hepatic fatty acid transporter and peroxisomal very long-chain acyl-CoA synthetase. *Am. J. Physiol. Metab.* **299(3)**, E384–E393 (2010).

170. Doege, H. *et al.* Silencing of hepatic fatty acid transporter protein 5 in vivo reverses diet-induced non-alcoholic fatty liver disease and improves hyperglycemia. *J. Biol. Chem.* **283**, 22186–22192 (2008).

171. Doege, H. *et al.* Targeted Deletion of FATP5 Reveals Multiple Functions in Liver Metabolism: Alterations in Hepatic Lipid Homeostasis. *Gastroenterology* **130**, 1245–1258 (2006).

172. Wei, Y., Rector, R. S., Thyfault, J. P., & Ibdah, J. A. Nonalcoholic fatty liver disease and mitochondrial dysfunction. *World J. Gastroenterol.* **14(2)**, 193 (2008).

173. Reddy, J. K. & Hashimoto, T. PEROXISOMAL β-OXIDATION AND PEROXISOME PROLIFERATOR–ACTIVATED RECEPTOR α: An Adaptive Metabolic System. *Annu. Rev. Nutr.* **21(1)**, 193–230 (2001).

174. Lu, K. Le *et al.* Hepatic β-oxidation and regulation of carnitine palmitoyltransferase (CPT) I in blunt snout bream Megalobrama amblycephala fed a high fat diet. *PLoS One* **9**, (2014).

175. Koo, S.-H. Nonalcoholic fatty liver disease: molecular mechanisms for the hepatic steatosis. *Clin. Mol. Hepatol.* **19**, 210 (2013).

176. Giangregorio, N., Tonazzi, A., Console, L. & Indiveri, C. Post-translational modification by acetylation regulates the mitochondrial carnitine/acylcarnitine transport protein. *Mol. Cell. Biochem.* **426**, 65–73 (2017).

177. Cox, K. B. *et al.* Gestational, pathologic and biochemical differences between very long-chain acyl-CoA dehydrogenase deficiency and long-chain acyl-CoA dehydrogenase deficiency in the mouse. *Hum Mol Genet.* **10**, 2069–77 (2001).

178. Tolwani, R. J. *et al.* Medium-chain acyl-CoA dehydrogenase deficiency in gene-targeted mice. *PLoS Genet.* **1**, 0205–0212 (2005).

179. Houtkooper, R. H., Pirinen, E. & Auwerx, J. Sirtuins as regulators of metabolism and healthspan. *Nat. Rev. Mol. Cell Biol.* **13**, 225–238 (2012).

180. Foster, D. W. Malonyl-CoA: the regulator of fatty acid synthesis and oxidation. *J. Clin. Invest.* **122(6)**, 1958–1959 (2012).

181. Jensen-Urstad, A. P. L. & Semenkovich, C. F. Fatty acid synthase and liver triglyceride metabolism: Housekeeper or messenger? *Biochim. Biophys. Acta - Mol. Cell Biol. Lipids* **1821**, 747–753 (2012).

182. Sanders, F. W. B. & Griffin, J. L. De novo lipogenesis in the liver in health and disease: More than just a shunting yard for glucose. *Biol. Rev.* **91**, 452–468 (2016).

183. Schwarz, J. M., Linfoot, P., Dare, D. & Aghajanian, K. Hepatic de novo lipogenesis in normoinsulinemic and hyperinsulinemic subjects consuming high-fat, low-carbohydrate and low-fat, high-carbohydrate isoenergetic diets. *Am. J. Clin. Nutr.* **77**, 43–50 (2003).

184. Maier, T., Leibundgut, M. & Ban, N. The crystal structure of a mammalian fatty acid synthase. *Science (80-.).* **321**, 1315–1322 (2008).

185. Mikkelsen, J., Hojrup, P., Rasmussen, M. M., Roepstorff, P. & Knudsen, J. Amino acid sequence around the active-site serine residue in the acyltransferase domain of goat mammary fatty acid synthetase. *Biochem J* **227**, 21–27 (1985).

186. Von Wettstein-Knowles, P., Olsen, J. G., McGuire, K. A. & Henriksen, A. Fatty acid synthesis: Role of active site histidines and lysine in Cys-His-His-type β-ketoacyl-acyl carrier protein synthases. *FEBS J.* **273**, 695–710 (2006).

187. Smith, S. & Tsai, S. C. The type I fatty acid and polyketide synthases: A tale of two megasynthases. *Nat. Prod. Rep.* **24**, 1041–1072 (2007).

188. Softic, S., Cohen, D. E. & Kahn, C. R. Role of Dietary Fructose and Hepatic De Novo Lipogenesis in Fatty Liver Disease. *Dig. Dis. Sci.* **61**, 1282–1293 (2016).

189. Chakravarty, B., Gu, Z., Chirala, S. S., Wakil, S. J. & Quiocho, F. A. Human fatty acid synthase: Structure and substrate selectivity of the thioesterase domain. *Proc. Natl. Acad. Sci.* **101**, 15567–15572 (2004).

190. Miyazaki, M., Kim, Y. C. & Ntambi, J. M. A lipogenic diet in mice with a disruption of the stearoyl-CoA desaturase 1 gene reveals a stringent requirement of endogenous monounsaturated fatty acids for triglyceride synthesis 7. *J Lipid Res.* **42**, 1018–1024 (2001).

191. Puri, P. *et al.* The plasma lipidomic signature of nonalcoholic steatohepatitis. *Hepatology* **50**, 1827–1838 (2009).

192. Jump, D. B., Clarke, S. D., Thelen, A. & Liimatta, M. Coordinate regulation of glycolytic and lipogenic gene expression by polyunsaturated fatty acids. *J. Lipid Res.* **35 %6**, 1076-1084 %& (1994).

193. Abu-Elheiga, L. *et al.* Mutant mice lacking acetyl-CoA carboxylase 1 are embryonically lethal. *Proc. Natl. Acad. Sci.* **102**, 12011–12016 (2005).

194. Chakravarthy, M. V. *et al.* 'New' hepatic fat activates PPARα to maintain glucose, lipid, and cholesterol homeostasis. *Cell Metab.* **1**, 309–322 (2005).

195. Bianchi, A. *et al.* Identification of an isozymic form of acetyl-CoA carboxylase. *J. Biol. Chem.* **265**, 1502–1509 (1990).

196. Ahmad, F., Ahmad, P. M., Pieretti, L. & Watters, G. T. Purification and subunit structure of rat mammary gland acetyl coenzyme A carboxylase. *J. Biol. Chem.* **253**, 1733–1737 (1978).

197. Kim, C.-W. *et al.* Induced polymerization of mammalian acetyl-CoA carboxylase by MIG12 provides a tertiary level of regulation of fatty acid synthesis. *Proc. Natl. Acad. Sci.* **107**, 9626–9631 (2010).

198. Boone, A. N., Chan, A., Kulpa, J. E. & Brownsey, R. W. Bimodal activation of acetyl-CoA carboxylase by glutamate. *J. Biol. Chem.* **275**, 10819–10825 (2000).

199. Brownsey, R. W., Boone, A. N., Elliott, J. E., Kulpa, J. E., & Lee, W. M. Regulation of acetyl-CoA carboxylase. *Biochem. Soc. Trans.* **34(2)**, 223 (2006).

200. Gaussin, V., Hue, L., Stalmans, W. & Bollen, M. Activation of hepatic acetyl-CoA carboxylase by glutamate and Mg2+ is mediated by protein phosphatase-2A. *J. Biochem.* **224**, 217–24 (1996).

201. Postic, C., & Girard, J. Contribution of de novo fatty acid synthesis to hepatic steatosis and insulin resistance: lessons from genetically engineered mice. *J. Clin. Invest.* **118**, 829–838 (2008).

202. Kawano, Y. & Cohen, D. E. Mechanisms of hepatic triglyceride accumulation in non-alcoholic fatty liver disease. *J. Gastroenterol.* **48**, 434–441 (2013).

203. Oosterveer, M. H. & Schoonjans, K. Hepatic glucose sensing and integrative pathways in the liver. *Cell. Mol. Life Sci.* **71**, 1453–1467 (2014).

204. Ferré, P. & Foufelle, F. Hepatic steatosis: a role for de novo lipogenesis and the transcription factor SREBP-1c. *Diabetes, Obes. Metab.* **12**, 83–92 (2010).

205. Sun, L.-P., Seemann, J., Goldstein, J. L. & Brown, M. S. Sterol-regulated transport of SREBPs from endoplasmic reticulum to Golgi: Insig renders sorting signal in Scap inaccessible to COPII proteins. *Proc. Natl. Acad. Sci.* **104**, 6519–6526 (2007).

206. Ricoult, S. J. H. & Manning, B. D. The multifaceted role of mTORC1 in the control of lipid metabolism. *EMBO Rep.* **14**, 242–251 (2013).

207. Chawla, A. Nuclear Receptors and Lipid Physiology: Opening the X-Files. *Science (80-.).* **294**,

1866–1870 (2001).

208. Dentin, R. *et al.* Glucose 6-phosphate, rather than xylulose 5-phosphate, is required for the activation of ChREBP in response to glucose in the liver. *J. Hepatol.* **56**, 199–209 (2012).

209. Arden, C. *et al.* Fructose 2,6-bisphosphate is essential for glucose-regulated gene transcription of glucose-6-phosphatase and other ChREBP target genes in hepatocytes. *Biochem. J.* **443**, 111–123 (2012).

210. Uyeda, K. & Repa, J. J. Carbohydrate response element binding protein, ChREBP, a transcription factor coupling hepatic glucose utilization and lipid synthesis. *Cell Metab.* **4**, 107–110 (2006).

211. Stein, O. & Stein, Y. Lipid synthesis, intracellular transport, storage, and secretion. I. Electron microscopic radioautographic study of liver after injection of tritiated palmitate or glycerol in fasted and ethanol-treated rats. *J. Cell Biol.* **33**, 319–339 (1967).

212. Harayama, T. & Riezman, H. Understanding the diversity of membrane lipid composition. *Nat. Rev. Mol. Cell Biol.* (2018). doi:10.1038/nrm.2017.138

213. Coleman, R. A. & Lee, D. P. Enzymes of triacylglycerol synthesis and their regulation. *Prog. Lipid Res.* **43**, 134–176 (2004).

214. Khatun, I. *et al.* Phospholipid transfer activity of microsomal triglyceride transfer protein produces apolipoprotein B and reduces hepatosteatosis while maintaining low plasma lipids in mice. *Hepatology* **55**, 1356–1368 (2012).

215. Wilfling, F., Haas, J. T., Walther, T. C. & Jr, R. V. F. Lipid droplet biogenesis. *Curr. Opin. Cell Biol.* **29**, 39–45 (2014).

216. Aon, M. A., Bhatt, N. & Cortassa, S. C. Mitochondrial and cellular mechanisms for managing lipid excess. *Front. Physiol.* **5**, 3218–3226 (2014).

217. Meikle, P. J. & Christopher, M. J. Lipidomics is providing new insight into the metabolic syndrome and its sequelae. *Curr. Opin. Lipidol.* **22**, 210–215 (2011).

218. Boden, G. Obesity, insulin resistance and free fatty acids. *Curr. Opin. Endocrinol. Diabetes Obes.* **18**, 139–143 (2011).

219. Ipsen, D. H., Lykkesfeldt, J. & Tveden-Nyborg, P. Molecular mechanisms of hepatic lipid accumulation in non-alcoholic fatty liver disease. *Cell. Mol. Life Sci.* **75**, 3313–3327 (2018).

220. Dasarathy, S. *et al.* Elevated hepatic fatty acid oxidation, high plasma fibroblast growth factor 21, and fasting bile acids in nonalcoholic steatohepatitis. *Eur. J. Gastroenterol. Hepatol.* **23**, 382–388 (2011).

221. Dasarathy, S. *et al.* Glycine and urea kinetics in nonalcoholic steatohepatitis in human: effect of intralipid infusion. *Am.J.Physiol Gastrointest.Liver Physiol* **297**, G567–G575 (2009).

222. Miele, L. *et al.* Hepatic mitochondrial beta-oxidation in patients with nonalcoholic steatohepatitis assessed by 13C-octanoate breath test. *Am. J. Gastroenterol.* **98**, 2335–2336 (2003).

223. Kotronen, A. *et al.* Liver fat and lipid oxidation in humans. *Liver Int.* **29**, 1439–1446 (2009).

224. Croci, I. *et al.* Whole-body substrate metabolism is associated with disease severity in patients with non-alcoholic fatty liver disease. *Gut* **62**, 1625–1633 (2013).

225. Auguet, T. *et al.* Altered fatty acid metabolism-related gene expression in liver from morbidly obese women with non-alcoholic fatty liver disease. *Int. J. Mol. Sci.* **15**, 22173–22187 (2014).

226. Lambert, J. E., Ramos-Roman, M. A., Browning, J. D. & Parks, E. J. Increased de novo lipogenesis is a distinct characteristic of individuals with nonalcoholic fatty liver disease. *Gastroenterology* **146**, 726–735 (2014).

227. Diraison, F., Moulin, P. & Beylot, M. Contribution of hepatic de novo lipogenesis and reesterification of plasma non esterified fatty acids to plasma triglyceride synthesis during non-alcoholic fatty liver disease. *Diabetes Metab.* **29**, 478–485 (2003).

228. Paradies, G., Paradies, V., Ruggiero, F. M. & Petrosillo, G. Oxidative stress, cardiolipin and mitochondrial dysfunction in nonalcoholic fatty liver disease. *World J. Gastroenterol.* **20**, 14205–14218 (2014).

229. Bhatti, J. S., Bhatti, G. K. & Reddy, P. H. Mitochondrial dysfunction and oxidative stress in metabolic disorders — A step towards mitochondria based therapeutic strategies. *Biochim. Biophys. Acta - Mol. Basis Dis.* **1863**, 1066–1077 (2017).

230. Chen, X. J. & Butow, R. A. The organization and inheritance of the mitochondrial genome. *Nat. Rev. Genet.* **6**, 815–825 (2005).

231. Palikaras, K. & Tavernarakis, N. Mitochondrial homeostasis: The interplay between mitophagy and mitochondrial biogenesis. *Exp. Gerontol.* **56**, 182–188 (2014).

232. Bournat, J. C. & Brown, C. W. Mitochondrial dysfunction in obesity. *Curr. Opin. Endocrinol. Diabetes. Obes.* **17**, 446–52 (2010).

233. Pessayre, D. & Fromenty, B. NASH: a mitochondrial disease. *J. Hepatol.* **42**, 928–940 (2005).

234. Valerio, A. *et al.* TNF- downregulates eNOS expression and mitochondrial biogenesis in fat and muscle of obese rodents. *J. Clin. Invest.* **116**, 2791–2798 (2006).

235. Santamaria, E. *et al.* Functional proteomics of nonalcoholic steatohepatitis: mitochondrial proteins as targets of S-adenosylmethionine. *Proc. Natl. Acad. Sci. U. S. A.* **100**, 3065–70 (2003).

236. Lasserre, J.-P. *et al.* Yeast as a system for modeling mitochondrial disease mechanisms and discovering therapies. *Dis. Model. Mech.* **8**, 509–526 (2015).

237. Kelley, D. E., He, J., Menshikova, E. V & Ritov, V. B. Dysfunction of mitochondria in human skeletal muscle in type 2 diabetes. *Diabetes* **51**, 2944–50 (2002).

238. Jheng, H.-F. *et al.* Mitochondrial Fission Contributes to Mitochondrial Dysfunction and Insulin Resistance in Skeletal Muscle. *Mol. Cell. Biol.* **32**, 309–319 (2012).

239. Caldwell, S. H. *et al.* Mitochondrial abnormalities in non-alcoholic steatohepatitis. *J. Hepatol.* **31**, 430–4 (1999).

240. McMurray, F., Patten, D. A. & Harper, M. E. Reactive Oxygen Species and Oxidative Stress in Obesity—Recent Findings and Empirical Approaches. *Obesity* **24**, 2301–2310 (2016).

241. Argyropoulos, G. *et al.* Effects of mutations in the human uncoupling protein 3 gene on the respiratory quotient and fat oxidation in severe obesity and type 2 diabetes. *J. Clin. Invest.* **102**, 1345–1351 (1998).

242. Xu, Y.-P. *et al.* Association between UCP3 gene polymorphisms and nonalcoholic fatty liver disease in Chinese children. *World J. Gastroenterol.* **19**, 5897–903 (2013).

243. Dalgaard, L. T. *et al.* A Prevalent Polymorphism in the Promoter of the *UCP3* Gene and Its Relationship to Body Mass Index and Long Term Body Weight Change in the Danish Population [1]. *J. Clin. Endocrinol. Metab.* **86**, 1398–1402 (2001).

244. Monteiro, R. & Azevedo, I. Chronic Inflammation in Obesity and the Metabolic Syndrome. *Mediators Inflamm.* **2010**, 1–10 (2010).

245. Maiese, K., Morhan, S. D. & Chong, Z. Z. Oxidative stress biology and cell injury during type 1 and type 2 diabetes mellitus. *Curr. Neurovasc. Res.* **4**, 63–71 (2007).

246. Graier, W. F., Trenker, M. & Malli, R. Mitochondrial Ca2+, the secret behind the function of uncoupling proteins 2 and 3? *Cell Calcium* **44**, 36–50 (2008).

247. Arsenijevic, D. *et al.* Disruption of the uncoupling protein-2 gene in mice reveals a role in immunity and reactive oxygen species production. *Nat. Genet.* **26**, 435–439 (2000).

248. Pérez, M. J. & Quintanilla, R. A. Development or disease: duality of the mitochondrial permeability transition pore. *Dev. Biol.* **426**, 1–7 (2017).

249. Rao, V. K., Carlson, E. A. & Yan, S. S. Mitochondrial permeability transition pore is a potential

drug target for neurodegeneration. *Biochim. Biophys. Acta - Mol. Basis Dis.* **1842**, 1267–1272 (2014).

250. Elrod, J. W. & Molkentin, J. D. Physiologic functions of cyclophilin D and the mitochondrial permeability transition pore. *Circ. J.* **77**, 1111–22 (2013).

251. Jonas, E. A., Porter, G. A., Beutner, G., Mnatsakanyan, N. & Alavian, K. N. Cell death disguised: The mitochondrial permeability transition pore as the c-subunit of the F1FO ATP synthase. *Pharmacol. Res.* **99**, 382–392 (2015).

252. Pesta, D. *et al.* Similar qualitative and quantitative changes of mitochondrial respiration following strength and endurance training in normoxia and hypoxia in sedentary humans. *Am. J. Physiol. Integr. Comp. Physiol.* **301**, R1078–R1087 (2011).

253. Campos, J. C. *et al.* Exercise reestablishes autophagic flux and mitochondrial quality control in heart failure. *Autophagy* **13**, 1304–1317 (2017).

254. Koliaki, C. *et al.* Adaptation of Hepatic Mitochondrial Function in Humans with Non-Alcoholic Fatty Liver Is Lost in Steatohepatitis. *Cell Metab.* **21**, 739–746 (2015).

255. Lohr, K. *et al.* Reduced mitochondrial mass and function add to age-related susceptibility toward diet-induced fatty liver in C57BL/6J mice. *Physiol. Rep.* **4**, (2016).

256. Wai, T. & Langer, T. Mitochondrial Dynamics and Metabolic Regulation. *Trends Endocrinol. Metab.* **27**, 105–117 (2016).

257. Ventura-Clapier, R., Garnier, A. & Veksler, V. Transcriptional control of mitochondrial biogenesis: the central role of PGC-1. *Cardiovasc. Res.* **79**, 208–217 (2008).

258. Jornayvaz, F. R. & Shulman, G. I. Regulation of mitochondrial biogenesis. *Essays Biochem.* **47**, 69–84 (2010).

259. Virbasius, J. V & Scarpulla, R. C. Activation of the human mitochondrial transcription factor A gene by nuclear respiratory factors: a potential regulatory link between nuclear and mitochondrial gene expression in organelle biogenesis. *Proc. Natl. Acad. Sci. U. S. A.* **91**, 1309–13 (1994).

260. Wright, D. C., Geiger, P. C., Han, D.-H., Jones, T. E. & Holloszy, J. O. Calcium Induces Increases in Peroxisome Proliferator-activated Receptor γ Coactivator-1α and Mitochondrial Biogenesis by a Pathway Leading to p38 Mitogen-activated Protein Kinase Activation. *J. Biol. Chem.* **282**, 18793–18799 (2007).

261. Feige, J. N. & Auwerx, J. Transcriptional coregulators in the control of energy homeostasis. *Trends Cell Biol.* **17**, 292–301 (2007).

262. Sparks, L. M. *et al.* A high-fat diet coordinately downregulates genes required for mitochondrial oxidative phosphorylation in skeletal muscle. *Diabetes* **54**, 1926–33 (2005).

263. Picca, A. *et al.* Mitochondrial quality control mechanisms as molecular targets in cardiac ageing. *Nat. Rev. Cardiol.* **15**, 543–554 (2018).

264. Scarpulla, R. C. Transcriptional Paradigms in Mammalian Mitochondrial Biogenesis and Function. *Physiol. Rev.* **88**, 611–638 (2008).

265. Dominy, J. E. & Puigserver, P. Mitochondrial Biogenesis through Activation of Nuclear Signaling Proteins. *Cold Spring Harb. Perspect. Biol.* **5**, a015008–a015008 (2013).

266. Hales, K. The machinery of mitochondrial fusion, division, and distribution, and emerging connections to apoptosis. *Mitochondrion* **4**, 285–308 (2004).

267. Youle, R. J. & van der Bliek, A. M. Mitochondrial Fission, Fusion, and Stress. *Science (80-.).* **337**, 1062–1065 (2012).

268. Cipolat, S., de Brito, O. M., Dal Zilio, B. & Scorrano, L. OPA1 requires mitofusin 1 to promote mitochondrial fusion. *Proc. Natl. Acad. Sci.* **101**, 15927–15932 (2004).

269. Hales, K. G. & Fuller, M. T. Developmentally regulated mitochondrial fusion mediated by a

conserved, novel, predicted GTPase. *Cell* **90**, 121–9 (1997).

270. Elgass, K., Pakay, J., Ryan, M. T. & Palmer, C. S. Recent advances into the understanding of mitochondrial fission. *Biochim. Biophys. Acta - Mol. Cell Res.* **1833**, 150–161 (2013).

271. Ashrafi, G. & Schwarz, T. L. The pathways of mitophagy for quality control and clearance of mitochondria. *Cell Death Differ.* **20**, 31–42 (2013).

272. Orenstein, S. J. & Cuervo, A. M. Chaperone-mediated autophagy: Molecular mechanisms and physiological relevance. *Semin. Cell Dev. Biol.* **21**, 719–726 (2010).

273. Ding, W.-X. & Yin, X.-M. Mitophagy: mechanisms, pathophysiological roles, and analysis. *Biol. Chem.* **393**, 547–64 (2012).

274. Geisler, S. *et al.* PINK1/Parkin-mediated mitophagy is dependent on VDAC1 and p62/SQSTM1. *Nat. Cell Biol.* **12**, 119–131 (2010).

275. Jin, S. M. & Youle, R. J. PINK1- and Parkin-mediated mitophagy at a glance. *J. Cell Sci.* **125**, 795–799 (2012).

276. Gegg, M. E. *et al.* Mitofusin 1 and mitofusin 2 are ubiquitinated in a PINK1/parkin-dependent manner upon induction of mitophagy. *Hum. Mol. Genet.* **19**, 4861–4870 (2010).

277. Kanki, T., Klionsky, D. J. & Okamoto, K. Mitochondria Autophagy in Yeast. *Antioxid. Redox Signal.* **14**, 1989–2001 (2011).

278. Tanida, I. Autophagy basics. *Microbiol. Immunol.* **55**, 1–11 (2011).

279. Gkikas, I., Palikaras, K. & Tavernarakis, N. The Role of Mitophagy in Innate Immunity. *Front. Immunol.* **9**, (2018).

280. Radoshevich, L. *et al.* ATG12 Conjugation to ATG3 Regulates Mitochondrial Homeostasis and Cell Death. *Cell* **142**, 590–600 (2010).

281. Youle, R. J. & Narendra, D. P. Mechanisms of mitophagy. *Nat. Rev. Mol. Cell Biol.* **12**, 9–14 (2011).

282. Shin, J.-H. *et al.* PARIS (ZNF746) Repression of PGC-1α Contributes to Neurodegeneration in Parkinson's Disease. *Cell* **144**, 689–702 (2011).

283. Lavallard, V. J. & Gual, P. Autophagy and Non-Alcoholic Fatty Liver Disease. *Biomed Res. Int.* **2014**, (2014).

284. Koga, H., Kaushik, S. & Cuervo, A. M. Altered lipid content inhibits autophagic vesicular fusion. *FASEB J.* **24**, 3052–3065 (2010).

285. González-Rodríguez, Á. *et al.* Impaired autophagic flux is associated with increased endoplasmic reticulum stress during the development of NAFLD. *Cell Death Dis.* **5**, e1179–e1179 (2014).

286. Kaur, J. & Debnath, J. Autophagy at the crossroads of catabolism and anabolism. *Nat. Rev. Mol. Cell Biol.* **16**, 461–472 (2015).

287. Lim, Y.-M. *et al.* Systemic autophagy insufficiency compromises adaptation to metabolic stress and facilitates progression from obesity to diabetes. *Nat. Commun.* **5**, 4934 (2014).

288. Moles, A., Tarrats, N., Fernández-Checa, J. C. & Marí, M. Cathepsins B and D drive hepatic stellate cell proliferation and promote their fibrogenic potential. *Hepatology* **49**, 1297–307 (2009).

289. Manchanda, M. *et al.* Cathepsin L and B as Potential Markers for Liver Fibrosis: Insights From Patients and Experimental Models. *Clin. Transl. Gastroenterol.* **8**, e99 (2017).

290. Fukuo, Y. *et al.* Abnormality of autophagic function and cathepsin expression in the liver from patients with non-alcoholic fatty liver disease. *Hepatol. Res.* **44**, 1026–1036 (2014).

291. Inami, Y. *et al.* Hepatic steatosis inhibits autophagic proteolysis via impairment of autophagosomal acidification and cathepsin expression. *Biochem. Biophys. Res. Commun.* **412**,

618–625 (2011).

292. Sherratt, H. S. Mitochondria: structure and function. *Rev. Neurol. (Paris).* **147**, 417–30 (1991).

293. Desideri, E., Vegliante, R. & Ciriolo, M. R. Mitochondrial dysfunctions in cancer: Genetic defects and oncogenic signaling impinging on TCA cycle activity. *Cancer Lett.* **356**, 217–223 (2015).

294. Akram, M. Citric Acid Cycle and Role of its Intermediates in Metabolism. *Cell Biochem. Biophys.* **68**, 475–478 (2014).

295. Lushchak, O. V., Piroddi, M., Galli, F. & Lushchak, V. I. Aconitase post-translational modification as a key in linkage between Krebs cycle, iron homeostasis, redox signaling, and metabolism of reactive oxygen species. *Redox Rep.* **19**, 8–15 (2014).

296. Cantu, D., Schaack, J. & Patel, M. Oxidative Inactivation of Mitochondrial Aconitase Results in Iron and H2O2-Mediated Neurotoxicity in Rat Primary Mesencephalic Cultures. *PLoS One* **4**, e7095 (2009).

297. Shadel, G. S. Mitochondrial DNA, aconitase 'wraps' it up. *Trends Biochem. Sci.* **30**, 294–296 (2005).

298. Singh, S. P. *et al.* Role of the electrophilic lipid peroxidation product 4-hydroxynonenal in the development and maintenance of obesity in mice. *Biochemistry* **47**, 3900–3911 (2008).

299. Zimniak, P. 4-Hydroxynonenal and fat storage: A paradoxical pro-obesity mechanism? *Cell Cycle* **9**, 3393–3394 (2010).

300. Bulku, A., Weaver, T. M. & Berkmen, M. B. Biochemical Characterization of Two Clinically-Relevant Human Fumarase Variants Defective for Oligomerization. *Open Biochem. J.* **12**, 1–15 (2018).

301. Dallner, G. & Sindelar, P. J. Regulation of ubiquinone metabolism. *Free Radic. Biol. Med.* **29**, 285–94 (2000).

302. Chaban, Y., Boekema, E. J. & Dudkina, N. V. Structures of mitochondrial oxidative phosphorylation supercomplexes and mechanisms for their stabilisation. *Biochim. Biophys. Acta - Bioenerg.* **1837**, 418–426 (2014).

303. Lobo-Jarne, T. & Ugalde, C. Respiratory chain supercomplexes: Structures, function and biogenesis. *Semin. Cell Dev. Biol.* **76**, 179–190 (2018).

304. Reinecke, F., Smeitink, J. A. M. & van der Westhuizen, F. H. OXPHOS gene expression and control in mitochondrial disorders. *Biochim. Biophys. Acta - Mol. Basis Dis.* **1792**, 1113–1121 (2009).

305. Schagger, H. & Pfeiffer, K. Supercomplexes in the respiratory chains of yeast and mammalian mitochondria. *EMBO J.* **19**, 1777–1783 (2000).

306. Pérez-Carreras, M. *et al.* Defective hepatic mitochondrial respiratory chain in patients with nonalcoholic steatohepatitis. *Hepatology* **38**, 999–1007 (2003).

307. Srivastava, S. *et al.* PGC-1α/β induced expression partially compensates for respiratory chain defects in cells from patients with mitochondrial disorders. *Hum. Mol. Genet.* **18**, 1805–1812 (2009).

308. Kudryavtseva, A. V. *et al.* Mitochondrial dysfunction and oxidative stress in aging and cancer. *Oncotarget* **7**, 44879–44905 (2016).

309. Mutinati, M. *et al.* Oxidative stress during pregnancy in the sheep. *Reprod. Domest. Anim.* **48**, 353–357 (2013).

310. Finkel, T. & Holbrook, N. J. Oxidants, oxidative stress and the biology of ageing. *Nature* **408**, 239–247 (2000).

311. Madesh, M. & Hajnóczky, G. VDAC-dependent permeabilization of the outer mitochondrial

membrane by superoxide induces rapid and massive cytochrome *c* release. *J. Cell Biol.* **155**, 1003–1016 (2001).

312. Bresciani, G., da Cruz, I. B. M. & González-Gallego, J. Manganese superoxide dismutase and oxidative stress modulation. *Adv. Clin. Chem.* **68**, 87–130 (2015).

313. Zelko, I. N., Mariani, T. J. & Folz, R. J. Superoxide dismutase multigene family: a comparison of the CuZn-SOD (SOD1), Mn-SOD (SOD2), and EC-SOD (SOD3) gene structures, evolution, and expression. *Free Radic. Biol. Med.* **33**, 337–49 (2002).

314. Marinho, H. S., Real, C., Cyrne, L., Soares, H. & Antunes, F. Hydrogen peroxide sensing, signaling and regulation of transcription factors. *Redox Biol.* **2**, 535–562 (2014).

315. Glorieux, C. & Calderon, P. B. Catalase, a remarkable enzyme: Targeting the oldest antioxidant enzyme to find a new cancer treatment approach. *Biol. Chem.* **398**, 1095–1108 (2017).

316. Cao, C. *et al.* Catalase is regulated by ubiquitination and proteosomal degradation. Role of the c-Abl and Arg tyrosine kinases. *Biochemistry* **42**, 10348–10353 (2003).

317. Deponte, M. Glutathione catalysis and the reaction mechanisms of glutathione-dependent enzymes. *Biochim. Biophys. Acta - Gen. Subj.* **1830**, 3217–3266 (2013).

318. Murphy, M. P. How mitochondria produce reactive oxygen species. *Biochem. J.* **417**, 1–13 (2009).

319. Dröge, W. Free Radicals in the Physiological Control of Cell Function. *Physiol. Rev.* **82**, 47–95 (2002).

320. Pessayre, D. Role of mitochondria in non-alcoholic fatty liver disease. *J. Gastroenterol. Hepatol.* **22**, S20–S27 (2007).

321. Nomoto, K., Tsuneyama, K., Takahashi, H., Murai, Y. & Takano, Y. Cytoplasmic Fine Granular Expression of 8-hydroxydeoxyguanosine Reflects Early Mitochondrial Oxidative DNA Damage in Nonalcoholic Fatty Liver Disease. *Appl. Immunohistochem. Mol. Morphol.* **PAP**, 71–5 (2007).

322. Vincent, H. K., Vincent, K. R., Bourguignon, C. & Braith, R. W. Obesity and postexercise oxidative stress in older women. *Med. Sci. Sports Exerc.* **37**, 213–9 (2005).

323. Amirkhizi, F. *et al.* Is obesity associated with increased plasma lipid peroxidation and oxidative stress in women? *ARYA Atheroscler.* **2**, (2010).

324. Ciapaite, J. *et al.* Metabolic control of mitochondrial properties by adenine nucleotide translocator determines palmitoyl-CoA effects. *FEBS J.* **273**, 5288–5302 (2006).

325. Yang, S. *et al.* Mitochondrial Adaptations to Obesity-Related Oxidant Stress. *Arch. Biochem. Biophys.* **378**, 259–268 (2000).

326. García-Ruiz, I. *et al.* Uric acid and anti-TNF antibody improve mitochondrial dysfunction in ob/ob mice. *Hepatology* **44**, 581–591 (2006).

327. Barry, J. The pregnant sheep as a model for human pregnancy. *Theriogenology* **69**, 55–67 (2009).

328. Chavatte-Palmer, P., Tarrade, A. & Rousseau-Ralliard, D. Diet before and during pregnancy and offspring health: The importance of animal models and what can be learned from them. *Int. J. Environ. Res. Public Health* **13**, (2016).

329. George, L. A. *et al.* Different levels of overnutrition and weight gain during pregnancy have differential effects on fetal growth and organ development. *Reprod. Biol. Endocrinol.* **8**, 75 (2010).

330. Council, N. R. *Nutrient Requirements of Small Ruminants*. (National Academies Press, 2007). doi:10.17226/11654

331. Quirós, P. M. Determination of Aconitase Activity: A Substrate of the Mitochondrial Lon Protease. in *Methods in molecular biology (Clifton, N.J.)* **1731**, 49–56 (2018).

332. Freitas, M. *et al.* Oxidative stress adaptation in aggressive prostate cancer may be counteracted by

the reduction of glutathione reductase. *FEBS Open Bio* **2**, 119–128 (2012).

333. Horn, H.-D. *Methods of enzymatic analysis*. (2011).

334. Spinazzi, M., Casarin, A., Pertegato, V., Salviati, L. & Angelini, C. Assessment of mitochondrial respiratory chain enzymatic activities on tissues and cultured cells. *Nat. Protoc.* **7**, 1235–1246 (2012).

335. Tsao, S.-M., Yin, M.-C. & Liu, W.-H. Oxidant Stress and B Vitamins Status in Patients With Non-Small Cell Lung Cancer. *Nutr. Cancer* **59**, 8–13 (2007).

336. Goossens, G. H. The Metabolic Phenotype in Obesity: Fat Mass, Body Fat Distribution, and Adipose Tissue Function. *Obes. Facts* **10**, 207–215 (2017).

337. Schattenberg, J. M. & Galle, P. R. Animal Models of Non-Alcoholic Steatohepatitis: Of Mice and Man. *Dig. Dis.* **28**, 247–254 (2010).

338. Stephenson, K. *et al.* Updates on Dietary Models of Nonalcoholic Fatty Liver Disease: Current Studies and Insights. *Gene Expr.* **18**, 5–17 (2018).

339. Lian, J. *et al.* Ces3/TGH Deficiency Attenuates Steatohepatitis. *Sci. Rep.* **6**, 25747 (2016).

340. Dai, G. *et al.* Maternal hepatic growth response to pregnancy in the mouse. *Exp. Biol. Med. (Maywood).* **236**, 1322–32 (2011).

341. Tuersunjiang, N. *et al.* Maternal obesity programs reduced leptin signaling in the pituitary and altered GH/IGF1 axis function leading to increased adiposity in adult sheep offspring. *PLoS One* **12**, e0181795 (2017).

342. Montminy, M. TRANSCRIPTIONAL REGULATION BY CYCLIC AMP. *Annu. Rev. Biochem.* **66**, 807–822 (1997).

343. Taylor, S. S., Knighton, D. R., Zheng, J., Ten Eyck, L. F. & Sowadski, J. M. Structural Framework for the Protein Kinase Family. *Annu. Rev. Cell Biol.* **8**, 429–462 (1992).

344. Ould Amer, Y. & Hebert-Chatelain, E. Mitochondrial cAMP-PKA signaling: What do we really know? *Biochim. Biophys. Acta - Bioenerg.* **1859**, 868–877 (2018).

345. Hossain, M. I., Roulston, C. L. & Stapleton, D. I. Molecular Basis of Impaired Glycogen Metabolism during Ischemic Stroke and Hypoxia. *PLoS One* **9**, e97570 (2014).

346. Peng, I.-C. *et al.* Glucagon regulates ACC activity in adipocytes through the CAMKKβ/AMPK pathway. *Am. J. Physiol. Endocrinol. Metab.* **302**, E1560-8 (2012).

347. Fang, X. *et al.* Phosphorylation and inactivation of glycogen synthase kinase 3 by protein kinase A. *Proc. Natl. Acad. Sci. U. S. A.* **97**, 11960–5 (2000).

348. Rider, M. H. *et al.* 6-phosphofructo-2-kinase/fructose-2,6-bisphosphatase: head-to-head with a bifunctional enzyme that controls glycolysis. *Biochem. J.* **381**, 561–79 (2004).

349. Rider, M. H. *et al.* The two forms of bovine heart 6-phosphofructo-2-kinase/fructose-2,6-bisphosphatase result from alternative splicing. *Biochem. J.* **285 (Pt 2)**, 405–11 (1992).

350. Portela, P., Moreno, S. & Rossi, S. Characterization of yeast pyruvate kinase 1 as a protein kinase A substrate, and specificity of the phosphorylation site sequence in the whole protein. *Biochem. J.* **396**, 117–26 (2006).

351. Lu, M. & Shyy, J. Y.-J. Sterol regulatory element-binding protein 1 is negatively modulated by PKA phosphorylation. *Am. J. Physiol. Physiol.* **290**, C1477–C1486 (2006).

352. Ahmadian, M. *et al.* PPARγ signaling and metabolism: the good, the bad and the future. *Nat. Med.* **19**, 557–66 (2013).

353. Berg, J. M., Tymoczko, J. L. & Stryer, L. Acetyl Coenzyme A Carboxylase Plays a Key Role in Controlling Fatty Acid Metabolism. (2002).

354. Liss, K. H. H. & Finck, B. N. PPARs and nonalcoholic fatty liver disease. *Biochimie* **136**, 65–74

(2017).

355. Serviddio, G., Bellanti, F. & Vendemiale, G. Free radical biology for medicine: learning from nonalcoholic fatty liver disease. *Free Radic. Biol. Med.* **65**, 952–968 (2013).

356. Sardanelli, A. M. *et al.* Topology of the mitochondrial cAMP-dependent protein kinase and its substrates. *FEBS Lett.* **396**, 276–278 (1996).

357. Acin-Perez, R. *et al.* Cyclic AMP Produced inside Mitochondria Regulates Oxidative Phosphorylation. *Cell Metab.* **9**, 265–276 (2009).

358. De Rasmo, D., Panelli, D., Sardanelli, A. M. & Papa, S. cAMP-dependent protein kinase regulates the mitochondrial import of the nuclear encoded NDUFS4 subunit of complex I. *Cell. Signal.* **20**, 989–997 (2008).

359. Prabu, S. K. *et al.* Protein Kinase A-mediated Phosphorylation Modulates Cytochrome *c* Oxidase Function and Augments Hypoxia and Myocardial Ischemia-related Injury. *J. Biol. Chem.* **281**, 2061–2070 (2006).

360. Shinzawa-Itoh, K. *et al.* Structures and physiological roles of 13 integral lipids of bovine heart cytochrome c oxidase. *EMBO J.* **26**, 1713–1725 (2007).

361. Tilokani, L., Nagashima, S., Paupe, V. & Prudent, J. Mitochondrial dynamics: overview of molecular mechanisms. *Essays Biochem.* **62**, 341–360 (2018).

362. Cribbs, J. T. & Strack, S. Reversible phosphorylation of Drp1 by cyclic AMP-dependent protein kinase and calcineurin regulates mitochondrial fission and cell death. *EMBO Rep.* **8**, 939–944 (2007).

363. Akabane, S. *et al.* PKA Regulates PINK1 Stability and Parkin Recruitment to Damaged Mitochondria through Phosphorylation of MIC60. *Mol. Cell* **62**, 371–384 (2016).

364. van der Laan, M., Horvath, S. E. & Pfanner, N. Mitochondrial contact site and cristae organizing system. *Curr. Opin. Cell Biol.* **41**, 33–42 (2016).

365. Yang, J., Li, J.-H., Wang, J. & Zhang, C.-Y. Molecular modeling of BAD complex resided in a mitochondrion integrating glycolysis and apoptosis. *J. Theor. Biol.* **266**, 231–241 (2010).

366. Virdee, K., Parone, P. A. & Tolkovsky, A. M. Phosphorylation of the pro-apoptotic protein BAD on serine 155, a novel site, contributes to cell survival. *Curr. Biol.* **10**, R883 (2000).

367. Harada, H. *et al.* Phosphorylation and Inactivation of BAD by Mitochondria-Anchored Protein Kinase A. *Mol. Cell* **3**, 413–422 (1999).

368. Hata, A. N., Engelman, J. A. & Faber, A. C. The BCL2 Family: Key Mediators of the Apoptotic Response to Targeted Anticancer Therapeutics. *Cancer Discov.* **5**, 475–87 (2015).

369. Cazanave, S. C. & Gores, G. J. The liver's dance with death: two Bcl-2 guardian proteins from the abyss. *Hepatology* **50**, 1009–13 (2009).

370. Breitschopf, K., Haendeler, J., Malchow, P., Zeiher, A. M. & Dimmeler, S. Posttranslational modification of Bcl-2 facilitates its proteasome-dependent degradation: molecular characterization of the involved signaling pathway. *Mol. Cell. Biol.* **20**, 1886–96 (2000).

371. Bodur, C., Kutuk, O., Tezil, T. & Basaga, H. Inactivation of Bcl-2 through IκB kinase (IKK)-dependent phosphorylation mediates apoptosis upon exposure to 4-hydroxynonenal (HNE). *J. Cell. Physiol.* **227**, 3556–3565 (2012).

372. Chiara, G. De *et al.* Bcl-2 Phosphorylation by p38 MAPK. *J. Biol. Chem.* **281**, 21353–21361 (2006).

373. Stiburek, L. *et al.* YME1L controls the accumulation of respiratory chain subunits and is required for apoptotic resistance, cristae morphogenesis, and cell proliferation. *Mol. Biol. Cell* **23**, 1010–23 (2012).

374. Harbauer, A. B., Zahedi, R. P., Sickmann, A., Pfanner, N. & Meisinger, C. The Protein Import

Machinery of Mitochondria—A Regulatory Hub in Metabolism, Stress, and Disease. *Cell Metab.* **19**, 357–372 (2014).

375. Wright, G., Terada, K., Yano, M., Sergeev, I. & Mori, M. Oxidative Stress Inhibits the Mitochondrial Import of Preproteins and Leads to Their Degradation. *Exp. Cell Res.* **263**, 107–117 (2001).

376. Houtkooper, R. H. *et al.* Mitonuclear protein imbalance as a conserved longevity mechanism. *Nature* **497**, 451–457 (2013).

377. Genova, M. L., Bianchi, C. & Lenaz, G. Supercomplex organization of the mitochondrial respiratory chain and the role of the Coenzyme Q pool: Pathophysiological implications. *BioFactors* **25**, 5–20 (2005).

378. Wang, Y., Mohsen, A.-W., Mihalik, S. J., Goetzman, E. S. & Vockley, J. Evidence for physical association of mitochondrial fatty acid oxidation and oxidative phosphorylation complexes. *J. Biol. Chem.* **285**, 29834–41 (2010).

379. de Brito, O. M. & Scorrano, L. Mitofusin 2 tethers endoplasmic reticulum to mitochondria. *Nature* **456**, 605–610 (2008).

380. Jarukamjorn, K., Jearapong, N., Pimson, C. & Chatuphonprasert, W. A High-Fat, High-Fructose Diet Induces Antioxidant Imbalance and Increases the Risk and Progression of Nonalcoholic Fatty Liver Disease in Mice. *Scientifica (Cairo).* **2016**, 1–10 (2016).

381. Sies, H. Hydrogen peroxide as a central redox signaling molecule in physiological oxidative stress: Oxidative eustress. *Redox Biol.* **11**, 613–619 (2017).

382. Cao, C., Leng, Y. & Kufe, D. Catalase Activity Is Regulated by c-Abl and Arg in the Oxidative Stress Response. *J. Biol. Chem.* **278**, 29667–29675 (2003).

383. Li, L. *et al.* A Western diet induced NAFLD in LDLR−− mice is associated with reduced hepatic glutathione synthesis. *Free Radic. Biol. Med.* **96**, 13–21 (2016).

384. Cho, C.-S. *et al.* Irreversible Inactivation of Glutathione Peroxidase 1 and Reversible Inactivation of Peroxiredoxin II by H_2O_2 in Red Blood Cells. *Antioxid. Redox Signal.* **12**, 1235–1246 (2010).

385. Filomeni, G., De Zio, D. & Cecconi, F. Oxidative stress and autophagy: the clash between damage and metabolic needs. *Cell Death Differ.* **22**, 377–388 (2015).

386. Kadowaki, M. & Karim, M. R. Cytosolic LC3 Ratio as a Quantitative Index of Macroautophagy. in *Methods in enzymology* **452**, 199–213 (2009).

387. He, C. & Klionsky, D. J. Regulation Mechanisms and Signaling Pathways of Autophagy. *Annu. Rev. Genet.* **43**, 67–93 (2009).

388. Nakaso, K. *et al.* Transcriptional activation of p62/A170/ZIP during the formation of the aggregates: possible mechanisms and the role in Lewy body formation in Parkinson's disease. *Brain Res.* **1012**, 42–51 (2004).

389. Kang, R., Zeh, H. J., Lotze, M. T. & Tang, D. The Beclin 1 network regulates autophagy and apoptosis. *Cell Death Differ.* **18**, 571–80 (2011).

390. Fukuo, Y. *et al.* Abnormality of autophagic function and cathepsin expression in the liver from patients with non-alcoholic fatty liver disease. *Hepatol. Res.* **44**, 1026–1036 (2014).

391. Gebhardt, R. & Matz-Soja, M. Liver zonation: Novel aspects of its regulation and its impact on homeostasis. *World J. Gastroenterol.* **20**, 8491–504 (2014).

392. Kessler, J., Rasmussen, S. & Kiserud, T. The fetal portal vein: normal blood flow development during the second half of human pregnancy. *Ultrasound Obstet. Gynecol.* **30**, 52–60 (2007).

393. Cox, L. A. *et al.* Gene expression profile differences in left and right liver lobes from mid-gestation fetal baboons: a cautionary tale. *J. Physiol.* **572**, 59–66 (2006).

394. Hocher, B. *et al.* Maternal eNOS deficiency determines a fatty liver phenotype of the offspring in

a sex dependent manner. *Epigenetics* **11**, 539–52 (2016).

395. Su, Y.-M., Lv, G.-R., Xie, J.-X., Wang, Z.-H. & Lin, H.-T. Maternal Hypoxia Increases the Susceptibility of Adult Rat Male Offspring to High-Fat Diet-Induced Nonalcoholic Fatty Liver Disease. *Endocrinology* **154**, 4377–4387 (2013).

396. Rueda-Clausen, C. F. *et al.* Hypoxia-Induced Intrauterine Growth Restriction Increases the Susceptibility of Rats to High-Fat Diet-Induced Metabolic Syndrome. *Diabetes* **60**, 507–516 (2011).

397. Bristow, J., Rudolph, A. M., Itskovitz, J. & Barnes, R. Hepatic oxygen and glucose metabolism in the fetal lamb. Response to hypoxia. *J. Clin. Invest.* **71**, 1047–61 (1983).

398. Becker, S. *et al.* Protective effect of maternal uteroplacental insufficiency on oxygen-induced retinopathy in offspring: removing bias of premature birth. *Sci. Rep.* **7**, 42301 (2017).

399. Sudhindran, S., Menon, R. N. & Balakrishnan, D. Challenges and Outcome of Left-lobe Liver Transplants in Adult Living Donor Liver Transplants. *J. Clin. Exp. Hepatol.* **2**, 181–7 (2012).

400. She, W. H., Chok, K. S., Fung, J. Y., Chan, A. C. & Lo, C. M. Outcomes of right-lobe and left-lobe living-donor liver transplantations using small-for-size grafts. *World J. Gastroenterol.* **23**, 4270–4277 (2017).

401. Humar, A. *et al.* Liver Regeneration After Adult Living Donor and Deceased Donor Split-Liver Transplants. (2004). doi:10.1002/lt.20096